Including Imperfections within the Displacement-based Koiter Methodology

Rolijne Veerle Pietersma

TU Delft

MSc Thesis

Including Imperfections within the Displacement-based Koiter Methodology

by

Rolijne Veerle Pietersma

to obtain the degree of Master of Science at the Delft University of Technology,
to be defended publicly on Tuesday September 19, 2023 at 14:00.

.

Student number: 4548841
Project duration: Augustus 20, 2022 – September 19, 2023
Thesis Committee: Dr. Saullo G. P. Castro
Dr. Eelco L. Jansen
Dr. Bianca Giovanardi
Dr. Otto K. Bergsma

An electronic version of this thesis is available at http://repository.tudelft.nl/.

Cover: Kintsugi Cylinder by Yoko Kawada Design

TU Delft

Preface

This thesis marks the end of my master's degree in Aerospace Engineering. It was a long and sometimes challenging journey and I would like to show my appreciation for everybody who supported me along the way.

To Saullo, who was always positive despite the whole process and always made me feel good about my work after our meetings. Your guidance helped me tremendously.

To Eelco, who jumped in on the project halfway. I appreciate the time and effort you took to share the knowledge you had about the Koiter methodology and your ability to explain everything clearly to me.

To my parents Alwin and Wilma for supporting me throughout everything and always telling me they were proud of me.

To my sister Karleen, who always believed in me and I could ask for anything.

To everybody at lacrosse, the games and social events were a welcome distraction from the struggles of my thesis.

To everybody in the ASM master room, you made it fun and motivating to come to university and work on the thesis together.

To Phil, for being a close friend throughout my whole master's degree and who I could always rely on.

To Natalia, for having good conversations about everything in our office.

And lastly, to everybody I have met in the last seven years of studying. You have all made it a wonderful experience and one I can look back at with joy.

Rolijne Veerle Pietersma
Delft, September 2023

Summary

The Koiter methodology is a reduced-order model that can predict the initial post-buckling characteristics of structures. Incorporating the Koiter approach within finite element simulations resulted in challenges. These included mesh-sensitive initial post-buckling coefficients, computationally expensive high-order derivatives, and phenomena such as locking, which led to unrealistic behaviour of structures. The displacement-based Koiter methodology is introduced to overcome these issues due to the clear connection between the theory and the implementation.

This research aimed to include imperfections in the displacement-based Koiter methodology and to develop an easily implementable and computationally efficient approach. This novel approach should be suitable for recurring processes such as sensitivity studies, ultimately leading to the creation of design guidelines for imperfection-insensitive cylinders. These cylinders are more weight-efficient compared to cylinders sensitive to imperfections and therefore ideal for aerospace applications, such as the outer shells of rockets.

To demonstrate the incorporation of imperfections within the displacement-based Koiter methodology, it was decided to apply the approach first to a plate with an imperfection utilising the single-mode expansion and Donnell-type kinematics. In order to achieve this goal, three steps are identified to include imperfections within the displacement-based methodology. First of all the total potential energy of an imperfect structure is expanded by performing three Taylor expansions. Two possibilities arise for this expansion, one formulation set up by Budiansky and another one derived by Pignataro. Following this, the perfect and imperfect functional derivatives are derived utilising the Donnell kinematics by means of Frechét derivatives. One can simplify this procedure by assuming that the pre-buckling is linear resulting in the out-of-plane rotations to be equal to zero, alternatively, one can disregard this assumption and have supposedly more accurate but consequently also more functional derivatives. A total of four solution possibilities arise due to the two assumptions related to the expansion of the total potential energy and the pre-buckling behaviour.

The last step is to perform an asymptotic analysis. The initial idea was to derive imperfect initial post-buckling coefficients a_I and b_I. These could be formulated by substituting the asymptotic expansions for the load and the displacement in the expansion for the total potential energy. The approach was unsuccessful in finding post-buckling coefficients since it was not possible to isolate any of the unknowns. Besides the fact that it was not possible to derive expressions for a_I and b_I, it was reflected that the coefficients would not be representative of reality as imperfect structures no longer have a bifurcation point and therefore it does not make sense to perform an asymptotic expansion in the vicinity of this critical load.

An alternative for the asymptotic expansion is to derive the imperfection form factors instead of the post-buckling coefficients. The asymptotic expansion for the load is adjusted to include the imperfection form factors α and β. To derive expressions for these coefficients, firstly the asymptotic expansion for the displacement is substituted into the expansion of the total potential energy. Then the load expansion including the terms α and β is replaced to derive an equilibrium equation. Due to the assumption of linear pre-buckling $\alpha = \beta$, it was possible to formulate an expression for α for a plate with linear pre-buckling. Initial results show that it matches literature, however, more imperfection shapes should be tested to conclude that the approach is correct.

The recommendations to verify that the inclusion of imperfection within the displacement-based Koiter methodology is successful are the following: reconstruct the displacement field and compare this to other non-linear solutions of imperfect plates. Secondly, it is recommended to compute the imperfection form factors for several different imperfection shapes with the displacement-based approach and compare it to the FE software DIANA which is able to compute the same form factors.

Contents

List of Figures

Nomenclature

Abbreviations

AFP	Automated Fibre Placement
BFSC	Bogner-Fox-Schmit-Castro
CFRP	Carbon Fibre Reinforced Plastic
CTS	Continuous Tow Shearing
DBKM	Displacement-based Koiter Methodology
FE	Finite Element
FEA	Finite Element Analysis
FEM	Finite Element Modelling
KDF	Knock-down Factor
MPLA	Multiple Perturbation Load Approach
QI	Quasi-Isotropic
SBPA	Single Boundary Perturbation Approach
SPDA	Single Perturbation Displacement Approach
SPLA	Single Perturbation Load Approach
TFP	Tailored Fibre Placement
VA	Variable Angle
VAFW	Variable Angle Filament Winding
VAT	Variable Angle Tow

Subscripts

$(\ )_{,x}, (\ )_{,y}, (\ )_{,z}$	Derivative w.r.t. x, y, z
$(\ )_0$	Fundamental Solution
$(\ )_c$	Bifurcation Point

Lower-case Roman

$\bar{\boldsymbol{u}}$	Imperfect displacement
$\bar{\boldsymbol{v}}$	Asymptotic expansion ($\boldsymbol{u} - \boldsymbol{u_c}$)
$\hat{\boldsymbol{u}}$	Imperfection shape
$\boldsymbol{u_I}$	First-order displacement field
$\boldsymbol{u_{III}}$	Third-order displacement field
$\boldsymbol{u_{II}}$	Second-order displacement field

$\boldsymbol{u}$	Displacements
ℓ	Dimensions finite element
a_I	First post-buckling coefficient
b_I	Second post-buckling coefficient
t_0	Original tow thickness

Upper-case Roman

$\bar{M}_i$	Imperfect bending stresses
$\bar{N}_i$	Imperfect membrane stresses
$\hat{\boldsymbol{N}}$	General distributed loading
A_{ij}	Membrane stiffness
B_{ij}	Membrane-bending coupling
D_{ij}	Bending stiffness
H_i	Hermite cubic functions
M_i	Perfect bending stresses
N_i	Perfect membrane stresses
$S^{\bar{w}}$	Shape functions of imperfect displacement field
S^u, S^v, S^w	Shape functions of displacement field

Superscripts

$(\dot{})$	Frechét derivative w.r.t. λ
$(\ )'$	Frechét derivative w.r.t. $\boldsymbol{u}$
$(\tilde{})$	Frechét derivative w.r.t. $\bar{\boldsymbol{u}}$

Lower-case Greek

α, β	Imperfection form factors
$\bar{\phi}$	Total potential energy functional structure
$\bar{\xi}$	Imperfection amplitude
$\bar{\boldsymbol{\kappa}}$	Rotational strain imperfect structure
$\bar{\boldsymbol{\varepsilon}}$	Extensional strain imperfect structure
$\boldsymbol{\kappa}$	Rotational strain perfect structure
$\boldsymbol{\varepsilon}$	Extensional strain perfect structure
λ	Load scalar paramater
ϕ	Total potential energy functional perfect structure
ψ	Total potential energy functional imperfect structure
θ	Tow shearing angle
ξ	Scalar Parameter

1

Introduction

Aerospace structures are designed to be lightweight. A structure that has more mass is less economical since it requires more thrust and lift to operate, consequently resulting in higher fuel requirements. For aircraft, the additional costs are estimated to be between $45 €/$kg and $385 €/$kg for fuel consumption when the weight of the plane is increased [1]. This cost increase is more significant for space structures and this is estimated to be around $10\,000 €$ per kilogram for Low Earth Orbit launchers [2]. These predictions for cost increase rely on several factors such as lifetime and application of the vehicle, and therefore it is difficult to obtain one cost estimation that is relevant for all space structures or all aircraft.

On top of being economical, reducing the weight of aerospace structures is more sustainable. The reduced fuel consumption due to designing lightweight configurations also minimizes the number of greenhouse gases emitted. The aviation industry is responsible for 3% of the total CO_2 emissions [3], most of these emissions are produced during the operational lifetime of the aircraft and therefore reducing the weight is the most sustainable approach to reduce this number.

To achieve these weight-efficient designs, aerospace structures are composed of thin-walled constructions prone to buckling. The load is redistributed within the structure due to the change in shape as a consequence of buckling, and this could potentially lead to yielding or even failure. Additionally, the aerodynamic shape is no longer maintained, resulting in a less efficient configuration due to the loss of lift and possible increased drag.

Several studies were carried out to accurately predict the buckling load of shells, resulting in the Elastic Buckling Theory. This theory solved the eigenvalue problem for shell structures to find the bifurcation point. The theory was able to predict the buckling load of plates and columns but it failed short for cylindrical shells. Large deviations between theory and experiment were observed for cylinders and these were attributed to imperfections. This has sparked interest in designing a cylindrical shell that is not sensitive to imperfections when axially compressed.

Up to this point, an imperfection-insensitive shell has not yet been achieved. One of the reasons no guidelines are available for this shell is due to the fact that repeated sensitivity studies are required to draw conclusions. Computationally expensive non-linear solvers are used to predict the buckling load of imperfect cylinders and these increase the running time of these sensitivity studies significantly. Therefore this research aims to introduce a new methodology that is efficient and simple to implement, namely the displacement-based Koiter methodology with the inclusion of imperfections. This novel tool could be used in sensitivity studies and eventually assist in the creation of design guidelines for imperfection-insensitive shells, but the focus of this study lies in the methodology.

The thesis is structured as follows, first, chapter 2 presents a literature review to outline the several possibilities to predict the buckling load of cylindrical shells and which techniques are available to reduce the sensitivity to imperfections. The chapter concludes by identifying the research gaps related to the buckling of cylindrical shells. From this conclusion, the research objective and scope are defined in chapter 3. The goal is to include imperfections within the displacement-based Koiter methodology and the necessary steps to achieve this are explained in chapter 4 to 7, as well as how effective this novel modelling technique is. Finally, the concluding remarks can be found in chapter 8 and future research is presented in chapter 9.

2

Literature Review

The initial objective of this thesis was to design a lightweight composite cylinder that is insensitive to imperfections. The first step in achieving this goal is to explore what has been done in the past, and this chapter provides a short overview of the existing literature relating to imperfection-sensitive cylindrical shells. The first section of this chapter introduces the revelation that cylinders are sensitive to imperfections, along with the factors that can reduce their buckling load (section 2.1). Subsequently, in section 2.2, various approaches to predicting the buckling load of imperfect cylinders are discussed. Building upon the definition of imperfection sensitivity presented in section 2.3, section 2.4 presents solution approaches aimed at reducing this sensitivity. The chapter concludes by identifying the gaps in the existing literature (section 2.5), which serve as the foundation for this thesis.

2.1. Discovery Imperfection Sensitivity

Thin-walled structures are commonly used in aerospace and marine industries, consisting of lightweight constructions that are prone to buckling, so extensive research has been done to predict the precise buckling load of various kinds of structures. The buckling load of structures is often predicted by means of solving eigenvalue problems that conclude the bifurcation point, at which the structure moves from the fundamental equilibrium path to the buckled path [4, 5]. When the theories were tested and validated, large deviations between the theoretical and the experimental buckling load were discovered. These discrepancies were unexpected since similar equations had worked well to predict the buckling load of plates and columns. Three main conclusions could be drawn from the experiments. First of all, the true buckling load was lower than the theoretical load, sometimes even as low as 10 % of the theoretical value. Secondly, there was scatter in the experimental data, even between identical cylinders and thirdly, the failures were unstable leading to catastrophic collapse [6, 5].

Koiter [7], Von Karman and Tsien [8], Donnell and Wan [9] could attribute the differences between the theoretical and experimental results of the buckling analysis of cylindrical shells to imperfections and thus cylindrical shells were defined as sensitive to imperfections. This discovery that imperfections can reduce the buckling load sparked much interest in finding solutions to reduce it and analysing imperfections themselves and other sources that could explain the discrepancies. Many revelations have been made since the early 1900s and it has been concluded that three factors have a significant effect on the buckling behaviour of thin-walled cylindrical shells; geometric imperfections, pre-buckling deformations and stresses, and lastly boundary conditions and non-uniform loading. Geometric imperfections lower the buckling load the most, but in combination with the other two factors, it explains the large deviations between theory and experiments.

2.2. Predicting the Buckling Load of Imperfect Shells

The prediction of buckling load can be divided into three main approaches: Empirical Design Factors, Koiter's Asymptotic Analysis and Finite Element Modelling. It was decided not to use Empirical Design Factors to predict the buckling load in this research since they are commonly used in preliminary design phases due to their simplistic and conservative nature. Moreover, the design factors are not appropriate for composite cylinders and therefore this approach is not discussed in detail.

2.2.1. Finite Element Modelling

Initially, empirical design factors were a simple fix to dealing with imperfections, but they resulted in overly conservative designs. Therefore researchers were looking for methods that could take imperfections into consideration for more accurate predictions of the buckling load. Finite Element Software was already being utilized to predict the behaviour of complex geometries, therefore making it the logical choice to also include imperfections in models to find more accurate buckling loads. At first linear solvers were used, but these did not yield satisfying results. As computational power increased exponentially over time, it was also possible to perform non-linear computations, which led to more accurate predictions. Now it is common to perform a detailed non-linear analysis of the cylinder within Finite Element software at the end of the design phase to predict the final buckling load. FEM is a powerful tool, however, one should also pay close attention when assembling the model and all assumptions should be carefully considered. The results of the model can depend on the input parameters, so the time to set up a model and verify the results is time-consuming. Within FEM there are three methods to model imperfections, which are Stress-Free superposition, Single Perturbation Methods, and Non-Stress-Free superposition. The last one is not discussed in detail, as this is the most complex and beyond the scope of this research.

The first methodology to replicate imperfections involves superimposing the defects onto the perfect cylinder. The coordinates of the nodes are translated to the position of the imperfection, resulting in a stress-free approach [10]. Depending, on how much information is available about the imperfection pattern there are different assumptions one can make about the imperfection shape. The simplest method is basing it on the eigenmode, however, this is often not realistic of true imperfection shapes [6]. More true to nature is to add a single dimple to the model, which causes a single buckle to occur as it was observed in experiments that a single dimple triggers the buckling mechanism of a cylinder [11]. Lastly, the most realistic imperfection shape is directly measured from a manufactured specimen and superimposed onto the cylinder, however, this is only possible when the cylinder is produced. This stress-free method can be easily implemented into finite element software. Despite the ease of implementation, one has to be careful that the translated nodes do not cause any axially-oriented buckling modes, resulting in a seemingly stronger cylinder since the imperfections act as stiffeners [12].

Due to the lack of data to provide realistic imperfection patterns for composite cylinders, simplified perturbation methods were introduced to overcome this problem [13, 14]. These methods include the Single Perturbation Load Approach (SPLA), Single Perturbation Displacement Approach (SPDA), and Single Boundary Perturbation Approach (SBPA). The SPLA is commonly used and therefore only this is discussed. SPLA assumes that the initial geometric imperfection can be simulated with a single perturbation load, which will cause a single buckle to occur as the cylinder is axially compressed. This was based on the research of Hühne [11] which observed that the buckling of imperfect structures is typically initiated with a single buckle. Secondly, SPLA assumes the presence of a minimum buckling load, which remains constant even as the perturbation load increases [15]. This critical load should be used as the design load. There are several limitations to this approach. First of all, this approach is suitable for displacement-controlled models and experiments, but not for load-controlled analyses [16]. Experiments are typically displacement-controlled, but real-life structures are somewhere between load- and displacement-controlled and therefore not truly suitable for this approach. Secondly, it was observed that certain cylinders failed below the predicted buckling load. This happened because non-geometric imperfections, such as load eccentricities, have a more significant effect and the SPLA method is unable to capture this [17]. Lastly, to obtain accurate results it is necessary to rely on non-linear finite element simulations which are computationally expensive.

2.2.2. Koiter's Asymptotic Analysis

An alternative to predict the initial post-buckling response of a cylinder is to make use of perturbation techniques. The pioneer for this perturbation approach was Koiter [7] and the perturbation methodology is also often referred to as the Asymptotic Koiter Analysis. Koiter was able to provide mathematical proof of why cylinders collapse before the predicted buckling load, whereas plates are capable of sustaining loads above them. The idea behind the perturbation technique is to expand the displacement field and load parameters around a known state. The main advantage of performing the expansion around this known state is to create a reduced linear model which is less computationally expensive, even when multiple modes interact. The reduced complexity and computational time are beneficial for repeated imperfection sensitivity studies of structures, which would become computationally expensive using

non-linear solvers.

The single mode asymptotic expansions for the load parameter and the displacement field are presented in Equation 2.1 and 2.2, respectively, where λ represents the load parameter, λ_c is the known critical load (typically the bifurcation load), ξ is a scalar parameter, and a_I and b_I are the Koiter factors. Moreover, $\boldsymbol{u_I}$ is the first-order displacement field which is either a single scaled buckling mode or a combination of scaled multiple buckling modes, $\boldsymbol{u_{II}}$ represents the second-order displacement field and is a correction to the first-order field, and lastly, $\boldsymbol{u_{III}}$ is the third-field order field but this is usually ignored [18].

$$\lambda - \lambda_c = a_I \lambda_c \xi + b_I \lambda_c \xi^2 \tag{2.1}$$

$$\boldsymbol{u} - \boldsymbol{u_c} = \xi \boldsymbol{u_I} + \xi^2 \boldsymbol{u_{II}} + \xi^3 \boldsymbol{u_{III}} \tag{2.2}$$

Typically for cylinders multiple buckling loads interact and the single expansion is not sufficient to predict the initial post-buckling behaviour. In the case of modes interacting the multi-modal expansions can be used which are expressed in Equation 2.3 and 2.4, where the subscripts j, k, ℓ represent the summation conventions [18].

$$\xi_I \left(\lambda - \lambda_I\right) = \lambda_I a_{Ijk} \xi_j \xi_k + \lambda_I b_{Ijk\ell} \xi_j \xi_k \xi_\ell + \cdots \tag{2.3}$$

$$\boldsymbol{u} - \boldsymbol{u_c} = \boldsymbol{v} = \xi_i \boldsymbol{u_i} + \xi_i \xi_j \boldsymbol{u}_{ij} + \cdots \tag{2.4}$$

The Koiter factors, also named the initial post-buckling coefficients, determine if a cylinder's post-buckling response is stable and are a direct indication of imperfection sensitivity. This relationship is shown visually in Figure 2.1. The first post-buckling coefficient, a_I, determines if the response is symmetric or not. The response is symmetric when a_I is equal to zero. When the first post-buckling coefficient is zero the initial post-buckling characteristics are determined by the second coefficient. When b_I is positive the structure can sustain load after buckling and is therefore stable. However, when the second post-buckling coefficient is negative the response is unstable since the structure collapses after the buckling load. If the first post-buckling coefficient is not equal to zero the response is unsymmetrical and therefore depending on the imperfection it will either have a stable or unstable response. This uncertainty in the post-buckling response is undesired and therefore if the first post-buckling coefficient is not equal to zero the behaviour is also categorised as unstable.

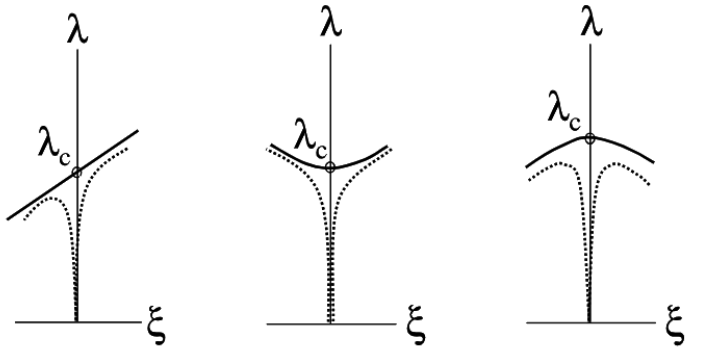

(a) $a \neq 0$ (unstable) (b) $a = 0,\ b > 0$ (stable) (c) $a = 0,\ b < 0$ (unstable)

Figure 2.1: "*Typical initial post-buckling responses. The solid and dotted lines indicate, respectively, the response of the perfect and imperfect structures.*" [19]

The Asymptotic Koiter Analysis is a powerful tool, however, difficulties arise for the implementation within Finite Element software. These challenges include the implementation of high-order energy derivatives, which can easily require large amounts of computational power. Moreover, one should pay close attention to the mechanical modelling as well as the finite element implementation, to avoid interpolation locking and extrapolation locking [20]. On top of this, it was found that the Koiter factor b_I is mesh sensitive, which would require additional analysis which is undesirable [21]. For these reasons,

the Koiter method is not available within many commercial FE software. The FE software DIANA[1] was able to overcome all of these issues and implement the Koiter analysis within their software.

To overcome the difficulties of implementing the Koiter method into finite element frameworks, Castro and Jansen [18, 22] formulated and performed a displacement-based expansion of the Koiter method. The method allows for a one-to-one correspondence between the formulation and the implementation. Moreover, the formulation can even be used within every displacement-based application [18]. The methodology for displacement-based Koiter can be concisely summarized by the following steps. First of all the potential energy of the system is presented and expanded by two Taylor expansions around the displacement field and the load parameter. The asymptotic expansions are substituted into the potential energy functional to find the coefficients a_I and b_I. The derivatives of the potential energy are found by means of Kinematics such as Donnell or Sanders. The method is expanded for both single-mode and multiple-modal. However, initial displacements have not yet been included in the implementation. The inclusion of imperfections would allow for an easily implementable procedure to assess the imperfection sensitivity of structures, which is also computationally inexpensive.

2.3. Definition Imperfection-Insensitive Shell

The goal of the present literature review is to create a design methodology for imperfection-insensitive cylinders. Many researchers have extensively studied imperfection sensitivity and solutions to prevent the decrease in buckling load. However, there is no consistent definition used to define an imperfection-insensitive cylinder. Therefore a final definition used within this literature research is presented here.

A uniform quantitative measurement to define sensitivity to imperfections is to use the knockdown factor (KDF), which is a ratio of the buckling load of the imperfect shell over the load of the perfect shell. The buckling load of the perfect shell can be found by means of linear eigenvalue analysis. On the other hand, the buckling load of the imperfect shell should be calculated by means of non-linear analysis to accurately take into account the non-linear effects of the imperfections on the buckling response [6]. A KDF equal to 1 is an imperfection-insensitive shell, however, this is impossible to achieve since the imperfections will have a minimal effect on the buckling load due to local stress concentrations that lower the overall critical load. All research related to imperfection-insensitive cylinders did not give any indication at which KDF a cylinder was insensitive and at which threshold value it is no longer considered insensitive. Therefore, it was decided to create this definition. If a cylinder is imperfection insensitive the KDF would be equal to 1. However, this would result in an unrealistic criterion. Therefore it was decided to take 0.95 as a threshold value, to allow for a more realistic criterion that could be achieved for certain designs, whilst not being too low that it is easily accomplished. Moreover, it was decided that an imperfection-insensitive cylinder should achieve this KDF for multiple imperfection amplitudes to avoid a design for one specific imperfection case. An imperfection range from -4 to 4 times the shell thickness should be considered as these are typically the size of imperfections [23]. This concludes the final definition of imperfection sensitivity.

2.4. Solutions against Imperfection Sensitivity

Naturally, researchers have attempted to find solutions to decrease the sensitivity to imperfections of cylindrical shells, ultimately paving the way to better designs since their behaviour is more predictable and the weight can be reduced. Two main solution groups are discussed, namely: the addition of reinforcing elements and variable angle (VA) composites. The goal of the research is to design an imperfection-insensitive cylinder so, each section concludes if a certain solution is able to achieve imperfection-insensitive shells, according to the previously established definition. Sandwich structures are another good alternative to decrease the sensitivity, however, it was decided not to explore this route since the buckling behaviour is more complex than traditional composite cylinders and therefore beyond the scope of this research. Moreover, the solutions presented here are limited to composite cylinders, due to their superior mechanical properties and low density compared to isotropic materials. Lastly, the solutions are restricted to axially compressed cylinders only.

[1] `https://manuals.dianafea.com/d107/en/1181807-1182380-effect-of-imperfection.html`, accessed 30 Aug. 2023

2.4.1. Additional Reinforcing Components

A simple solution to the unexpected decreasing load of compressed cylinders was to reinforce the cylinders with axially and circumferential stringers and hoops. It was observed that stiffened cylinders have an increased buckling load and are less sensitive to imperfections, compared to their equivalent unstiffened cylinder [24]. The addition of stable post-buckling elements increases the stability of the whole structure reducing the sensitivity to imperfections [25]. A short overview of research related to creating an imperfection-insensitive shell utilising reinforcing structures is presented.

Wagner et al. [26] designed a cylinder with 18 inward aluminium stringers, and three CFRP hoops with the goal of it being imperfection insensitive by stopping the formation of significant dimple imperfections. Unfortunately, the design was not imperfection insensitive, since the authors claim the KDF was equal to 0.87, however, this is calculated by dividing the experimental results by the non-linear Analysis buckling load. This definition of the KDF does not match with what is defined for this literature review which states that the KDF can be calculated by means of the experimental result over the theoretical linear buckling load. Unfortunately, the linear buckling load is not provided in the paper and thus the KDF by the definition used in this literature review cannot be computed. The paper also claims that the three hoops lower the sensitivity to imperfections since the KDF is higher for the cylinder that is reinforced. However, the KDFs in comparison were calculated in two different manners, resulting in an unfair comparison. A more fair comparison still leads to the conclusion that the reinforced cylinder is less sensitive to imperfections, but the difference is less significant so it is a strong statement to claim it reduces the sensitivity. It is evident that an imperfection-insensitive design was not achieved.

Hao et al. [27] also concluded that the addition of reinforcing stiffeners lowered the sensitivity to imperfections of cylinders, compared to monolithic equals. The imperfection pattern was based on the eigenmode obtained from the linear buckling analysis. An imperfection-insensitive shell was not achieved.

Hao et al. [28] and Wang et al. [29] both concluded that hierarchical stiffened shells have a lower imperfection sensitivity. Hierarchical stiffened shells are composed of major and minor stiffeners. The downside of this reinforcing strategy is the additional weight of all the stringers and the additional weight of the connection components. In conclusion, it is clear that adding reinforcing components lowers the sensitivity to imperfections, but no imperfection-insensitive design has been achieved yet.

2.4.2. Variable Angle Manufacturing Techniques

Another possible solution to lower the sensitivity to imperfections is to use variable-angle tow (VAT) composites, which are enabled by novel manufacturing techniques able to steer the fibre (or tow) in a curved trajectory, as opposed to the traditional straight paths. This allows for variations of the mechanical properties within one layer, leading to more optimised designs [30], reducing the occurrence of instabilities, and designs that are less sensitive to imperfections. The following manufacturing techniques allow for VAT composites; automated fibre placement (AFP), continuous tow-shearing (CTS), tailored fibre placement (TFP), and variable angle filament winding (VAFW). The first three are presented below, alongside a discussion evaluating whether these manufacturing processes could enable imperfection-insensitive cylinders, according to the available literature. VAFW is not discussed since Wang et al. [31] concluded that VAFW does not allow for designs with lower sensitivity to imperfections compared to the constant angle cylinders.

Automated Fibre Placement is a manufacturing technique that was developed in the 1980s and made commercial at the end of the decade. It was unique during development in the fact that the tape was cut into individual tows, leading to the possibility of more complex designs, such as double-curved surfaces. A schematic overview of the process is presented in Figure 2.2. Originally AFP was intended for straight fibre paths, but later on, the technique was used to experiment with curved trajectories as well. Unfortunately, there are several limitations related to VAT AFP manufactured structures. The curvilinear paths are achieved by in-plane bending and therefore the minimum radius is limited. Small radii result in fibre wrinkling or even breaking. The minimum radius is around $500mm$ [32]. Moreover, it is not possible to achieve tessellation of the placed tows. The inner radius is smaller compared to the outer radius since the head moves along with the path direction and as a result, there are always tow gaps or tow overlaps [32]. As a consequence, there is an uneven thickness distribution, or tows have to be cut resulting in unfavourable stress concentrations. Despite these disadvantages, AFP has been used to fabricate VA cylinders. Wu et al. [33, 34] concluded that AFP enables designs that lower the sensitivity to imperfections. This reduced sensitivity is based on the fact that the cylinder had locally stiffer regions

and buckling is more likely to happen locally, thus preventing geometric imperfections from triggering the overall buckling of the complete structure. The designed cylinder had a KDF equal to 0.96. Therefore, it can be concluded that AFP enables designs that can be used to lower the sensitivity to defects of cylinders, and Wu even manufactured a cylinder that was imperfection insensitive. Nonetheless, research into designing an imperfection-sensitive shell utilizing AFP should be continued since Wu's imperfection-insensitive cylinder is a single case, and the conclusions of this research could establish new design guidelines for cylinders.

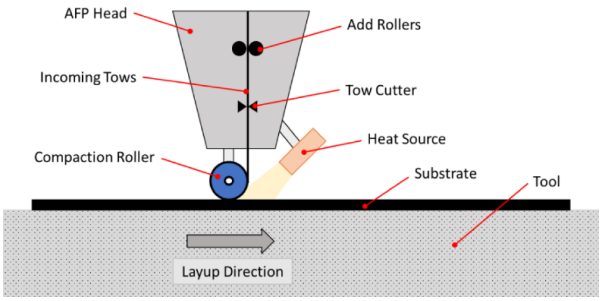

Figure 2.2: Simplified overview of automated fibre placement [35].

Continuous Tow-Shearing is an alternative fibre placement manufacturing technique that was developed to eliminate the fibre buckling and wrinkling that occurred due to the in-plane bending verified in fibre-steered parts manufactured by AFP. The first CTS prototypes were developed in 2012 [32] and therefore it is a fairly recent manufacturing technique. The shearing is achieved by keeping the steering head parallel to the shifting direction. The main advantage of CTS is that the minimum shearing radius is significantly smaller when compared to AFP, which allows for more complex designs. The smaller radius is attained because the steering head remains stationary, as opposed to the rotating head utilised in the AFP technique. The minimum radius for CTS is typically equal to around $50mm$, whereas the typical radius of curvature for AFP is $500mm$, so a significant decrease. Moreover, due to shearing there no longer is a need for tow gaps or tow overlaps. All the tows are shifted in the same direction due to the constant direction of the head and therefore they can follow the towpath exactly, as shown in Figure 2.3.

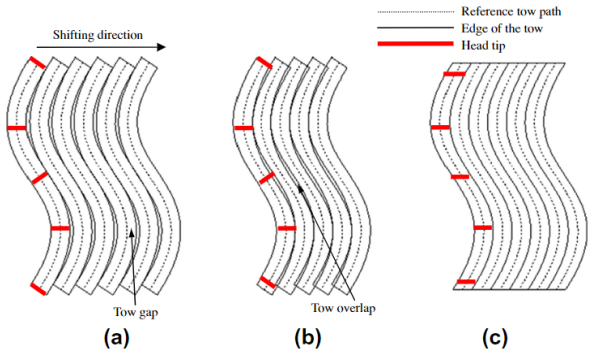

Figure 2.3: *"Difference of the tow arrangement and head rotation: (a) conventional AFP (tow gap), (b) conventional AFP (tow overlap), and (c) CTS"*[32].

One of the results of this novel manufacturing technique is the coupling between the thickness of the tow and the shearing angle, which enables embedded stringers and hoops [36, 37]. This relationship is also presented in Equation 2.5, where t is the thickness of the tow after shearing, t_0 is the original tow thickness, and θ is the angle at which the tow is sheared.

$$t = \frac{t_0}{\cos(\theta)} \tag{2.5}$$

The main disadvantage of the CTS technique is that it is not as developed as AFP, with the hardware being significantly more expensive. Moreover, at the moment it is only possible to shear tows that are

not angled yet, so the initial shearing angle, T_0 has to be equal to zero. If one wants to shear, for example, from 30 to 50 degrees, one would have to shear from 0 to 50 and remove the 0 to 20 region, as shown in Figure 2.4. This limitation has to be taken into account during the realization of the design to create a structure that can be manufactured.

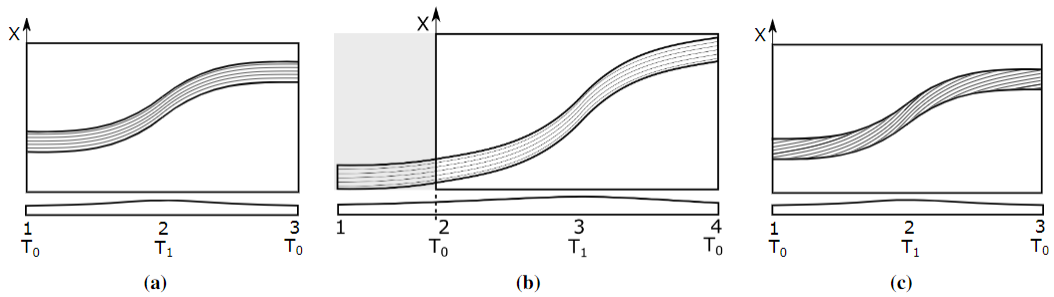

Figure 2.4: *" Differentiation between current and idealistic manufacturing methods where: (a) is a $90\langle 0|50\rangle^1$ laminate for both methods, (b) is a $90\langle 30|50\rangle^1$ laminate for the current manufacturing method and (c) is shearing $90\langle 30|50\rangle^1$ for the idealistic manufacturing method."* [38]

CTS shows the potential to create imperfection-insensitive cylinders, due to the embedded stringers and hoops, unfortunately, this has not yet been achieved. Lincoln et al. [39, 38] and Santos et al. [40] have both performed optimisation algorithms on cylinders to achieve an optimal design, and both concluded that this novel manufacturing technique enables cylindrical shell designs with lower sensitivity to imperfections.

Lastly, Tailored Fiber Placement (TFP) is an embroidery-based manufacturing technique. The first papers relating to the procedure date back to 1998, therefore it is not as novel as CTS. The idea behind the technique involves a needle yarn stitching a roving in a zigzag motion onto a base material. The base material can be either a fabric or a non-woven composite. The needle yarn is typically polyester. Standard production techniques, like Resin Transfer Moulding and Vacuum Bag Injection Process, are used to consolidate the final product [41]. The main advantage of this technique is that it is able to achieve an extremely small steering radius equal to about $5mm$ [42]. The technique is limited to two-dimensional surfaces, so in order to create a cylinder, one must join two ends. Almeida. et al [42] performed a study on AFP cylinders and concluded that the TFP procedure enables designs that have reduced sensitivity to imperfections, similar to the other VA manufacturing techniques. However, the imperfection amplitude in this study was extremely small only 5% of the shell thickness. To the best knowledge, this is the only information available that relates the TFP technique to imperfection-sensitive cylinders.

2.5. Conclusion and Research Gaps

It can be concluded that imperfections lower the buckling load of cylindrical shells. Three categories of imperfections can be identified, namely geometric imperfections, pre-buckling deformations and stresses, and lastly boundary conditions and non-uniform loading. Geometric imperfections lower the buckling load the most, but in combination with the other two factors, it explains the large deviations between theory and experiments.

Naturally, researchers have tried to determine methods to accurately predict the buckling load of imperfect cylinders, leading to three main solution groups. First of all, empirical design factors based on experimental data can be used to estimate the imperfect buckling load, however, these factors are conservative and not specifically designed for composite cylinders. Secondly, finite element software can be used to predict the buckling load of imperfect structures. Geometric imperfections can be modelled by translating the nodes to the desired imperfection shape or by assuming the imperfection initiates as a dimple. The drawback of including imperfections in finite element software is that they rely on non-linear analysis to accurately solve the problem making them computationally expensive and not suitable for repeated processes such as optimisation techniques. Lastly, a less computationally expensive modelling technique is Koiter's Asymptotic Expansion. This methodology predicts the initial post-buckling behaviour only in the neighbourhood of a known state and relies on a linear expansion,

thus reducing the complexity of the problem. Challenges arise when the Koiter methodology is implemented within Finite Elements Simulations. To overcome these problems, the displacement-based methodology proposed by Castro and Jansen [22] can be used. There is a close correspondence between the theory and the implementation minimizing the room for mistakes. Thus, far no imperfections have been included in this displacement-based methodology and it is always assumed that the pre-buckling is linear thereby simplifying the problem.

In addition to exploring methods for predicting the buckling load, researchers have attempted to minimize the impact of imperfections. Two approaches to reduce the sensitivity to imperfections can be identified. The first method involves adding reinforcing elements such as stringers and hoops into the designs. Secondly, variable angle manufacturing techniques can be used to create stronger designs. Lincoln et al. [38] concluded that a CTS-manufactured cylinder had a constant KDF for an increasing amplitude load. Santos and Castro [40] also concluded that CTS enables cylinders with lower sensitivity to imperfections. The VA technique creates embedded stringers and hoops due to the coupling between the shearing angle and the thickness making it more weight efficient than adding reinforcing components. Moreover, this novel manufacturing technique allows for more complex shapes compared to AFP since the minimum allowed steering radius is smaller and there is no need for tow gaps or overlaps. TFP can achieve an even smaller steering radius and achieved surprisingly high KDFs, however, the KDFs in the available literature were calculated with extremely small imperfections. It is unsure if this technique lowers the sensitivity for the increased amplitudes of imperfections as well. Lastly, the literature related to the VAFW manufacturing technique did not suggest that it enables designs with lower sensitivity to defects.

Lastly, it is important to point out that currently there is no generally accepted definition for imperfection insensitivity. To address this issue and allow for quantitative comparison between different studies, a definition for imperfection insensitivity was created and used within this literature review. This definition is based on the fact that it is common to present the KDFs in research papers focused on imperfect cylinders. An imperfection-insensitive shell is one where the knockdown factor (KDF) is equal to 0.95 or higher for imperfection amplitudes ranging from -4 to 4 times the shell thickness. The knockdown factor is defined as the non-linear predicted buckling load of the imperfect shell over the linear buckling load based on an eigenvalue analysis of the perfect shell. An alternative approach could be to formulate a definition centred on the initial post-buckling parameters derived from Koiter's Asymptotic analysis. These parameters serve as a direct measure of imperfection sensitivity and are a good alternative for the proposed definition.

3

Research Definition

3.1. Research Objective

In the literature review three research aspects are addressed concerning imperfection-insensitive shells, namely the formulation of the buckling load and initial post-buckling characteristics, secondly minimizing the impact of imperfections by means of reinforcing elements or VA manufacturing techniques and lastly, the lack of existence of a general definition for an imperfection-insensitive shell. This thesis focuses on the formulation of the initial post-buckling characteristics, rather than minimizing the impact of imperfections. By prioritising the formulation, a more efficient methodology can be created to predict the post-buckling characteristics of imperfect structures, which in turn can also be used as a tool to find new or improved solutions to reduce the effect of imperfections. Whilst it is also important that a definition for an imperfection-insensitive shell is established, the impact of creating this definition was not deemed large enough and therefore this was not explored further for this research.

Based on the findings from the literature review, it is evident that imperfections have not been integrated into the displacement-based Koiter methodology. Therefore, the research objective of this thesis is defined as follows.

Research Objective

Incorporate imperfections within the displacement-based Koiter methodology, aiming to develop an easily implementable and computationally efficient approach.

This novel approach should be suitable for recurring processes like optimisation algorithms and sensitivity studies. It could be used as a tool in the creation of design guidelines for imperfection-insensitive cylinders. However, this thesis focuses on the methodology itself, thus exploring its applications is beyond the scope of the research.

Koiter's asymptotic analysis is not novel and there are examples of it being used in combination with Finite element simulations [19, 43, 44]. The goal of incorporating imperfections into the displacement-based Koiter methodology is to establish an approach that is easier to implement due to the direct correspondence between the theory and the execution. Moreover, the methodology should be equally or even more computationally efficient else the purpose of using Koiter's analysis is lost.

3.2. Research Scope

Three main steps can be identified for the displacement-based Koiter approach, namely the expansion of the total potential energy functional, the derivation of the functional derivatives, and the asymptotic analysis. Each step is based on certain assumptions and therefore to achieve the goal of including imperfections in the displacement-based Koiter methodology these assumptions can be included or disregarded resulting in several solution possibilities. First of all, there are two possible approaches for expanding the total potential energy: one is based on Pignataro's formulation [45], and the other follows Budiansky's convention [4]. The derivation of the functional derivatives initiates from the strains. One can either assume that the pre-buckling is linear, consequently simplifying the strains, or one can

presume non-linear pre-buckling. These two assumptions lead to four solution possibilities, which are listed below. The first letter indicates which approach to expanding the total potential energy is used, either Pignataro (P) or Budiasnky (B). The last letter denotes if the assumption linear pre-buckling is made (L) or non-linear pre-buckling is presumed (N).

1. PL
2. BL
3. PN
4. BN

The final step is to derive the initial post-buckling characteristics by means of an asymptotic expansion. Two possibilities to define these properties arise, namely a less traditional approach of finding the imperfection post-buckling characteristics a_I and b_I. On the other hand, there is the more traditional approach of introducing two new coefficients known as the imperfection form factors α and β which define how sensitive a structure is to imperfections. Both alternatives for the asymptotic expansion are performed for the four solution opportunities to see which approach is more accurate.

To illustrate the inclusion of imperfections within the displacement-based Koiter approach, it was chosen to include imperfections to a perfect plate for the single mode expansion first. This decision is made due to the fact that the initial post-buckling behaviour of a plate can be approximated with simpler kinematics such as Donnell. Since the inclusion of imperfections within a displacement-based environment has never been attempted, it is expected to make some errors along the way. The methodology will have to be adjusted and this is more easily done for simpler kinematics and choosing single-mode mode over multi-modal. Once the imperfections have been successfully implemented within the displacement-based Koiter methodology for plates, the same approach can be readily applied to more complex applications such as a cylinder, different kinematics, or multi-modal expansion. Therefore, the work presented for this research focuses on the inclusion of imperfection within the displacement-based Koiter methodology for plates based on Donnell Kinematics and only includes the single-mode expansion.

3.3. Hypotheses

Based on the four solution possibilities several hypotheses are established

H1: Hypothesis on the assumption linear pre-buckling

The assumption of linear pre-buckling simplifies the procedure of finding the initial post-buckling coefficients by means of the displacement-based Koiter methodology, but the results are less accurate.

H2: Hypothesis on the derivations of the initial post-buckling properties

- H2.1 Initial imperfect post-buckling coefficients (a_I and b_I) can be derived by means of the displacement-based Koiter methodology.
- H2.2 The initial imperfect post-buckling coefficients (a_I and b_I) are more efficient in predicting the post-buckling behaviour of a structure, compared to the imperfect form factors.

3.4. Research Outline

The work of Castro and Jansen forms the foundation of this thesis, therefore a comprehensive overview of the displacement-based Koiter methodology without imperfections is presented in chapter 4. In this chapter, certain assumptions are made and formulations are derived, which are revisited when imperfections are introduced into the methodology. This dedicated chapter ensures a clear distinction between the prior work and the novel steps taken in this study. Following the explanation of the perfect methodology, the expansion of the total potential including imperfections is presented in chapter 5. This forms the first step in including imperfections in the methodology and includes the two possibilities and the differences between them. Subsequently, chapter 6 outlines the various options for deriving the functional derivatives. Finally, the derivation of the initial post-buckling characteristics for both the traditional and less traditional approach is shown in chapter 7 as well as a conclusion on how accurate they are and if the hypotheses were correct.

4

Displacement-based Koiter Methodology

The displacement-based Koiter methodology [18, 22] aimed to improve the implementation of the Koiter expansion within finite element simulations. Previous attempts of the perturbation methodology within finite element context had led to initial post-buckling coefficients that were mesh sensitive, computationally expensive higher-order derivatives, and phenomena such as locking in the implementation resulting in unrealistic behaviour of structures. Rahman [19] and Tiso [43] were able to overcome these issues resulting in the Koiter methodology being available in the FE Software Diana. The main drawback is that the methodology is convoluted and difficult to interpret. The research of Castro and Jansen creates a strong connection between theory and implementation, facilitating the overall implementation process. The methodology forms the basis of this thesis and therefore an explanation of the necessary steps taken is provided in this chapter. Three key steps can be identified for the displacement-based Koiter methodology. The process begins with the expansion of the total potential energy functional, which is presented section 4.1. Subsequently, the derivation of the functional derivatives used within the expansion of the potential energy is outlined in section 4.2. Finally, the formulation of the initial post-buckling coefficients is addressed in section 4.3.

4.1. Expansion of the Total Potential Energy Functional

The methodology starts with a general-purpose formulation of the potential energy based on the work of Budiansky [4]. The potential energy functional (ϕ) is dependent on both the displacements ($\boldsymbol{u}$) and a scalar load parameter (λ). The variational equation of equilibrium must equal zero as presented in Equation 4.1 where $\boldsymbol{u_0}$ is a known displacement field that is dependent on a scalar parameter λ. The Fréchet Derivative $\phi'\delta\boldsymbol{u}$ is used to show the dependence of the variation on the displacement and to express the tensor product between the derivative and the displacement-field vector ($\delta\boldsymbol{u}$). The first differentiation is multiplied by one displacement vector but the second differentiation is multiplied by two displacement vectors and this logic continues for the higher order derivatives, as shown in Equation 4.2.

$$\phi'[\boldsymbol{u_0}(\lambda), \lambda]\delta\boldsymbol{u} = 0 \tag{4.1}$$

$$\begin{aligned}
\delta\phi &= \phi'\delta\boldsymbol{u} \\
\delta^2\phi &= \phi''\delta\boldsymbol{u}\delta\boldsymbol{u} \\
\delta^3\phi &= \phi'''\delta\boldsymbol{u}\delta\boldsymbol{u}\delta\boldsymbol{u} \\
\delta^4\phi &= \phi^{iv}\delta\boldsymbol{u}\delta\boldsymbol{u}\delta\boldsymbol{u}\delta\boldsymbol{u}
\end{aligned} \tag{4.2}$$

It is assumed that the bifurcation point lies on the equilibrium path such that $\boldsymbol{u_c} = \boldsymbol{u_0}(\lambda_c)$ and therefore the static equilibrium at the bifurcation point is equal to Equation 4.3.

$$\phi'[\boldsymbol{u_c}, \lambda_c]\delta\boldsymbol{u} = 0 \tag{4.3}$$

Next, a Taylor expansion around the known bifurcation point ($\boldsymbol{u_c}$) is performed utilising the displacement perturbation $\boldsymbol{v}$, equivalent to Equation 4.4. The Taylor expansion is shown in Equation 4.5, where ($'$) represents the Frechét differentiation with respect to the displacement.

$$\boldsymbol{v} = \boldsymbol{u}(\lambda) - \boldsymbol{u_c} \tag{4.4}$$

$$\phi' \left[\boldsymbol{u_c}, \lambda_c\right] \delta\boldsymbol{u} = \phi'_c \delta\boldsymbol{u} + \phi''_c \boldsymbol{v}\delta\boldsymbol{u} + \frac{1}{2}\phi'''_c \boldsymbol{v}^2 \delta u + \frac{1}{6}\phi^{iv}_c \boldsymbol{v}^3 \delta\boldsymbol{u} + \cdots = 0 \tag{4.5}$$

Finally, a second Taylor expansion is conducted around the critical load factor (λ_c), where ($\dot{}$) represents the Frechét differentiation with respect to the load factor.

$$\begin{aligned}
\phi'[\boldsymbol{u_c}, \lambda_c]\delta\boldsymbol{u} = &\left(\phi''_c + \dot{\phi}''_c \left(\lambda - \lambda_c\right) + \frac{1}{2}\ddot{\phi}''_c \left(\lambda - \lambda_c\right)^2 + \cdots\right) \boldsymbol{v}\delta\boldsymbol{u} \\
&+ \frac{1}{2}\left(\phi'''_c + \dot{\phi}'''_c \left(\lambda - \lambda_c\right) + \frac{1}{2}\ddot{\phi}'''_c \left(\lambda - \lambda_c\right)^2 + \cdots\right) \boldsymbol{v}^2\delta\boldsymbol{u} \\
&+ \frac{1}{6}\left(\phi^{iv}_c + \dot{\phi}^{iv}_c \left(\lambda - \lambda_c\right) + \frac{1}{2}\ddot{\phi}^{iv}_c \left(\lambda - \lambda_c\right)^2 + \cdots\right) \boldsymbol{v}^3\delta\boldsymbol{u} + \cdots = 0
\end{aligned} \tag{4.6}$$

4.2. Functional Derivatives utilising Frechét Derivatives

The subsequent step involves finding the functional derivatives (ϕ^n_c, $\dot{\phi}^n_c$, and $\ddot{\phi}^n_c$) that appear in the expanded potential energy. These functional derivatives are based on stresses, which in turn depend on the strains, therefore all three aspects are elaborated on in subsection 4.2.1 to 4.2.3.

4.2.1. Strains

Kinematic relations are used to find the strains and their derivatives with respect to the displacements and load factor. Depending on which kinematic relationship is chosen the complexity of the problem can be increased to include more non-linear terms. For example, the Donnell kinematics ignore various non-linear terms and are sufficient to accurately represent the initial post-buckling behaviour of a plate. However, the Donnell relationship is not accurate enough to accurately compute the post-buckling coefficients of axially compressed cylinders and therefore the Sanders Kinematics are preferred [22]. As mentioned in the scope of this thesis, the Donnell kinematics are used to demonstrate the inclusion of imperfections within the displacement-based Koiter methodology, but the same line of reasoning can be applied to different structures and kinematic relations. The three-dimensional strains can be expressed as $\boldsymbol{\varepsilon}(x, y, z) = \boldsymbol{\varepsilon}(x, y) + z\boldsymbol{\kappa}(x, y)$ and the extensional and rotational strains for a plate are presented in Equation 4.7 and 4.8.

$$\boldsymbol{\varepsilon} = \left\{ \begin{array}{c} \varepsilon_{xx} \\ \varepsilon_{yy} \\ \gamma_{xy} \end{array} \right\} = \left\{ \begin{array}{c} u_{,x} + \frac{1}{2}\left(w_{,x}\right)^2 \\ v_{,y} + \frac{1}{2}\left(w_{,y}\right)^2 \\ u_{,y} + v_{,x} + w_{,x}w_{,y} \end{array} \right\} \tag{4.7}$$

$$\boldsymbol{\kappa} = \left\{ \begin{array}{c} \kappa_{xx} \\ \kappa_{yy} \\ \kappa_{xy} \end{array} \right\} = \left\{ \begin{array}{c} -w_{,xx} \\ -w_{,yy} \\ -2w_{,xy} \end{array} \right\} \tag{4.8}$$

The displacement field can be approximated using the known shape functions $\boldsymbol{S}^{u,v,w}$ as shown down below.

$$\begin{aligned}
u, v, w^\top &= \boldsymbol{S}^u \boldsymbol{u} \\
\boldsymbol{S}^u &= \left[\begin{array}{c} \boldsymbol{S}^u \\ \boldsymbol{S}^v \\ \boldsymbol{S}^w \end{array} \right]
\end{aligned} \tag{4.9}$$

The displacement in each direction u, v, w can also be represented by using the summation convention for repeated indices as shown in Equation 4.10.

$$\begin{aligned} u &= S_a^u u_a \\ v &= S_a^v u_a \\ w &= S_a^w u_a \end{aligned} \tag{4.10}$$

The Frechét notation is still applicable to the strains and is equal to the notation presented in Equation 4.2. Simplifying the strains to $\varepsilon_1 = \varepsilon_{xx}$, $\varepsilon_2 = \varepsilon_{yy}$, $\varepsilon_3 = \gamma_{xy}$, $\kappa_1 = \kappa_{xx}$, $\kappa_2 = \kappa_{yy}$, and $\kappa_3 = \kappa_{xy}$ the repeated index notation can be utilised, resulting in the first and second differentiation of the strain to follow the notation presented in Equation 4.11.

$$\begin{aligned} \delta\varepsilon_i &= \varepsilon'_{ia}\delta u_a \\ \delta\kappa_i &= \kappa'_{ia}\delta u_a \\ \delta\left(\delta\varepsilon_i\right) &= \varepsilon''_{iab}\delta u_a \delta u_b \\ \delta\left(\delta\kappa_i\right) &= \kappa''_{iab}\delta u_a \delta u_b \end{aligned} \tag{4.11}$$

Following these notations, the first Frechét differentiation with respect to the displacement is shown in Equation 4.12 and 4.13

$$\boldsymbol{\varepsilon}'_a = \left\{ \begin{array}{c} S^u_{a,x} + S^w_{a,x} w_{,x} \\ S^v_{a,y} + S^w_{a,y} w_{,y} \\ S^u_{a,y} + S^v_{a,y} + S^w_{a,x} w_{,y} + S^w_{a,y} w_{,x} \end{array} \right\} \tag{4.12}$$

$$\boldsymbol{\kappa}'_a = \left\{ \begin{array}{c} -S^w_{a,xx} \\ -S^w_{a,yy} \\ -2S^w_{a,xy} \end{array} \right\} \tag{4.13}$$

The second differentiation with respect to the displacement is represented by Equation 4.14 and 4.15.

$$\boldsymbol{\varepsilon}''_{ab} = \left\{ \begin{array}{c} S^w_{a,x} S^w_{b,x} \\ S^w_{a,y} S^w_{b,y} \\ S^w_{a,x} S^w_{b,y} + S^w_{a,y} S^w_{b,x} \end{array} \right\} \tag{4.14}$$

$$\boldsymbol{\kappa}''_{ab} = \mathbf{0} \tag{4.15}$$

The differentiation with respect to the load factor (λ) can be found by keeping in mind that $\boldsymbol{u} = \lambda \boldsymbol{u_0}$, and therefore the first differentiation equals Equation 4.16 and 4.17.

$$\dot{\boldsymbol{\varepsilon}} = \left\{ \begin{array}{c} u_{0,x} + \lambda w^2_{0,x} \\ v_{0,y} + \lambda w^2_{0,y} \\ u_{0,y} + v_{0,x} + 2\lambda w_{0,x} w_{0,y} \end{array} \right\} \tag{4.16}$$

$$\dot{\boldsymbol{\kappa}} = \left\{ \begin{array}{c} -w_{0,xx} \\ -w_{0,yy} \\ -2w_{0,xy} \end{array} \right\} \tag{4.17}$$

The second differentiation with respect to the load factor results in Equation 4.18 and 4.19.

$$\ddot{\boldsymbol{\varepsilon}} = \begin{Bmatrix} w_{0,x}^2 \\ w_{0,y}^2 \\ 2w_{0,x}w_{0,y} \end{Bmatrix} \tag{4.18}$$

$$\ddot{\boldsymbol{\kappa}} = \mathbf{0} \tag{4.19}$$

Now moving on to the differentiation with respect to both the displacement and load factor:

$$\dot{\boldsymbol{\varepsilon}}'_{\boldsymbol{a}} = \begin{Bmatrix} w_{0,x}S_{a,x}^w \\ w_{0,y}S_{a,y}^w \\ w_{0,x}S_{a,y}^w + w_{0,y}S_{a,x}^w \end{Bmatrix} \tag{4.20}$$

$$\dot{\boldsymbol{\kappa}}'_{\boldsymbol{a}} = \mathbf{0} \tag{4.21}$$

Since $\dot{\boldsymbol{\varepsilon}}'_{\boldsymbol{a}}$ and $\dot{\boldsymbol{\kappa}}'_{\boldsymbol{a}}$ are not a function of the load parameter λ, $\ddot{\boldsymbol{\varepsilon}}'_a$ and $\ddot{\boldsymbol{\kappa}}'_a$ are both equal to a zero vector, as well as λ, $\dot{\boldsymbol{\varepsilon}}''_a$ and $\dot{\boldsymbol{\kappa}}''_a$. This concludes all the derivatives of the strain.

4.2.2. Stresses

The stresses can be easily computed from the strains, by making use of the classical constitutive relations for laminate composites. The stresses are simplified to the following notation $N_1 = N_{xx}$, $N_2 = N_{yy}$, $N_3 = N_{xy}$, $M_1 = M_{xx}$, $M_2 = M_{yy}$, and $M_3 = M_{xy}$ and as a result the stress-strain relation can be represented by the repeated index notation, as shown in Equation 4.22 where A_{ij} is equal to the membrane stiffness, B_{ij} represents the membrane-bending coupling, and D_{ij} is the bending stiffness.

$$\begin{aligned} N_i &= A_{ij}\varepsilon_j + B_{ij}\kappa_j \\ M_i &= B_{ij}\varepsilon_j + D_{ij}\kappa_j \end{aligned} \tag{4.22}$$

Now all the differentiations of the stress can be found and these are presented below.

$$\begin{aligned} N'_{ia} &= A_{ij}\varepsilon'_{ja} + B_{ij}\kappa'_{ja} \\ M'_{ia} &= B_{ij}\varepsilon'_{ja} + D_{ij}\kappa'_{ja} \end{aligned} \tag{4.23}$$

$$\begin{aligned} N''_{iab} &= A_{ij}\varepsilon''_{jab} \\ M''_{iab} &= B_{ij}\varepsilon''_{jab} \end{aligned} \tag{4.24}$$

$$\begin{aligned} \dot{N}_i &= A_{ij}\dot{\varepsilon}_j + B_{ij}\dot{\kappa}_j \\ \dot{M}_i &= B_{ij}\dot{\varepsilon}_j + D_{ij}\dot{\kappa}_j \end{aligned} \tag{4.25}$$

$$\begin{aligned} \ddot{N}_i &= A_{ij}\ddot{\epsilon}_j \\ \ddot{M}_i &= B_{ij}\ddot{\epsilon}_j \end{aligned} \tag{4.26}$$

$$\begin{aligned} \dot{N}'_{ia} &= A_{ij}\dot{\varepsilon}'_{ja} \\ \dot{M}'_{ia} &= B_{ij}\dot{\varepsilon}'_{ja} \end{aligned} \tag{4.27}$$

4.2.3. Functional Derivatives

The final step is to combine the stresses with the strains and find the functional derivatives. A reminder that the methodology of the displacement-based Koiter analysis is demonstrated here using a plate, but the same logic can be applied to any structure. The total potential energy of a plate is equal to Equation 4.28, where the assumption is made that a general distributed loading $\hat{\boldsymbol{N}}$ vector is applied to the boundaries of a plate and where $\delta\Omega = dxdy$.

$$\phi = \frac{1}{2}\int_{\Omega} \left(N_i\varepsilon_i + M_i\kappa_i\right) d\Omega - \int_{\delta\Omega} \lambda\hat{\boldsymbol{N}}^{\top}\boldsymbol{u}d(\delta\Omega) \tag{4.28}$$

The stationary total potential energy (ϕ') is defined at the bifurcation point $[\boldsymbol{u_c}, \lambda_c]$ is presented in Equation 4.29.

$$\phi_c' \delta \boldsymbol{u} = \frac{1}{2} \int_\Omega \left(\delta N_i \varepsilon_i + N_i \delta \varepsilon_i + \delta M_i \kappa_i + M_i \delta \kappa_i \right) d\Omega - \int_{\delta\Omega} \lambda \hat{\boldsymbol{N}}^\top \delta \boldsymbol{u} d(\delta\Omega) \tag{4.29}$$

The variation $\delta \boldsymbol{u}$ is assumed to be $\delta \boldsymbol{u} = \boldsymbol{u_a} = \{\cdots, u_a, \cdots\}^T$, such that the first Frechét derivative with respect to the displacement of the total potential energy is equal to Equation 4.30.

$$\phi_c' \boldsymbol{u_a} = \left[\frac{1}{2} \int_\Omega \left(N_{ia}' \varepsilon_i + N_i \varepsilon_{ia}' + M_{ia}' \kappa_i + M_i \kappa_{ia}' \right) d\Omega - \int_{\delta\Omega} \lambda \widehat{\boldsymbol{N}}^\top S^u_{ax=\ell_x} d(\delta\Omega) \right] u_a \tag{4.30}$$

The second Frechét derivative is equal to Equation 4.31

$$\begin{aligned} \phi_c'' \boldsymbol{u_a u_b} = \Bigg[\frac{1}{2} \int_\Omega \Big(& N_{iab}'' \varepsilon_i + N_{ia}' \varepsilon_{ib}' + N_{ib}' \varepsilon_{ia}' + N_i \varepsilon_{iab}'' + M_{iab}'' \kappa_i + M_{ia}' \kappa_{ib}' + M_{ib}' \kappa_{ia}' \\ & + M_i \cancelto{0}{\kappa_{iab}''} \Big) d\Omega \Bigg] u_a u_b \\ = \Bigg[\frac{1}{2} \int_\Omega \Big(& N_{iab}'' \varepsilon_i + N_{ia}' \varepsilon_{ib}' + N_{ib}' \varepsilon_{ia}' + N_i \varepsilon_{iab}'' + M_{iab}'' \kappa_i + M_{ia}' \kappa_{ib}' + M_{ib}' \kappa_{ia}' \Big) d\Omega \Bigg] u_a u_b \end{aligned} \tag{4.31}$$

The third derivative is presented in Equation 4.32

$$\begin{aligned} \phi_c''' \boldsymbol{u_a u_b u_c} = \Bigg[\frac{1}{2} \int_\Omega \Big(& \cancelto{0}{N_{iabc}'''} \varepsilon_i + N_{iab}'' \varepsilon_{ic}' + N_{iac}'' \varepsilon_{ib}' + N_{ia}' \varepsilon_{ibc}'' + N_{ibc}'' \varepsilon_{ia}' + N_{ib}' \varepsilon_{iac}'' \\ & + N_{ic}' \varepsilon_{iab}'' + N_i \cancelto{0}{\varepsilon_{iabc}'''} + \cancelto{0}{M_{iabc}'''} \kappa_i + M_{iab}'' \kappa_{ic}' + M_{iac}'' \kappa_{ib}' + M_{ia}' \cancelto{0}{\kappa_{ibc}''} \\ & + M_{ibc}'' \kappa_{ia}' + M_{ib}' \cancelto{0}{\kappa_{iac}''} \Big) d\Omega \Bigg] u_a u_b u_c \\ = \Bigg[\frac{1}{2} \int_\Omega \Big(& N_{iab}'' \varepsilon_{ic}' + N_{iac}'' \varepsilon_{ib}' + N_{ia}' \varepsilon_{ibc}'' + N_{ibc}'' \varepsilon_{ia}' + N_{ib}' \varepsilon_{iac}'' \\ & + N_{ic}' \varepsilon_{iab}'' + M_{iab}'' \kappa_{ic}' + M_{iac}'' \kappa_{ib}' + M_{ibc}'' \kappa_{ia}' \Big) d\Omega \Bigg] u_a u_b u_c \end{aligned} \tag{4.32}$$

Finally, the fourth derivative is shown in Equation 4.33

$$\begin{aligned} \phi_c^{iv} \boldsymbol{u_a u_b u_c u_d} = \Bigg[\frac{1}{2} \int_\Omega \Big(& \cancelto{0}{N_{iabd}'''} \varepsilon_{ic}' + N_{iab}'' \varepsilon_{icd}'' + \cancelto{0}{N_{iacd}'''} \varepsilon_{ib}' + N_{iac}'' \varepsilon_{ibd}'' + N_{iad}'' \varepsilon_{ibc}'' + N_{ia}' \cancelto{0}{\varepsilon_{ibcd}'''} \\ & + \cancelto{0}{N_{ibcd}'''} \varepsilon_{ia}' + N_{ibc}'' \varepsilon_{iad}'' + N_{ibd}'' \varepsilon_{iac}'' + N_{ib}' \cancelto{0}{\varepsilon_{iacd}'''} + N_{icd}'' \varepsilon_{iab}'' + N_{ic}' \cancelto{0}{\varepsilon_{iabd}'''} \\ & + \cancelto{0}{M_{iabd}'''} \kappa_{ic}' + M_{iab}'' \cancelto{0}{\kappa_{icd}''} + \cancelto{0}{M_{iacd}'''} \kappa_{ib}' + M_{iac}'' \cancelto{0}{\kappa_{ibd}''} + \cancelto{0}{M_{ibcd}'''} \kappa_{ia}' + M_{ibc}'' \cancelto{0}{\kappa_{iad}''} \Big) d\Omega \Bigg] u_a u_b u_c u_d \\ = \Bigg[\frac{1}{2} \int_\Omega \Big(& N_{iab}'' \varepsilon_{icd}'' + N_{iac}'' \varepsilon_{ibd}'' + N_{iad}'' \varepsilon_{ibc}'' + N_{ibc}'' \varepsilon_{iad}'' + N_{ibd}'' \varepsilon_{iac}'' + N_{icd}'' \varepsilon_{iab}'' \Big) d\Omega \Bigg] u_a u_b u_c u_d \end{aligned} \tag{4.33}$$

From Equation 4.31 the first and second derivatives with respect to the load factor (λ) can be found, represented respectively in Equation 4.34 and 4.35.

$$
\begin{aligned}
\dot{\phi}_c'' \boldsymbol{u_a u_b} = &\left[\frac{1}{2}\int_\Omega \Big(\cancelto{0}{\dot{N}_{iab}''\varepsilon_i} + N_{iab}''\dot{\varepsilon}_i + \dot{N}_{ia}'\varepsilon_{ib}' + N_{ia}'\dot{\varepsilon}_{ib}' + \dot{N}_{ib}'\varepsilon_{ia}' + N_{ib}'\dot{\varepsilon}_{ia}' + \dot{N}_i\varepsilon_{iab}'' + N_i\cancelto{0}{\dot{\varepsilon}_{iab}''} \right. \\
&\left. + \cancelto{0}{\dot{M}_{iab}''\kappa_i} + M_{iab}''\dot{\kappa}_i + \dot{M}_{ia}'\kappa_{ib}' + M_{ia}'\cancelto{0}{\dot{\kappa}_{ib}'} + \dot{M}_{ib}'\kappa_{ia}' + M_{ib}'\cancelto{0}{\dot{\kappa}_{ia}'} \Big) d\Omega \right] u_a u_b \\
= &\left[\frac{1}{2}\int_\Omega \Big(N_{iab}''\dot{\varepsilon}_i + \dot{N}_{ia}'\varepsilon_{ib}' + N_{ia}'\dot{\varepsilon}_{ib}' + \dot{N}_{ib}'\varepsilon_{ia}' + N_{ib}'\dot{\varepsilon}_{ia}' + \dot{N}_i\varepsilon_{iab}'' \right. \\
&\left. + M_{iab}''\dot{\kappa}_i + \dot{M}_{ia}'\kappa_{ib}' + \dot{M}_{ib}'\kappa_{ia}' \Big) d\Omega \right] u_a u_b
\end{aligned}
\tag{4.34}
$$

$$
\begin{aligned}
\ddot{\phi}_c'' \boldsymbol{u_a u_b} = &\left[\frac{1}{2}\int_\Omega \Big(\cancelto{0}{\ddot{N}_{iab}''\varepsilon_i} + \dot{N}_{iab}''\dot{\varepsilon}_i + \cancelto{0}{\ddot{N}_{ia}'\varepsilon_{ib}'} + \dot{N}_{ia}'\dot{\varepsilon}_{ib}' + \dot{N}_{ia}'\dot{\varepsilon}_{ib}' + N_{ia}'\cancelto{0}{\ddot{\varepsilon}_{ib}'} + \cancelto{0}{\ddot{N}_{ib}'\varepsilon_{ia}'} + \dot{N}_{ib}'\dot{\varepsilon}_{ia}' \right. \\
&+ \dot{N}_{ib}'\dot{\varepsilon}_{ia}' + N_{ib}'\cancelto{0}{\ddot{\varepsilon}_{ia}'} + \ddot{N}_i\varepsilon_{iab}'' + \dot{N}_i\cancelto{0}{\dot{\varepsilon}_{iab}''} + \cancelto{0}{\dot{M}_{iab}''\dot{\kappa}_i} + M_{iab}''\cancelto{0}{\ddot{\kappa}_i} + \cancelto{0}{\ddot{M}_{ia}'\kappa_{ib}'} + \dot{M}_{ia}'\cancelto{0}{\dot{\kappa}_{ib}'} \\
&\left. + \cancelto{0}{\ddot{M}_{ib}'\kappa_{ia}'} + \dot{M}_{ib}'\cancelto{0}{\dot{\kappa}_{ia}'} \Big) d\Omega \right] u_a u_b \\
= &\left[\frac{1}{2}\int_\Omega \Big(N_{iab}''\ddot{\varepsilon}_i + 2\dot{N}_{ia}'\dot{\varepsilon}_{ib}' + 2\dot{N}_{ib}'\dot{\varepsilon}_{ia}' + \ddot{N}_i\varepsilon_{iab}'' \Big) d\Omega \right] u_a u_b
\end{aligned}
\tag{4.35}
$$

Lastly, from Equation 4.32 the derivative with respect to λ is concluded, as shown in Equation 4.36.

$$
\begin{aligned}
\dot{\phi}_c''' \boldsymbol{u_a u_b u_c} = &\left[\frac{1}{2}\int_\Omega \Big(\cancelto{0}{\dot{N}_{iab}''\varepsilon_{ic}'} + N_{iab}''\dot{\varepsilon}_{ic}' + \cancelto{0}{\dot{N}_{iac}''\varepsilon_{ib}'} + N_{iac}''\dot{\varepsilon}_{ib}' + \dot{N}_{ia}'\varepsilon_{ibc}'' + N_{ia}'\cancelto{0}{\dot{\varepsilon}_{ibc}''} + \cancelto{0}{\dot{N}_{ibc}''\varepsilon_{ia}'} \right. \\
&+ N_{ibc}''\dot{\varepsilon}_{ia}' + \dot{N}_{ib}'\varepsilon_{iac}'' + N_{ib}'\cancelto{0}{\dot{\varepsilon}_{iac}''} + \dot{N}_{ic}'\varepsilon_{iab}'' + N_{ic}'\cancelto{0}{\dot{\varepsilon}_{iab}''} + \cancelto{0}{\dot{M}_{iab}''\kappa_{ic}'} + M_{iab}''\cancelto{0}{\dot{\kappa}_{ic}'} \\
&\left. + \cancelto{0}{\dot{M}_{iac}''\kappa_{ib}'} + M_{iac}''\cancelto{0}{\dot{\kappa}_{ib}'} + \cancelto{0}{\dot{M}_{ibc}''\kappa_{ia}'} + M_{ibc}''\cancelto{0}{\dot{\kappa}_{ia}'} \Big) d\Omega \right] u_a u_b u_c \\
= &\left[\frac{1}{2}\int_\Omega \Big(N_{iab}''\dot{\varepsilon}_{ic}' + N_{iac}''\dot{\varepsilon}_{ib}' + \dot{N}_{ia}'\varepsilon_{ibc}'' + N_{ibc}''\dot{\varepsilon}_{ia}' + \dot{N}_{ib}'\varepsilon_{iac}'' + \dot{N}_{ic}'\varepsilon_{iab}'' \Big) d\Omega \right] u_a u_b u_c
\end{aligned}
\tag{4.36}
$$

The high order terms $\ddot{\phi}'''$, $\dot{\phi}^{iv}$, $\ddot{\phi}^{iv}$ equal zero. This concludes the derivation of the functional derivatives. The present derivation serves as an illustration of how to compute the functional derivative utilising the Donell kinematics for a plate. However, the same reasoning can be applied to a different structure such as a cylinder or alternative kinematics relation, like Sanders.

4.3. Asymptotic Analysis

The single mode asymptotic expansions for the load parameter and the displacement field are presented in Equation 4.37 and 4.38, respectively, where λ represents the load parameter, λ_c is the known critical load (typically the bifurcation load), ξ is a scalar parameter, and a_I and b_I are the Koiter factors. Moreover, $\boldsymbol{u_I}$ is the first-order displacement field which is either a single buckling mode or a combination of multiple buckling modes scaled with respect to the thickness of the plate, $\boldsymbol{u_{II}}$ represents the second-order displacement field and is a correction to the first-order field, and lastly, $\boldsymbol{u_{III}}$ is the third-field order field but this is usually ignored.

$$
\lambda - \lambda_c = a_I \lambda_c \xi + b_I \lambda_c \xi^2 \tag{4.37}
$$

$$\boldsymbol{u} - \boldsymbol{u_c} = \boldsymbol{v} = \xi \boldsymbol{u_I} + \xi^2 \boldsymbol{u_{II}} + \xi^3 \boldsymbol{u_{III}} \tag{4.38}$$

By substituting the asymptotic expansions into the potential energy function expansion, the initial post-buckling coefficients can be determined. Replacing Equation 4.37 and 4.38 into Equation 4.6, and disregarding terms multiplied with $\boldsymbol{u_{III}}$, leads to Equation 4.39 where the terms are grouped according to ξ^2, ξ^3 and higher order terms are left out.

$$\begin{aligned} &\xi^2 \Big(\frac{1}{2}\boldsymbol{u_I}^2 \phi_c''' + \boldsymbol{u_{II}} \phi_c'' + a_I \lambda_c \boldsymbol{u_I} \dot{\phi}_c'' \Big) \delta\boldsymbol{u} + \\ &\xi^3 \left(\frac{1}{6}\boldsymbol{u_I}^3 \phi_c^{iv} + a_I \lambda_c \boldsymbol{u_{II}} \dot{\phi}_c'' + \frac{1}{2} a_I \lambda_c \boldsymbol{u_I}^2 \dot{\phi}_c''' + \frac{1}{2} a_I^2 \lambda_c^2 \boldsymbol{u_I} \ddot{\phi}_c'' + \boldsymbol{u_I u_{II}} \phi_c''' + b_I \lambda_c \boldsymbol{u_I} \dot{\phi}_c'' \right) \delta\boldsymbol{u} \\ &+ \cdots = 0 \end{aligned} \tag{4.39}$$

The terms multiplied with ξ^2 and ξ^3 must both equal zero to satisfy the equilibrium condition. The assumption $\delta\boldsymbol{u} = \boldsymbol{u_I}$ can be made, resulting in the orthogonality of the second-order displacement which leads to the simplification that $\dot{\phi}_c'' \boldsymbol{u_I u_{II}} = 0$. Utilising this simplification the expression for a_I and b_I for the single-mode expansion are equal to Equation 4.40 and 4.41

$$a_I = -\frac{1}{2\lambda_c} \frac{\boldsymbol{u_I}^3 \phi_c'''}{\boldsymbol{u_I}^2 \dot{\phi}_c''} \tag{4.40}$$

$$b_I = -\left(\frac{1}{6}\boldsymbol{u_I}^4 \phi_c^{iv} + \frac{1}{2} a_I \lambda_c \boldsymbol{u_I}^3 \dot{\phi}_c''' + \frac{1}{2} a_I^2 \lambda_c^2 \boldsymbol{u_I}^2 \ddot{\phi}_c'' + \boldsymbol{u_I}^2 \boldsymbol{u_{II}} \phi_c''' \right) / \left(\lambda_c \boldsymbol{u_I}^2 \dot{\phi}_c'' \right) \tag{4.41}$$

The second-order displacement field ($\boldsymbol{u_{II}}$) is found by using the terms related to ξ^2 which must hold for all arbitrary variations of $\delta\boldsymbol{u}$ and can be rewritten to find the second-order field.

$$\overline{\boldsymbol{u}}_{\boldsymbol{II}} = [\phi_c'']^{-1} \left(-\frac{1}{2}\phi_c''' \boldsymbol{u_I}^2 - a_I \lambda_c \boldsymbol{u_I} \dot{\phi}_c'' \right) \tag{4.42}$$

Equation 4.42 does allow for multiple solutions, however, to ensure the second-order field is orthogonal to the first-order field the Gram-Schmidt orthogonalization is performed, as presented here. Now a_I and b_I can be computed.

$$\boldsymbol{u_{II}} = \overline{\boldsymbol{u}}_{\boldsymbol{II}} - \boldsymbol{u_I} \frac{\langle \overline{\boldsymbol{u}}_{\boldsymbol{II}}, \boldsymbol{u_I} \rangle}{\langle \boldsymbol{u_I}, \boldsymbol{u_I} \rangle} \tag{4.43}$$

It is important to highlight that the expressions for a_I and b_I are general and do not rely on any assumption made about the structure. These coefficients can be derived directly from the expansion of the total potential energy, which is also not specific to any structure. Moreover, it should be pointed out that all the proceeding steps apply to any energy-based methodology. Castro and Jansen developed the methodology to ease the implementation within finite element simulations and this implementation is discussed in the following section, however, the formulation thus far is general and applicable to other energy methods as well.

4.4. Finite Element Implementation

A crucial assumption for Koiter's asymptotic expansion is that it relies on the expansion around a known state. This known state is traditionally the buckling point. This assumption does imply that a method to calculate this known state is required. It was concluded from the literature review there are several options to calculate the buckling load. Castro and Jansen define the known state as the linear buckling mode, which is calculated based on solving an eigenvalue problem. To set up this eigenvalue problem the Bogner-Fox-Schmit-Castro (BFSC) plate element is utilised for implementation within finite element models. This novel element is a modification of the Bogner-Fox-Schmit element and it is introduced to overcome the poor convergence of the second-order displacement field which in turn also affects the second post-buckling coefficient. An additional four degrees of freedom per node are added to the BFS element, resulting in an element that has four nodes and 10 degrees of freedom per node. These additional degrees of freedom allow for third-order interpolation of the in-plane displacements.

The displacements are approximated utilising Equation 4.44, where $\boldsymbol{u}_{ei}$ represents the vector containing the 10 DOFs of the i^{th} node.

$$u, v, w = \sum_{i=1}^{4} \boldsymbol{S}_i^{u,v,w} \boldsymbol{u}_{ei} \tag{4.44}$$

The shape functions $\boldsymbol{S}_i^{u,v,w}$ arange in the matrices according to Equation 4.45, with the cubic Hermite functions H_i, H_i^x, H_i^y, and H_i^{xy} equal to Equation 4.46. The dimensions of the finite element along the x and y axis are represented by ℓ_x and ℓ_y. Finally, the values for the natural coordinates, ξ_j and η_i are given in Equation 4.47

$$\begin{aligned}
\boldsymbol{S}_i^u &= \begin{bmatrix} H_i & H_i^x & H_i^y & 0 & 0 & 0 & 0 & 0 & 0 & 0 \end{bmatrix} \\
\boldsymbol{S}_i^v &= \begin{bmatrix} 0 & 0 & 0 & H_i & H_i^x & H_i^y & 0 & 0 & 0 & 0 \end{bmatrix} \\
\boldsymbol{S}_i^v &= \begin{bmatrix} 0 & 0 & 0 & 0 & 0 & 0 & H_i & H_i^x & H_i^y & H_i^{xy} \end{bmatrix}
\end{aligned} \tag{4.45}$$

$$\begin{aligned}
H_i &= \frac{1}{16}\left(\xi+\xi_i\right)^2\left(\xi\xi_i-2\right)\left(\eta+\eta_i\right)^2\left(\eta\eta_i-2\right) \\
H_i^x &= -\frac{\ell_x}{32}\xi_i\left(\xi+\xi_i\right)^2\left(\xi\xi_i-1\right)\left(\eta+\eta_i\right)^2\left(\eta\eta_i-2\right) \\
H_i^y &= -\frac{\ell_y}{32}\left(\xi+\xi_i\right)^2\left(\xi\xi_i-2\right)\eta_i\left(\eta+\eta_i\right)^2\left(\eta\eta_i-1\right) \\
H_i^{xy} &= \frac{\ell_x\ell_y}{64}\xi_i\left(\xi+\xi_i\right)^2\left(\xi\xi_i-1\right)\eta_i\left(\eta+\eta_i\right)^2\left(\eta\eta_i-1\right)
\end{aligned} \tag{4.46}$$

Node	ξ_i	η_i
1	-1	-1
2	$+1$	-1
3	$+1$	$+1$
4	-1	$+1$

(4.47)

The natural coordinate can be easily computed from the finite element dimension according to the conversions presented below.

$$\xi = \frac{2x}{\ell_x} - 1 \tag{4.48}$$

$$\eta = \frac{2y}{\ell_y} - 1 \tag{4.49}$$

Lastly, the derivative of the shape functions required for the derivative of the strain has to be computed in natural coordinates utilising Equation 4.50 and Equation 4.51.

$$\frac{\partial}{\partial x} = \frac{\ell_x}{2}\frac{\partial}{\partial \xi} \tag{4.50}$$

$$\frac{\partial}{\partial y} = \frac{\ell_y}{2}\frac{\partial}{\partial \eta} \tag{4.51}$$

The buckling load of the plate is calculated to define the known state that forms the basis of the Koiter expansion. This process initiates with creating a mesh, based on the required number of nodes. Subsequently, the boundary conditions are applied to the necessary nodes after which an external load is applied to the edges of the plate. The buckling load and shapes are computed by solving an eigenvalue problem. The BFSC element was able to accurately predict the linear buckling load. With the buckling load found, the functional derivative can be computed.

The third- and fourth-order tensors ϕ_c''' and ϕ_c^{iv} can easily require huge amounts of space if one does not take action to minimize this. Instead of computing the whole individual tensor, the product between the tensor and the displacements is calculated to reduce the size of the array required to store this information. This allows for a computationally inexpensive procedure. The functional derivatives are calculated on an element level and added together with the corresponding weights to compute the final functional derivatives. These in turn are used to calculate the initial post-buckling coefficients a_I and b_I.

5

Expansion of the Total Potential Energy Functional

The first step in including imperfections into the displacement-based Koiter methodology is to expand the total potential energy. Opposed to the methodology without imperfections, the total potential energy now consists of both the perfect and the imperfect structure. The presence of imperfections in the structure introduces a dependence on the imperfection shape and therefore an expansion around this imperfection shape is required. Two different approaches to expanding the total potential energy were found. First of all, the expansion according to Pignataro [45] is presented in section 5.1. Following this, the work of Budiansky [4] is given in section 5.2. The chapter concludes with a comparison between the two approaches.

5.1. Formulation by Pignataro

If a structure is imperfect, as in it contains a displacement before any load is applied, the potential energy functional is a combination of the perfect and the imperfect structure, as shown in Equation 5.1. The perfect structure is still only dependent on the displacement ($\boldsymbol{u}$) and the load parameter (λ), the imperfect structure is dependent on the same two factors on top of the initial displacement ($\bar{\boldsymbol{u}}$).

$$\bar{\phi} = \phi\left[\boldsymbol{u}(\lambda);\lambda\right] + \psi\left[\boldsymbol{u}(\lambda), \bar{\boldsymbol{u}};\lambda\right] \tag{5.1}$$

The potential energy must equal zero if the imperfection is set to zero and therefore the following must be true.

$$\psi\left[\boldsymbol{u}(\lambda), \boldsymbol{0};\lambda\right] = 0 \tag{5.2}$$

The variational equation of equilibrium is equal to zero, and therefore Equation 5.3 is applicable for an imperfect structure. Note that ($'$) still represents the Frechét derivative with respect to the displacement and the displacement is still dependent on the load parameter however the concise notation of just $\boldsymbol{u}$ instead of $\boldsymbol{u}(\lambda)$.

$$\phi'\left[\boldsymbol{u};\lambda\right]\delta\boldsymbol{u} + \psi'\left[\boldsymbol{u}, \bar{\boldsymbol{u}};\lambda\right]\delta\boldsymbol{u} = \boldsymbol{0} \tag{5.3}$$

Subsequently, the first Taylor expansion around the known initial out-of-plane displacement $\bar{\boldsymbol{u}}_{\boldsymbol{0}}$ is carried out. It is assumed that the initial displacement of the imperfection is small and can therefore be approximated to zero. As a consequence of this assumption, only the linear terms remain. The expansion of the potential including this assumption is presented below, where ($\tilde{}$) represents the Frechét differentiation with respect to the initial imperfection $\bar{\boldsymbol{u}}$.

$$\phi'\left[\boldsymbol{u};\lambda\right]\delta\boldsymbol{u} + \cancelto{0,}{\psi'\left[\boldsymbol{u},\boldsymbol{0};\lambda\right]\delta\boldsymbol{u}}^{\text{Eq. 5.2}} + \tilde{\psi}'\left[\boldsymbol{u},\boldsymbol{0};\lambda\right]\bar{\boldsymbol{u}}\delta\boldsymbol{u} + \cancelto{0,}{\frac{1}{2}\tilde{\tilde{\psi}}'\left[\boldsymbol{u},\boldsymbol{0};\lambda\right]\bar{\boldsymbol{u}}^2\delta\boldsymbol{u}}^{\text{Non-linear}} = \boldsymbol{0} \tag{5.4}$$

Following this, the total potential energy is expanded around the known displacement ($\boldsymbol{u_0}$).

$$\begin{aligned}\Big[\cancelto{0,\text{Eq. Perfect Structure}}{\phi'\left[\boldsymbol{u_0};\lambda\right]}+\phi''\left[\boldsymbol{u_0};\lambda\right]\left(\boldsymbol{u}-\boldsymbol{u_0}\right)+\frac{1}{2}\phi'''\left[\boldsymbol{u_0};\lambda\right]\left(\boldsymbol{u}-\boldsymbol{u_0}\right)^2+\frac{1}{6}\phi^{iv}\left[\boldsymbol{u_0};\lambda\right]\left(\boldsymbol{u}-\boldsymbol{u_0}\right)^3+\cdots\Big]\delta\boldsymbol{u}+\\ \Big[\tilde{\psi}'\left[\boldsymbol{u_0},\boldsymbol{0};\lambda\right]\bar{\boldsymbol{u}}+\tilde{\psi}''\left[\boldsymbol{u},\boldsymbol{0};\lambda\right]\bar{\boldsymbol{u}}\left(\boldsymbol{u}-\boldsymbol{u_0}\right)+\frac{1}{2}\tilde{\psi}'''\left[\boldsymbol{u},\boldsymbol{0};\lambda\right]\bar{\boldsymbol{u}}\left(\boldsymbol{u}-\boldsymbol{u_0}\right)^2+\cdots\Big]\delta\boldsymbol{u}=\boldsymbol{0}\end{aligned} \tag{5.5}$$

To complete the expansion of the total potential energy, a final Taylor expansion around the critical load parameter (λ_c) is performed.

$$\begin{aligned}&\Big[\phi''\left[\boldsymbol{u_c};\lambda_c\right]+\dot{\phi}''\left[\boldsymbol{u_c};\lambda_c\right]\left(\lambda-\lambda_c\right)+\frac{1}{2}\ddot{\phi}''\left[\boldsymbol{u_c};\lambda_c\right]\left(\lambda-\lambda_c\right)^2\Big]\left(\boldsymbol{u}-\boldsymbol{u_c}\right)\delta\boldsymbol{u}+\\ &\frac{1}{2}\Big[\phi'''\left[\boldsymbol{u_c};\lambda_c\right]+\dot{\phi}'''\left[\boldsymbol{u_c};\lambda_c\right]\left(\lambda-\lambda_c\right)+\frac{1}{2}\ddot{\phi}'''\left[\boldsymbol{u_c};\lambda_c\right]\left(\lambda-\lambda_c\right)^2\Big]\left(\boldsymbol{u}-\boldsymbol{u_c}\right)^2\delta\boldsymbol{u}+\\ &\frac{1}{6}\Big[\phi^{iv}\left[\boldsymbol{u_c};\lambda_c\right]+\dot{\phi}^{iv}\left[\boldsymbol{u_c};\lambda_c\right]\left(\lambda-\lambda_c\right)+\frac{1}{2}\ddot{\phi}^{iv}\left[\boldsymbol{u_c};\lambda_c\right]\left(\lambda-\lambda_c\right)^2\Big]\left(\boldsymbol{u}-\boldsymbol{u_c}\right)^3\delta\boldsymbol{u}+\\ &\Big[\tilde{\psi}'\left[\boldsymbol{u_c},\boldsymbol{0};\lambda_c\right]+\dot{\tilde{\psi}}'\left[\boldsymbol{u_c},\boldsymbol{0};\lambda_c\right]\left(\lambda-\lambda_c\right)+\frac{1}{2}\ddot{\tilde{\psi}}'\left[\boldsymbol{u_c},\boldsymbol{0};\lambda_c\right]\left(\lambda-\lambda_c\right)^2\Big]\bar{\boldsymbol{u}}\delta\boldsymbol{u}+\\ &\Big[\tilde{\psi}''\left[\boldsymbol{u},\boldsymbol{0};\lambda_c\right]+\dot{\tilde{\psi}}''\left[\boldsymbol{u},\boldsymbol{0};\lambda_c\right]\left(\lambda-\lambda_c\right)+\frac{1}{2}\ddot{\tilde{\psi}}''\left[\boldsymbol{u},\boldsymbol{0};\lambda_c\right]\left(\lambda-\lambda_c\right)^2\Big]\bar{\boldsymbol{u}}\left(\boldsymbol{u}-\boldsymbol{u_c}\right)\delta\boldsymbol{u}+\\ &\frac{1}{2}\Big[\tilde{\psi}'''\left[\boldsymbol{u},\boldsymbol{0};\lambda_c\right]+\dot{\tilde{\psi}}'''\left[\boldsymbol{u},\boldsymbol{0};\lambda_c\right]\left(\lambda-\lambda_c\right)+\frac{1}{2}\ddot{\tilde{\psi}}'''\left[\boldsymbol{u},\boldsymbol{0};\lambda_c\right]\left(\lambda-\lambda_c\right)^2\Big]\bar{\boldsymbol{u}}\left(\boldsymbol{u}-\boldsymbol{u_c}\right)^2\delta\boldsymbol{u}=\boldsymbol{0}\end{aligned} \tag{5.6}$$

It is convenient to rewrite the initial imperfection ($\bar{\boldsymbol{u}}$) to Equation 5.7, such that $\hat{\boldsymbol{u}}$ is the imperfection shape and $\bar{\xi}$ is the imperfection amplitude.

$$\bar{\boldsymbol{u}}=\bar{\xi}\hat{\boldsymbol{u}} \tag{5.7}$$

Equation 5.6 can be rewritten in enhanced notation equal to Equation 5.8. This includes the simplification $\boldsymbol{v}=\boldsymbol{u}-\boldsymbol{u_0}(\lambda_c)$ and Equation 5.7.

$$\begin{aligned}&\Big[\phi_c''+\dot{\phi}_c''\left(\lambda-\lambda_c\right)+\frac{1}{2}\ddot{\phi}_c''\left(\lambda-\lambda_c\right)^2\Big]\boldsymbol{v}\delta\boldsymbol{u}+\frac{1}{2}\Big[\phi_c'''+\dot{\phi}_c'''\left(\lambda-\lambda_c\right)+\frac{1}{2}\ddot{\phi}_c'''\left(\lambda-\lambda_c\right)^2\Big]\boldsymbol{v}^2\delta\boldsymbol{u}+\\ &\frac{1}{6}\Big[\phi_c^{iv}+\dot{\phi}_c^{iv}\left(\lambda-\lambda_c\right)+\frac{1}{2}\ddot{\phi}_c^{iv}\left(\lambda-\lambda_c\right)^2\Big]\boldsymbol{v}^3\delta\boldsymbol{u}+\Big[\tilde{\psi}_c'+\dot{\tilde{\psi}}_c'\left(\lambda-\lambda_c\right)+\frac{1}{2}\ddot{\tilde{\psi}}_c'\left(\lambda-\lambda_c\right)^2\Big]\bar{\xi}\hat{\boldsymbol{u}}\delta\boldsymbol{u}+\\ &\Big[\tilde{\psi}_c''+\dot{\tilde{\psi}}_c''\left(\lambda-\lambda_c\right)+\frac{1}{2}\ddot{\tilde{\psi}}_c''\left(\lambda-\lambda_c\right)^2\Big]\bar{\xi}\hat{\boldsymbol{u}}\boldsymbol{v}\delta\boldsymbol{u}+\\ &\frac{1}{2}\Big[\tilde{\psi}_c'''+\dot{\tilde{\psi}}_c'''\left(\lambda-\lambda_c\right)+\frac{1}{2}\ddot{\tilde{\psi}}_c'''\left(\lambda-\lambda_c\right)^2\Big]\bar{\xi}\hat{\boldsymbol{u}}\boldsymbol{v}^2\delta\boldsymbol{u}=\boldsymbol{0}\end{aligned} \tag{5.8}$$

This concludes the expansion of the potential energy, based on the assumptions made by Pignataro. Thus far no assumptions have been made about the structure or the imperfection pattern and therefore this derivation applies to any imperfect structure not only a plate.

5.2. Fomulation by Budiansky

Budiansky's expansion of the potential energy initiates similarly to Pignataro's approach and assumes the potential energy of an imperfect structure can be split into perfect and imperfect. The variational equation of equilibrium remains zero, and the definitions previously presented in Equation 5.1 to 5.3 are still applicable. However, the two methodologies follow a different path from this point on as Budiansky performs a Taylor expansion around a known displacement position $\boldsymbol{u_0}$ instead of the initial imperfection.

$$\begin{aligned}\phi'\left[\boldsymbol{u_0};\lambda\right]\delta\boldsymbol{u}+\phi''\left[\boldsymbol{u_0};\lambda\right]\left(\boldsymbol{u}-\boldsymbol{u_0}\right)\delta\boldsymbol{u}+\frac{1}{2}\phi'''\left[\boldsymbol{u_0};\lambda\right]\left(\boldsymbol{u}-\boldsymbol{u_0}\right)^2\delta\boldsymbol{u}+\frac{1}{6}\phi^{iv}\left[\boldsymbol{u_0};\lambda\right]\left(\boldsymbol{u}-\boldsymbol{u_0}\right)^3\delta\boldsymbol{u}+\\ \psi'\left[\boldsymbol{u_0},\bar{\boldsymbol{u}};\lambda\right]\delta\boldsymbol{u}+\psi''\left[\boldsymbol{u_0},\bar{\boldsymbol{u}};\lambda\right]\left(\boldsymbol{u}-\boldsymbol{u_0}\right)\delta\boldsymbol{u}+\frac{1}{2}\psi'''\left[\boldsymbol{u_0},\bar{\boldsymbol{u}};\lambda\right]\left(\boldsymbol{u}-\boldsymbol{u_0}\right)^2\delta\boldsymbol{u}=\boldsymbol{0}\end{aligned} \tag{5.9}$$

Following from this a Taylor expansion around the imperfection $\bar{\boldsymbol{u}}_{\boldsymbol{0}}$ is carried out. The known initial displacement is assumed to be small and therefore it can be approximated to be zero, similar to Pignataro. By Equation 5.2 all derivatives of $\psi\left[\boldsymbol{u},\boldsymbol{0};\lambda\right]$ equal zero and $\phi'\left[\boldsymbol{u_0};\lambda\right]$ disappears due to the equilibrium of the unbuckled perfect structure, demonstrated in Equation 4.1. The expansion of the potential including these assumptions is presented below, where $\tilde{}$ represents the Frechét differentiation with respect to the initial known geometric imperfection.

$$\begin{aligned}\cancelto{0,}{\phi'\left[\boldsymbol{u_0};\lambda\right]\delta\boldsymbol{u}}^{\text{Eq. Perfect Structure}}+\phi''\left[\boldsymbol{u_0};\lambda\right]\left(\boldsymbol{u}-\boldsymbol{u_0}\right)\delta\boldsymbol{u}+\frac{1}{2}\phi'''\left[\boldsymbol{u_0};\lambda\right]\left(\boldsymbol{u}-\boldsymbol{u_0}\right)^2\delta\boldsymbol{u}+\frac{1}{6}\phi^{iv}\left[\boldsymbol{u_0};\lambda\right]\left(\boldsymbol{u}-\boldsymbol{u_0}\right)^3+\\ \left[\cancelto{0}{\psi'\left[\boldsymbol{u_0},\boldsymbol{0};\lambda\right]}+\tilde{\psi}'\left[\boldsymbol{u_0},\boldsymbol{0};\lambda\right]\bar{\boldsymbol{u}}+\frac{1}{2}\tilde{\tilde{\psi}}'\left[\boldsymbol{u_0},\boldsymbol{0};\lambda\right]\bar{\boldsymbol{u}}^2\right]\delta\boldsymbol{u}+\\ \left[\cancelto{0}{\psi''\left[\boldsymbol{u_0},0;\lambda\right]}+\tilde{\psi}''\left[\boldsymbol{u_0},0;\lambda\right]\bar{\boldsymbol{u}}+\frac{1}{2}\tilde{\tilde{\psi}}''\left[\boldsymbol{u_0},0;\lambda\right]\bar{\boldsymbol{u}}^2\right]\left(\boldsymbol{u}-\boldsymbol{u_0}\right)\delta\boldsymbol{u}+\\ \frac{1}{2}\left[\cancelto{0}{\psi'''\left[\boldsymbol{u_0},\boldsymbol{0};\lambda\right]}+\tilde{\psi}'''\left[\boldsymbol{u_0},\boldsymbol{0};\lambda\right]\bar{\boldsymbol{u}}+\frac{1}{2}\tilde{\tilde{\psi}}'''\left[\boldsymbol{u_0},\boldsymbol{0};\lambda\right]\bar{\boldsymbol{u}}^2\right]\left(\boldsymbol{u}-\boldsymbol{u_0}\right)^2\delta\boldsymbol{u}=0\end{aligned} \tag{5.10}$$

The imperfection can still be rewritten to be a multiplication of the imperfection amplitude and the imperfection shape, as shown in Equation 5.7. Therefore Equation 5.10 can be rewritten to the following.

$$\begin{aligned}\phi''\left[\boldsymbol{u_0};\lambda\right]\left(\boldsymbol{u}-\boldsymbol{u_0}\right)\delta\boldsymbol{u}+\frac{1}{2}\phi'''\left[\boldsymbol{u_0};\lambda\right]\left(\boldsymbol{u}-\boldsymbol{u_0}\right)^2\delta\boldsymbol{u}+\frac{1}{6}\phi^{iv}\left[\boldsymbol{u_0};\lambda\right]\left(\boldsymbol{u}-\boldsymbol{u_0}\right)^3+\\ \left[\tilde{\psi}'\left[\boldsymbol{u_0},\boldsymbol{0};\lambda\right]\bar{\xi}\hat{\boldsymbol{u}}+\frac{1}{2}\tilde{\tilde{\psi}}'\left[\boldsymbol{u_0},\boldsymbol{0};\lambda\right]\bar{\xi}^2\hat{\boldsymbol{u}}^2\right]\delta\boldsymbol{u}+\\ \left[\tilde{\psi}''\left[\boldsymbol{u_0},0;\lambda\right]\bar{\xi}\hat{\boldsymbol{u}}+\frac{1}{2}\tilde{\tilde{\psi}}''\left[\boldsymbol{u_0},0;\lambda\right]\bar{\xi}^2\hat{\boldsymbol{u}}^2\right]\left(\boldsymbol{u}-\boldsymbol{u_0}\right)\delta\boldsymbol{u}+\\ \frac{1}{2}\left[\tilde{\psi}'''\left[\boldsymbol{u_0},\boldsymbol{0};\lambda\right]\bar{\xi}\hat{\boldsymbol{u}}+\frac{1}{2}\tilde{\tilde{\psi}}'''\left[\boldsymbol{u_0},\boldsymbol{0};\lambda\right]\bar{\xi}^2\hat{\boldsymbol{u}}^2\right]\left(\boldsymbol{u}-\boldsymbol{u_0}\right)^2\delta\boldsymbol{u}=0\end{aligned} \tag{5.11}$$

A last Taylor expansion is performed around the critical load λ_c. Note that in the equation above the notation of $\boldsymbol{u_0}$ was used, however, this changes to $\boldsymbol{u_c}$ due to the assumption $\boldsymbol{u_c}=\boldsymbol{u_0}(\lambda_c)$.

$$\begin{aligned}\left[\phi''\left[\boldsymbol{u_c};\lambda_c\right]+\dot{\phi}''\left[\boldsymbol{u_c};\lambda_c\right]\left(\lambda-\lambda_c\right)+\frac{1}{2}\ddot{\phi}''\left[\boldsymbol{u_c};\lambda_c\right]\left(\lambda-\lambda_c\right)^2\right]\left(\boldsymbol{u}-\boldsymbol{u_c}\right)\delta\boldsymbol{u}+\\ \frac{1}{2}\left[\phi'''\left[\boldsymbol{u_c};\lambda_c\right]+\dot{\phi}'''\left[\boldsymbol{u_c};\lambda_c\right]\left(\lambda-\lambda_c\right)+\frac{1}{2}\ddot{\phi}'''\left[\boldsymbol{u_c};\lambda_c\right]\left(\lambda-\lambda_c\right)^2\right]\left(\boldsymbol{u}-\boldsymbol{u_c}\right)^2\delta\boldsymbol{u}+\\ \frac{1}{6}\left[\phi^{iv}\left[\boldsymbol{u_c};\lambda_c\right]+\dot{\phi}^{iv}\left[\boldsymbol{u_c};\lambda_c\right]\left(\lambda-\lambda_c\right)+\frac{1}{2}\ddot{\phi}^{iv}\left[\boldsymbol{u_c};\lambda_c\right]\left(\lambda-\lambda_c\right)^2\right]\left(\boldsymbol{u}-\boldsymbol{u_c}\right)^3\delta\boldsymbol{u}+\\ \left[\tilde{\psi}'\left[\boldsymbol{u_c},\boldsymbol{0};\lambda_c\right]+\dot{\tilde{\psi}}'\left[\boldsymbol{u_c},\boldsymbol{0};\lambda_c\right]\left(\lambda-\lambda_c\right)+\frac{1}{2}\ddot{\tilde{\psi}}'\left[\boldsymbol{u_c},\boldsymbol{0};\lambda_c\right]\left(\lambda-\lambda_c\right)^2\right]\bar{\xi}\hat{\boldsymbol{u}}\delta\boldsymbol{u}+\\ \frac{1}{2}\left[\tilde{\tilde{\psi}}'\left[\boldsymbol{u_c},\boldsymbol{0};\lambda_c\right]+\dot{\tilde{\tilde{\psi}}}'\left[\boldsymbol{u_c},\boldsymbol{0};\lambda_c\right]\left(\lambda-\lambda_c\right)+\frac{1}{2}\ddot{\tilde{\tilde{\psi}}}'\left[\boldsymbol{u_c},\boldsymbol{0};\lambda_c\right]\left(\lambda-\lambda_c\right)^2\right]\bar{\xi}^2\hat{\boldsymbol{u}}^2\delta\boldsymbol{u}+\\ \left[\tilde{\psi}''\left[\boldsymbol{u_c},\boldsymbol{0};\lambda_c\right]+\dot{\tilde{\psi}}''\left[\boldsymbol{u_c},\boldsymbol{0};\lambda_c\right]\left(\lambda-\lambda_c\right)+\frac{1}{2}\ddot{\tilde{\psi}}''\left[\boldsymbol{u_c},\boldsymbol{0};\lambda_c\right]\left(\lambda-\lambda_c\right)^2\right]\bar{\xi}\hat{\boldsymbol{u}}\left(\boldsymbol{u}-\boldsymbol{u_c}\right)\delta\boldsymbol{u}+\\ \frac{1}{2}\left[\tilde{\tilde{\psi}}''\left[\boldsymbol{u_c},\boldsymbol{0};\lambda_c\right]+\dot{\tilde{\tilde{\psi}}}''\left[\boldsymbol{u_c},\boldsymbol{0};\lambda_c\right]\left(\lambda-\lambda_c\right)+\frac{1}{2}\ddot{\tilde{\tilde{\psi}}}''\left[\boldsymbol{u_c},\boldsymbol{0};\lambda_c\right]\left(\lambda-\lambda_c\right)^2\right]\bar{\xi}^2\hat{\boldsymbol{u}}^2\left(\boldsymbol{u}-\boldsymbol{u_c}\right)\delta\boldsymbol{u}+\end{aligned} \tag{5.12}$$

$$\begin{aligned}\frac{1}{2}\left[\tilde{\psi}'''\left[\boldsymbol{u_c},\boldsymbol{0};\lambda_c\right]+\dot{\tilde{\psi}}'''\left[\boldsymbol{u_c},\boldsymbol{0};\lambda_c\right](\lambda-\lambda_c)+\frac{1}{2}\ddot{\tilde{\psi}}'''\left[\boldsymbol{u_c},\boldsymbol{0};\lambda_c\right](\lambda-\lambda_c)^2\right]\bar{\xi}\hat{\boldsymbol{u}}\left(\boldsymbol{u}-\boldsymbol{u_c}\right)^2\delta\boldsymbol{u}+\\ \frac{1}{4}\left[\tilde{\tilde{\psi}}'''\left[\boldsymbol{u_c},\boldsymbol{0};\lambda_c\right]+\dot{\tilde{\tilde{\psi}}}'''\left[\boldsymbol{u_c},\boldsymbol{0};\lambda_c\right](\lambda-\lambda_c)+\frac{1}{2}\ddot{\tilde{\tilde{\psi}}}'''\left[\boldsymbol{u_c},\boldsymbol{0};\lambda_c\right](\lambda-\lambda_c)^2\right]\bar{\xi}^2\hat{\boldsymbol{u}}^2\left(\boldsymbol{u}-\boldsymbol{u_c}\right)^2\delta\boldsymbol{u}=0\end{aligned} \tag{5.12}$$

The enhanced notation of Equation 5.12 is presented down below, which utilises the assumption $\boldsymbol{v}=\boldsymbol{u}-\boldsymbol{u_0}(\lambda_c)$.

$$\begin{aligned}\left[\phi_c''+\dot{\phi}_c''(\lambda-\lambda_c)+\frac{1}{2}\ddot{\phi}_c''(\lambda-\lambda_c)^2\right]\boldsymbol{v}\delta\boldsymbol{u}+\frac{1}{2}\left[\phi_c'''+\dot{\phi}_c'''(\lambda-\lambda_c)+\frac{1}{2}\ddot{\phi}_c'''(\lambda-\lambda_c)^2\right]\boldsymbol{v}^2\delta\boldsymbol{u}+\\ \frac{1}{6}\left[\phi_c^{iv}+\dot{\phi}_c^{iv}(\lambda-\lambda_c)+\frac{1}{2}\ddot{\phi}_c^{iv}(\lambda-\lambda_c)^2\right]\boldsymbol{v}^3\delta\boldsymbol{u}+\left[\tilde{\psi}_c'+\dot{\tilde{\psi}}_c'(\lambda-\lambda_c)+\frac{1}{2}\ddot{\tilde{\psi}}_c'(\lambda-\lambda_c)^2\right]\bar{\xi}\hat{\boldsymbol{u}}\delta\boldsymbol{u}+\\ \frac{1}{2}\left[\tilde{\tilde{\psi}}_c'+\dot{\tilde{\tilde{\psi}}}_c'(\lambda-\lambda_c)+\frac{1}{2}\ddot{\tilde{\tilde{\psi}}}_c'(\lambda-\lambda_c)^2\right]\bar{\xi}^2\hat{\boldsymbol{u}}^2\delta\boldsymbol{u}+\left[\tilde{\psi}_c''+\dot{\tilde{\psi}}_c''(\lambda-\lambda_c)+\frac{1}{2}\ddot{\tilde{\psi}}_c''(\lambda-\lambda_c)^2\right]\bar{\xi}\hat{\boldsymbol{u}}\boldsymbol{v}\delta\boldsymbol{u}+\\ \frac{1}{2}\left[\tilde{\tilde{\psi}}_c''+\dot{\tilde{\tilde{\psi}}}_c''(\lambda-\lambda_c)+\frac{1}{2}\ddot{\tilde{\tilde{\psi}}}_c''(\lambda-\lambda_c)^2\right]\bar{\xi}^2\hat{\boldsymbol{u}}^2\boldsymbol{v}\delta\boldsymbol{u}+\\ \frac{1}{2}\left[\tilde{\psi}_c'''+\dot{\tilde{\psi}}_c'''(\lambda-\lambda_c)+\frac{1}{2}\ddot{\tilde{\psi}}_c'''(\lambda-\lambda_c)^2\right]\bar{\xi}\hat{\boldsymbol{u}}\boldsymbol{v}^2\delta\boldsymbol{u}+\\ \frac{1}{4}\left[\tilde{\tilde{\psi}}_c'''+\dot{\tilde{\tilde{\psi}}}_c'''(\lambda-\lambda_c)+\frac{1}{2}\ddot{\tilde{\tilde{\psi}}}_c'''(\lambda-\lambda_c)^2\right]\bar{\xi}^2\hat{\boldsymbol{u}}^2\boldsymbol{v}^2\delta\boldsymbol{u}=0\end{aligned} \tag{5.13}$$

This concludes the expansion of the potential energy according to Budiansky. Once again, the derivation is not structure-specific since no assumptions about the characteristics of the structure have been made. Whilst the scope defined this research to be related to plates only, this specific step is general. Moreover, no specific imperfection pattern is assumed yet and therefore it can take any shape from a combination of eigenmodes or sinusoidal waves.

5.3. Comparison between Pignataro and Budiansky

Pignataro and Budiansky propose similar approaches to the expansion of potential energy, but there are two differences. Firstly, the sequence of their expansions is different. Budiansky initially performs an expansion around the displacement whereas Pignataro kicks off with an expansion around the initial imperfection. Nonetheless, the sequence of the expansion does not influence the outcome and if either methodology had initiated with a different expansion it would have resulted in the same conclusion. The key difference between the two of them is that Budiansky does include non-linear functional derivatives of the imperfect structure ($\tilde{\tilde{\psi}}^{(n)}$, $\dot{\tilde{\tilde{\psi}}}^{(n)}$ and $\ddot{\tilde{\tilde{\psi}}}^{(n)}$) as opposed to Pignataro who assumes these are equal to zero.

6

Functional Derivatives utilising Frechét Derivatives

The second step in including imperfections within the displacement-based Koiter methodology involves determining all functional derivatives used in the expanded potential energy. To derive the final expression for the functional derivatives, the strains and stresses are required, thus these two steps in the methodology are also highlighted. There is one assumption one can make when deriving the derivatives. The pre-buckling can be presumed to be linear, simplifying the procedure of finding the functional derivatives significantly. The alternative is to ignore the linearity of the pre-buckling, but as a consequence, this increases the complexity of the methodology.

The outline of this chapter is as follows. The derivatives of the strain, without the assumption of linear pre-buckling, are presented in section 6.1. The influence of the assumption linear pre-buckling is discussed in section 6.2. Next, the stresses are computed in section 6.3. The stresses are directly derived from the strains, therefore section 6.4 shows the stresses derived with the assumption of linear pre-buckling in mind. The functional derivatives are formulated in section 6.5 and 6.6, without and including the assumption related to linear pre-buckling respectively. Finally, the chapter concludes with a short overview of the non-zero functional derivatives for each of the four possibilities.

6.1. Strains

The Donnell Kinematic relation for an imperfect plate is presented in Equation 6.1, which can be split into the perfect (Equation 6.2 and 6.3) and imperfect strains (Equation 6.4). The perfect strains and rotations are used to calculate the perfect functional derivatives (ϕ) and the imperfect strains are used to calculate the imperfect functional derivatives (ψ).

$$\boldsymbol{\epsilon} = \begin{Bmatrix} u_{,x} + \frac{1}{2}\left(w_{,x}\right)^2 + \bar{w}_{,x}w_{,x} \\ v_{,y} + \frac{1}{2}\left(w_{,y}\right)^2 + \bar{w}_{,y}w_{,y} \\ u_{,y} + v_{,x} + w_{,x}w_{,y} + \bar{w}_{,y}w_{,x} + \bar{w}_{,x}w_{,y} \end{Bmatrix} + z \begin{Bmatrix} -w_{,xx} \\ -w_{,yy} \\ -2w_{,xy} \end{Bmatrix} \tag{6.1}$$

$$\boldsymbol{\varepsilon} = \begin{Bmatrix} \varepsilon_{xx} \\ \varepsilon_{yy} \\ \gamma_{xy} \end{Bmatrix} = \begin{Bmatrix} u_{,x} + \frac{1}{2}\left(w_{,x}\right)^2 \\ v_{,y} + \frac{1}{2}\left(w_{,y}\right)^2 \\ u_{,y} + v_{,x} + w_{,x}w_{,y} \end{Bmatrix} \tag{6.2}$$

$$\boldsymbol{\kappa} = \begin{Bmatrix} \kappa_{xx} \\ \kappa_{yy} \\ \kappa_{xy} \end{Bmatrix} = \begin{Bmatrix} -w_{,xx} \\ -w_{,yy} \\ -2w_{,xy} \end{Bmatrix} \tag{6.3}$$

$$\bar{\boldsymbol{\varepsilon}} = \begin{Bmatrix} \bar{\varepsilon}_{xx} \\ \bar{\varepsilon}_{yy} \\ \bar{\gamma}_{xy} \end{Bmatrix} = \begin{Bmatrix} \bar{w}_{,x} w_{,x} \\ \bar{w}_{,y} w_{,y} \\ \bar{w}_{,y} w_{,x} + \bar{w}_{,x} w_{,y} \end{Bmatrix} \tag{6.4}$$

Luckily, the perfect strain derivatives have previously been computed by Castro and Jansen and can be reused. The necessary steps to derive these are illustrated in section 4.2, therefore only the imperfect derivatives of the strains are presented here.

The displacement due to the imperfection can be approximated by using known shape function $\boldsymbol{S}^{\bar{w}}$ and following a similar repeated index notation to what is presented in Equation 4.9, 4.10, and 4.11. Note that only imperfections that are out-of-plane are considered, thus only the shape function $\boldsymbol{S}^{\bar{w}}$ is required. The first Frechét derivative with respect to the displacement for the imperfect strains is presented in Equation 6.5 and the second derivative is equal to Equation 6.6. It is known that the imperfection shape is not dependent on the displacement field hence the second differentiation is equal to a zero vector.

$$\bar{\boldsymbol{\varepsilon}}'_{\boldsymbol{a}} = \begin{Bmatrix} \cancelto{0}{\bar{w}'_{,x} w_{,x}} + S^w_{a,x} \bar{w}_{,x} \\ \cancelto{0}{\bar{w}'_{,y} w_{,y}} + S^w_{a,y} \bar{w}_{,y} \\ \cancelto{0}{\bar{w}'_{,x} w_{,y}} + S^w_{a,y} \bar{w}_{,x} + \cancelto{0}{\bar{w}'_{,y} w_{,x}} + S^w_{a,x} \bar{w}_{,y} \end{Bmatrix} = \begin{Bmatrix} S^w_{a,x} \bar{w}_{,x} \\ S^w_{a,y} \bar{w}_{,y} \\ S^w_{a,y} \bar{w}_{,x} + S^w_{a,x} \bar{w}_{,y} \end{Bmatrix} \tag{6.5}$$

$$\bar{\boldsymbol{\varepsilon}}''_{\boldsymbol{ab}} = \begin{Bmatrix} S^w_{a,x} \cancelto{0}{\bar{w}'_{,x}} \\ S^w_{a,y} \cancelto{0}{\bar{w}'_{,y}} \\ S^w_{a,y} \cancelto{0}{\bar{w}'_{,x}} + S^w_{a,x} \cancelto{0}{\bar{w}'_{,y}} \end{Bmatrix} = \begin{Bmatrix} 0 \\ 0 \\ 0 \end{Bmatrix} \tag{6.6}$$

For the differentiations with respect to load factor (λ), the following is still known to be true $\boldsymbol{u_c} = \lambda_c \boldsymbol{u_0}$. Moreover, it is known that the initial imperfection does not increase as the load increases and therefore $\bar{w}_{,x}$ is not dependent on λ, thus the first derivative is equivalent to Equation 6.7. Other higher-order derivatives with respect to the load factor equal zero vectors, since none of the terms are dependent on the load factor.

$$\dot{\bar{\boldsymbol{\varepsilon}}} = \begin{Bmatrix} \bar{w}_{,x} w_{0,x} \\ \bar{w}_{,y} w_{0,y} \\ \bar{w}_{,x} w_{0,y} + \bar{w}_{,y} w_{0,x} \end{Bmatrix} \tag{6.7}$$

The Frechét derivative with respect to both the load factor (λ) and the displacement ($\boldsymbol{u}$) can be derived from Equation 6.5 and is equal to zero since the imperfections are not dependent on the load factor.

$$\dot{\bar{\boldsymbol{\varepsilon}}}'_{\boldsymbol{a}} = \boldsymbol{0} \tag{6.8}$$

Moving on to the derivatives concerning the imperfection field. Only the initial imperfection is dependent on the imperfection shape so therefore the first derivative is equal to Equation 6.9. All higher-order derivatives are equal to zero since none of the terms are dependent on the imperfection.

$$\tilde{\bar{\boldsymbol{\varepsilon}}}_{\boldsymbol{k}} = \begin{Bmatrix} \tilde{\bar{w}}_{,x} w_{,x} + \bar{w}_{,x} \cancelto{0}{\tilde{w}_{,x}} \\ \tilde{\bar{w}}_{,y} w_{,y} + \bar{w}_{,y} \cancelto{0}{\tilde{w}_{,y}} \\ \tilde{\bar{w}}_{,y} w_{,x} + \bar{w}_{,y} \cancelto{0}{\tilde{w}_{,x}} + \tilde{\bar{w}}_{,x} w_{,y} + \bar{w}_{,x} \cancelto{0}{\tilde{w}_{,y}} \end{Bmatrix} = \begin{Bmatrix} S^{\bar{w}}_{k,x} w_{,x} \\ S^{\bar{w}}_{k,y} w_{,y} \\ S^{\bar{w}}_{k,y} w_{,x} + S^{\bar{w}}_{k,x} w_{,y} \end{Bmatrix} \tag{6.9}$$

From Equation 6.9 the derivative with respect to both the imperfection field and the displacement can be found, as shown in Equation 6.10. All other higher-order derivatives related to both the imperfection and the displacement equal zero.

$$\tilde{\bar{\varepsilon}}'_{\boldsymbol{ka}} = \left\{ \begin{array}{c} S^{\bar{w}}_{k,x} S^{w}_{a,x} \\ S^{\bar{w}}_{k,y} S^{w}_{a,y} \\ S^{\bar{w}}_{k,y} S^{w}_{a,x} + S^{\bar{w}}_{k,x} S^{w}_{a,y} \end{array} \right\} \tag{6.10}$$

Finally, from Equation 6.9, the derivative with respect to both the imperfection and the load parameter is computed and presented in Equation 6.11. Again all high-order derivatives depending on the imperfection and the load factor become zero. The Frechét derivative with respect to all three parameters is also equal to zero.

$$\dot{\tilde{\bar{\varepsilon}}}_{\boldsymbol{k}} = \left\{ \begin{array}{c} S^{\bar{w}}_{k,x} w_{0,x} \\ S^{\bar{w}}_{k,y} w_{0,y} \\ S^{\bar{w}}_{k,y} w_{0,x} + S^{\bar{w}}_{k,x} w_{0,y} \end{array} \right\} \tag{6.11}$$

This concludes the derivations of the imperfect strains. The imperfect strains that are not non-zero are listed below as these are used in the next steps of the derivation.

$$\begin{array}{cc} \bar{\varepsilon} & \bar{\varepsilon}'_a \\ \dot{\bar{\varepsilon}} & \tilde{\bar{\varepsilon}}_k \\ \tilde{\bar{\varepsilon}}'_{ka} & \dot{\tilde{\bar{\varepsilon}}}_k \end{array}$$

6.2. Strains for Linear Pre-buckling

If the pre-buckling state $\boldsymbol{u}_0$ is evaluated linearly for a plate with no bending-extension coupling and only in-plane pre-buckling loads, the out-of-plane displacement (w_0) equals zero. This assumption is only applicable for small rotations. Besides the out-of-plane displacement (w_0) dropping to zero, the term w and its derivatives also disappear due the fact that $\boldsymbol{u_c} = \boldsymbol{u_0}(\lambda_c)$. The full expressions for both the perfect and imperfect strains can be found in subsection A.1.1 and A.1.2. This assumption that w_0 is equal to zero for linear pre-buckling is only applicable for a plate and not a cylinder. If the displacement-based Koiter methodology is modified for cylinder one should pay attention to the case of linear pre-buckling as it is not as simple as for a plate.

6.3. Stresses

The stresses are computed utilising the classical constitutive relations for laminate composites and using repeated index notation, similar to what was done for the perfect displacement-based Koiter methodology. The stresses for the perfect structure have been previously computed by Castro and Jansen and can be found completely in subsection 4.2.2. The imperfect stresses are based only on the imperfect strains and are therefore equivalent to Equation 6.12.

$$\begin{array}{l} \bar{N}_i = A_{ij} \bar{\varepsilon}_j \\ \bar{M}_i = B_{ij} \bar{\varepsilon}_j \end{array} \tag{6.12}$$

The derivatives of the imperfect stresses can easily be formulated using the imperfect strains and are presented here.

$$\begin{array}{l} \bar{N}'_{ia} = A_{ij} \bar{\varepsilon}'_{ja} \\ \bar{M}'_{ia} = B_{ij} \bar{\varepsilon}'_{ja} \end{array} \tag{6.13}$$

$$\begin{array}{l} \dot{\bar{N}}_i = A_{ij} \dot{\bar{\varepsilon}}_j \\ \dot{\bar{M}}_i = B_{ij} \dot{\bar{\varepsilon}}_j \end{array} \tag{6.14}$$

$$\begin{array}{l} \tilde{\bar{N}}_{ik} = A_{ij} \tilde{\bar{\varepsilon}}_{jk} \\ \tilde{\bar{M}}_{ik} = B_{ij} \tilde{\bar{\varepsilon}}_{jk} \end{array} \tag{6.15}$$

$$\begin{aligned}\tilde{\bar{N}}'_{ika} &= A_{ij}\tilde{\bar{\varepsilon}}'_{jka} \\ \tilde{\bar{M}}'_{ika} &= B_{ij}\tilde{\bar{\varepsilon}}'_{jka}\end{aligned} \tag{6.16}$$

$$\begin{aligned}\dot{\tilde{\bar{N}}}_{ik} &= A_{ij}\dot{\tilde{\bar{\varepsilon}}}_{ik} \\ \dot{\tilde{\bar{M}}}_{ik} &= B_{ij}\dot{\tilde{\bar{\varepsilon}}}_{ik}\end{aligned} \tag{6.17}$$

This concludes the derivation of the imperfect stresses. All higher-order derivatives that are not presented above are equal to zero since the strains are also equal to zero. An overview of the non-zero imperfect strains can be found at the end of section 6.1.

6.4. Stresses for Linear Pre-buckling

The assumption of linear pre-buckling influences the stresses as well since they are dependent on the strains. Since the computation of the stresses from the strains is self-explanatory, the final expressions of the derivatives of the imperfect stresses including the assumption linear pre-buckling are only presented in section A.2.

6.5. Functional Derivatives

The final step is to derive the functional derivatives. To complete the derivation, the imperfect stresses are multiplied with the strains to find the imperfect functional derivatives. The full derivation of the perfect functional derivatives has previously been executed by Castro and Jansen and presented in section 4.2. The potential energy of an imperfect plate is equal to $\phi + \psi$. The contribution the imperfections have on the potential energy is represented in Equation 6.18.

$$\psi = \frac{1}{2}\int_\Omega \left(\bar{N}_i\bar{\varepsilon}_i + N_i\bar{\varepsilon}_i + \bar{N}_i\varepsilon_i + \bar{M}_i\kappa_i\right) d\Omega \tag{6.18}$$

The equilibrium of the imperfect structure is presented in Equation 6.19, which can also be rewritten to Equation 6.20. An overview of all the perfect and imperfect stresses and strains that remain after the differentiation is given in Table 6.1. All other terms are equal to zero vectors, therefore these terms are crossed during the derivation of all imperfect functional derivatives.

$$\psi'_c\delta\boldsymbol{u} = \frac{1}{2}\int_\Omega \left(\delta\bar{N}_i\bar{\varepsilon}_i + \bar{N}_i\delta\bar{\varepsilon}_i + \delta N_i\bar{\varepsilon}_i + N_i\delta\bar{\varepsilon}_i + \delta\bar{N}_i\varepsilon_i + \bar{N}_i\delta\varepsilon_i + \delta\bar{M}_i\kappa_i + \bar{M}_i\delta\kappa_i\right) d\Omega \tag{6.19}$$

$$\psi'_c\boldsymbol{u_a} = \left[\frac{1}{2}\int_\Omega \left(\bar{N}'_{ia}\bar{\varepsilon}_i + \bar{N}_i\bar{\varepsilon}'_{ia} + N'_{ia}\bar{\varepsilon}_i + N_i\bar{\varepsilon}'_{ia} + \bar{N}'_{ia}\varepsilon_i + \bar{N}_i\varepsilon'_{ia} + \bar{M}'_{ia}\kappa_i + \bar{M}_i\kappa'_{ia}\right) d\Omega\right] u_a \tag{6.20}$$

The second, third and fourth derivatives with respect to the displacement are presented in Equation 6.21, 6.22, and 6.23.

$$\begin{aligned}\psi''_c\boldsymbol{u_a u_b} = \Bigg[\frac{1}{2}\int_\Omega \Bigg(&\cancelto{0}{\bar{N}''_{iab}\bar{\varepsilon}_i} + \bar{N}'_{ia}\bar{\varepsilon}'_{ib} + \bar{N}'_{ib}\bar{\varepsilon}'_{ia} + \bar{N}_i\cancelto{0}{\bar{\varepsilon}''_{iab}} + N''_{iab}\bar{\varepsilon}_i + N'_{ia}\bar{\varepsilon}'_{ib} \\ &+ N'_{ib}\bar{\varepsilon}'_{ia} + N_i\cancelto{0}{\bar{\varepsilon}''_{iab}} + \cancelto{0}{\bar{N}''_{iab}\bar{\varepsilon}_i} + \bar{N}'_{ia}\varepsilon'_{ib} + \bar{N}'_{ib}\varepsilon'_{ia} \\ &+\bar{N}_i\varepsilon''_{iab} + \cancelto{0}{\bar{M}''_{iab}\kappa_i} + \bar{M}'_{ia}\kappa'_{ib} + \bar{M}'_{ib}\kappa'_{ia} + \bar{M}_i\cancelto{0}{\kappa''_{iab}}\Bigg) d\Omega\Bigg] u_a u_b \\ = \Bigg[\frac{1}{2}\int_\Omega &\left(\bar{N}'_{ia}\bar{\varepsilon}'_{ib} + \bar{N}'_{ib}\bar{\varepsilon}'_{ia} + N''_{iab}\bar{\varepsilon}_i + N'_{ia}\bar{\varepsilon}'_{ib} + N'_{ib}\bar{\varepsilon}'_{ia}\right. \\ &\left.+\bar{N}'_{ia}\varepsilon'_{ib} + \bar{N}'_{ib}\varepsilon'_{ia} + \bar{N}_i\varepsilon''_{iab} + \bar{M}'_{ia}\kappa'_{ib} + \bar{M}'_{ib}\kappa'_{ia}\right) d\Omega\Bigg] u_a u_b\end{aligned} \tag{6.21}$$

Strains		Stresses	
Perfect	Imperfect	Perfect	Imperfect
$\boldsymbol{\varepsilon}$	$\bar{\boldsymbol{\varepsilon}}$	N_i and M_i	$\bar{N}_i$ and $\bar{M}_i$
$\boldsymbol{\kappa}$	$\bar{\boldsymbol{\varepsilon}}'_{\boldsymbol{a}}$	N'_{ia} and M'_{ia}	$\bar{N}'_{ia}$ and $\bar{M}'_{ia}$
$\boldsymbol{\varepsilon}'_a$	$\dot{\bar{\boldsymbol{\varepsilon}}}$	N''_{iab} and M''_{iab}	$\dot{\bar{N}}_i$ and $\dot{\bar{M}}_i$
$\boldsymbol{\kappa}'_a$	$\tilde{\bar{\boldsymbol{\varepsilon}}}_{\boldsymbol{k}}$	$\dot{N}_i$ and $\dot{M}_i$	$\tilde{\bar{N}}_{ik}$ and $\tilde{\bar{M}}_{ik}$
$\boldsymbol{\varepsilon}''_{ab}$	$\tilde{\bar{\boldsymbol{\varepsilon}}}'_{\boldsymbol{ka}}$	$\ddot{N}_i$ and $\ddot{M}_i$	$\tilde{\bar{N}}'_{ika}$ and $\tilde{\bar{M}}'_{ika}$
$\dot{\boldsymbol{\varepsilon}}$	$\dot{\tilde{\bar{\boldsymbol{\varepsilon}}}}_{\boldsymbol{k}}$	$\dot{N}'_{ia}$ and $\dot{M}'_{ia}$	$\dot{\tilde{\bar{N}}}_{ik}$ and $\dot{\tilde{\bar{M}}}_{ik}$
$\dot{\boldsymbol{\kappa}}$			
$\ddot{\boldsymbol{\varepsilon}}$			
$\dot{\boldsymbol{\varepsilon}}'_{\boldsymbol{a}}$			

Table 6.1: Overview all relevant strains and stresses for the perfect and imperfect structure

$$
\begin{aligned}
\psi'''_c \boldsymbol{u_a u_b u_c} = \Bigg[\frac{1}{2}\int_\Omega \Bigg(& \cancelto{0}{\bar{N}''_{iac}\bar{\varepsilon}'_{ib}} + \bar{N}'_{ia}\cancelto{0}{\bar{\varepsilon}''_{ibc}} + \cancelto{0}{\bar{N}''_{ibc}\bar{\varepsilon}'_{ia}} + \bar{N}'_{ib}\cancelto{0}{\bar{\varepsilon}''_{iac}} + \cancelto{0}{N'''_{iabc}\bar{\varepsilon}_i} + N''_{iab}\bar{\varepsilon}'_{ic} + N''_{iac}\bar{\varepsilon}'_{ib} \\
& + N'_{ia}\cancelto{0}{\bar{\varepsilon}''_{ibc}} + N''_{ibc}\bar{\varepsilon}'_{ia} + N'_{ib}\cancelto{0}{\bar{\varepsilon}''_{iac}} + \cancelto{0}{\bar{N}''_{iac}\bar{\varepsilon}'_{ib}} + \bar{N}'_{ia}\varepsilon''_{ibc} + \cancelto{0}{\bar{N}''_{ibc}\bar{\varepsilon}'_{ia}} + \bar{N}'_{ib}\varepsilon''_{iac} \\
& + \bar{N}'_{ic}\varepsilon''_{iab} + \bar{N}_i\cancelto{0}{\varepsilon'''_{iabc}} + \cancelto{0}{\bar{M}''_{iac}\kappa'_{ib}} + \bar{M}'_{ia}\cancelto{0}{\kappa''_{ibc}} + \cancelto{0}{\bar{M}''_{ibc}\kappa'_{ia}} + \bar{M}'_{ib}\cancelto{0}{\kappa''_{iac}}\Bigg) d\Omega\Bigg] u_a u_b u_c \\
= & \left[\frac{1}{2}\int_\Omega \left(N''_{iab}\bar{\varepsilon}'_{ic} + N''_{iac}\bar{\varepsilon}'_{ib} + N''_{ibc}\bar{\varepsilon}'_{ia} + \bar{N}'_{ia}\varepsilon''_{ibc} + \bar{N}'_{ib}\varepsilon''_{iac} + \bar{N}'_{ic}\varepsilon''_{iab}\right) d\Omega\right] u_a u_b u_c
\end{aligned}
\tag{6.22}
$$

$$
\begin{aligned}
\psi^{iv}_c \boldsymbol{u_a u_b u_c u_d} = \Bigg[\frac{1}{2}\int_\Omega \Bigg(& \cancelto{0}{N'''_{iabd}\bar{\varepsilon}'_{ic}} + N''_{iab}\cancelto{0}{\bar{\varepsilon}''_{icd}} + \cancelto{0}{N'''_{iacd}\bar{\varepsilon}'_{ib}} + N''_{iac}\cancelto{0}{\bar{\varepsilon}''_{ibd}} + \cancelto{0}{N'''_{ibcd}\bar{\varepsilon}'_{ia}} + N''_{ibc}\cancelto{0}{\bar{\varepsilon}''_{iad}} \\
& + \cancelto{0}{\bar{N}''_{iad}\bar{\varepsilon}''_{ibc}} + \bar{N}'_{ia}\cancelto{0}{\varepsilon'''_{ibcd}} + \cancelto{0}{\bar{N}''_{ibd}\bar{\varepsilon}''_{iac}} + \bar{N}'_{ib}\cancelto{0}{\varepsilon'''_{iacd}} + \cancelto{0}{\bar{N}''_{icd}\bar{\varepsilon}''_{iab}} + \bar{N}'_{ic}\cancelto{0}{\varepsilon'''_{iabd}}\Bigg) d\Omega\Bigg] u_a u_b u_c u_d \\
& = \mathbf{0}
\end{aligned}
\tag{6.23}
$$

The next step is to compute the functional derivatives with respect to the initial displacement ($\bar{\boldsymbol{u}}$) and displacement field ($\boldsymbol{u}$). From Equation 6.20 the first derivative with respect to both $\bar{\boldsymbol{u}}$ and $\boldsymbol{u}$ is equal to Equation 6.24.

$$
\begin{aligned}
\tilde{\psi}'_c \boldsymbol{u_a \bar{u}_k} = \Bigg[\frac{1}{2}\int_\Omega \Bigg(& \tilde{\bar{N}}'_{iak}\bar{\varepsilon}_i + \bar{N}'_{ia}\tilde{\bar{\varepsilon}}_{ik} + \tilde{\bar{N}}_{ik}\bar{\varepsilon}'_{ia} + \bar{N}_i\tilde{\bar{\varepsilon}}'_{iak} + \cancelto{0}{\tilde{\bar{N}}'_{iak}\bar{\varepsilon}_i} + N'_{ia}\tilde{\bar{\varepsilon}}_{ik} + \cancelto{0}{\tilde{\bar{N}}_{ik}\bar{\varepsilon}'_{ia}} + N_i\tilde{\bar{\varepsilon}}'_{iak} \\
& + \tilde{\bar{N}}'_{iak}\varepsilon_i + \bar{N}'_{ia}\cancelto{0}{\tilde{\bar{\varepsilon}}_{ik}} + \tilde{\bar{N}}_{ik}\varepsilon'_{ia} + \bar{N}_i\cancelto{0}{\tilde{\bar{\varepsilon}}'_{iak}} + \tilde{\bar{M}}'_{iak}\kappa_i + \bar{M}'_{ia}\cancelto{0}{\tilde{\bar{\kappa}}_{ik}} + \tilde{\bar{M}}_{ik}\kappa'_{ia} + \bar{M}_i\cancelto{0}{\tilde{\bar{\kappa}}'_{iak}}\Bigg) d\Omega\Bigg] u_a \bar{u}_k \\
= & \left[\frac{1}{2}\int_\Omega \left(\tilde{\bar{N}}'_{iak}\bar{\varepsilon}_i + \bar{N}'_{ia}\tilde{\bar{\varepsilon}}_{ik} + \tilde{\bar{N}}_{ik}\bar{\varepsilon}'_{ia} + \bar{N}_i\tilde{\bar{\varepsilon}}'_{iak} + N'_{ia}\tilde{\bar{\varepsilon}}_{ik}\right.\right. \\
& \left.\left. + N_i\tilde{\bar{\varepsilon}}'_{iak} + \tilde{\bar{N}}'_{iak}\varepsilon_i + \tilde{\bar{N}}_{ik}\varepsilon'_{ia} + \tilde{\bar{M}}'_{iak}\kappa_i + \tilde{\bar{M}}_{ik}\kappa'_{ia}\right) d\Omega\right] u_a \bar{u}_k
\end{aligned}
\tag{6.24}
$$

From Equation 6.24 the first and second differentiation about the load factor (λ) can be computed, as presented in Equation 6.25 and 6.26. The third derivative to the load factor is equal to zero.

$$
\begin{aligned}
\dot{\tilde{\psi}}'_c \boldsymbol{u_a \bar{u}_k} = \Bigg[\frac{1}{2} \int_\Omega \Bigg(& \cancelto{0}{\dot{\tilde{\bar{N}}}'_{iak} \bar{\varepsilon}_i} + \tilde{\bar{N}}'_{iak} \dot{\tilde{\varepsilon}}_i + \cancelto{0}{\dot{\bar{N}}'_{ia} \tilde{\bar{\varepsilon}}_{ik}} + \bar{N}'_{ia} \dot{\tilde{\bar{\varepsilon}}}_{ik} + \dot{\tilde{\bar{N}}}_{ik} \bar{\varepsilon}'_{ia} + \cancelto{0}{\tilde{\bar{N}}_{ik} \dot{\bar{\varepsilon}}'_{ia}} + \dot{\bar{N}}_i \tilde{\bar{\varepsilon}}'_{iak} \\
& + \bar{N}_i \cancelto{0}{\dot{\tilde{\bar{\varepsilon}}}'_{iak}} + \dot{\bar{N}}'_{ia} \tilde{\bar{\varepsilon}}_{ik} + N'_{ia} \dot{\tilde{\bar{\varepsilon}}}_{ik} + \dot{N}_i \tilde{\bar{\varepsilon}}'_{iak} + N_i \cancelto{0}{\dot{\tilde{\bar{\varepsilon}}}'_{iak}} + \cancelto{0}{\dot{\tilde{\bar{N}}}_{iak} \varepsilon_i} + \tilde{\bar{N}}'_{iak} \dot{\varepsilon}_i \\
& + \dot{\tilde{\bar{N}}}_{ik} \varepsilon'_{ia} + \tilde{\bar{N}}_{ik} \dot{\varepsilon}'_{ia} + \cancelto{0}{\dot{\tilde{\bar{M}}}_{iak} \kappa_i} + \tilde{\bar{M}}'_{iak} \dot{\kappa}_i + \dot{\tilde{\bar{M}}}_{ik} \kappa'_{ia} + \tilde{\bar{M}}_{ik} \cancelto{0}{\dot{\kappa}'_{ia}} \Bigg) d\Omega \Bigg] u_a \bar{u}_k \\
= \Bigg[\frac{1}{2} \int_\Omega \Bigg(& \tilde{\bar{N}}'_{iak} \dot{\tilde{\varepsilon}}_i + \bar{N}'_{ia} \dot{\tilde{\bar{\varepsilon}}}_{ik} + \dot{\tilde{\bar{N}}}_{ik} \bar{\varepsilon}'_{ia} + \dot{\bar{N}}_i \tilde{\bar{\varepsilon}}'_{iak} + \dot{N}'_{ia} \tilde{\bar{\varepsilon}}_{ik} + N'_{ia} \dot{\tilde{\bar{\varepsilon}}}_{ik} + \dot{N}_i \tilde{\bar{\varepsilon}}'_{iak} \\
& + \tilde{\bar{N}}'_{iak} \dot{\varepsilon}_i + \dot{\tilde{\bar{N}}}_{ik} \varepsilon'_{ia} + \tilde{\bar{N}}_{ik} \dot{\varepsilon}'_{ia} + \tilde{\bar{M}}'_{iak} \dot{\kappa}_i + \dot{\tilde{\bar{M}}}_{ik} \kappa'_{ia} \Bigg) d\Omega \Bigg] u_a \bar{u}_k
\end{aligned}
\tag{6.25}
$$

$$
\begin{aligned}
\ddot{\tilde{\psi}}'_c \boldsymbol{u_a \bar{u}_k} = \Bigg[\frac{1}{2} \int_\Omega \Bigg(& \cancelto{0}{\ddot{\tilde{\bar{N}}}'_{iak} \dot{\varepsilon}_i} + \cancelto{0}{\tilde{\bar{N}}'_{iak} \ddot{\varepsilon}_i} + \cancelto{0}{\ddot{\bar{N}}'_{ia} \tilde{\bar{\varepsilon}}_{ik}} + \cancelto{0}{\dot{\bar{N}}'_{ia} \dot{\tilde{\bar{\varepsilon}}}_{ik}} + \cancelto{0}{\ddot{\tilde{\bar{N}}}_{ik} \bar{\varepsilon}'_{ia}} + \cancelto{0}{\dot{\tilde{\bar{N}}}_{ik} \dot{\bar{\varepsilon}}'_{ia}} + \cancelto{0}{\ddot{\bar{N}}_i \tilde{\bar{\varepsilon}}'_{iak}} + \cancelto{0}{\dot{\bar{N}}_i \dot{\tilde{\bar{\varepsilon}}}'_{iak}} \\
& + \cancelto{0}{\ddot{\bar{N}}'_{ia} \tilde{\bar{\varepsilon}}_{ik}} + \dot{\bar{N}}'_{ia} \dot{\tilde{\bar{\varepsilon}}}_{ik} + \dot{\bar{N}}'_{ia} \dot{\tilde{\bar{\varepsilon}}}_{ik} + N'_{ia} \cancelto{0}{\ddot{\tilde{\bar{\varepsilon}}}_{ik}} + \ddot{\bar{N}}_i \tilde{\bar{\varepsilon}}'_{iak} + \dot{N}_i \dot{\tilde{\bar{\varepsilon}}}'_{iak} + \cancelto{0}{\ddot{\tilde{\bar{N}}}'_{iak} \varepsilon_i} + \tilde{\bar{N}}'_{iak} \ddot{\varepsilon}_i \\
& + \cancelto{0}{\ddot{\tilde{\bar{N}}}_{ik} \varepsilon'_{ia}} + \dot{\tilde{\bar{N}}}_{ik} \dot{\varepsilon}'_{ia} + \cancelto{0}{\ddot{\tilde{\bar{N}}}_{ik} \dot{\varepsilon}'_{ia}} + \tilde{\bar{N}}_{ik} \cancelto{0}{\ddot{\varepsilon}'_{ia}} + \cancelto{0}{\dot{\tilde{\bar{M}}}'_{iak} \kappa_i} + \tilde{\bar{M}}'_{iak} \cancelto{0}{\dot{\kappa}_i} + \cancelto{0}{\ddot{\tilde{\bar{M}}}_{ik} \kappa'_{ia}} + \dot{\tilde{\bar{M}}}_{ik} \cancelto{0}{\dot{\kappa}'_{ia}} \Bigg) d\Omega \Bigg] u_a \bar{u}_k \\
= \Bigg[\frac{1}{2} \int_\Omega \Bigg(& 2 \dot{\bar{N}}'_{ia} \dot{\tilde{\bar{\varepsilon}}}_{ik} + \ddot{\bar{N}}_i \tilde{\bar{\varepsilon}}'_{iak} + \tilde{\bar{N}}'_{iak} \ddot{\varepsilon}_i + \dot{\tilde{\bar{N}}}_{ik} \dot{\varepsilon}'_{ia} \Bigg) d\Omega \Bigg] u_a
\end{aligned}
\tag{6.26}
$$

From Equation 6.24, the second derivation with respect to the imperfection field can be found resulting in a third-order tensor and it is equal to Equation 6.27.

$$
\begin{aligned}
\tilde{\tilde{\psi}}'_c \boldsymbol{u_a \bar{u}_k \bar{u}_l} = \Bigg[\frac{1}{2} \int_\Omega \Bigg(& \cancelto{0}{\dot{\tilde{\tilde{\bar{N}}}}_{iakl} \bar{\varepsilon}_i} + \tilde{\tilde{\bar{N}}}'_{iak} \tilde{\tilde{\varepsilon}}_{il} + \tilde{\tilde{\bar{N}}}'_{ial} \tilde{\tilde{\varepsilon}}_{ik} + \bar{N}'_{ia} \cancelto{0}{\dot{\tilde{\tilde{\varepsilon}}}_{ikl}} + \cancelto{0}{\dot{\tilde{\tilde{\bar{N}}}}_{ikl} \bar{\varepsilon}'_{ia}} + \tilde{\bar{N}}_{ik} \tilde{\tilde{\varepsilon}}'_{ial} + \tilde{\bar{N}}_{il} \tilde{\tilde{\varepsilon}}'_{iak} \\
& + \bar{N}_i \cancelto{0}{\dot{\tilde{\tilde{\varepsilon}}}'_{iakl}} + \cancelto{0}{\dot{\bar{N}}'_{ial} \tilde{\tilde{\varepsilon}}_{ik}} + N'_{ia} \cancelto{0}{\dot{\tilde{\tilde{\varepsilon}}}_{ikl}} + \cancelto{0}{\dot{\bar{N}}_{il} \tilde{\bar{\varepsilon}}'_{iak}} + N_i \cancelto{0}{\dot{\tilde{\tilde{\varepsilon}}}'_{iakl}} + \cancelto{0}{\dot{\tilde{\tilde{\bar{N}}}}'_{iakl} \varepsilon_i} + \cancelto{0}{\tilde{\bar{N}}'_{iak} \dot{\varepsilon}_{il}} \\
& + \cancelto{0}{\dot{\tilde{\tilde{\bar{N}}}}_{ikl} \varepsilon'_{ia}} + \tilde{\bar{N}}_{ik} \cancelto{0}{\dot{\tilde{\bar{\varepsilon}}}'_{ial}} + \cancelto{0}{\dot{\tilde{\tilde{\bar{M}}}}'_{iakl} \kappa_i} + \tilde{\bar{M}}'_{iak} \cancelto{0}{\dot{\tilde{\kappa}}_{il}} + \cancelto{0}{\dot{\tilde{\tilde{\bar{M}}}}_{ikl} \kappa'_{ia}} + \tilde{\bar{M}}_{ik} \cancelto{0}{\dot{\tilde{\kappa}}'_{ial}} \Bigg) d\Omega \Bigg] u_a \bar{u}_k \bar{u}_l \\
= \Bigg[\frac{1}{2} \int_\Omega \Big(& \tilde{\tilde{\bar{N}}}'_{iak} \tilde{\tilde{\varepsilon}}_{il} + \tilde{\tilde{\bar{N}}}'_{ial} \tilde{\tilde{\varepsilon}}_{ik} + \tilde{\bar{N}}_{ik} \tilde{\tilde{\varepsilon}}'_{ial} + \tilde{\bar{N}}_{il} \tilde{\tilde{\varepsilon}}'_{iak} \Big) d\Omega \Bigg] u_a \bar{u}_k \bar{u}_l
\end{aligned}
\tag{6.27}
$$

Equation 6.27 is used to find the derivatives to the load factor (λ) as shown in Equation 6.28 and 6.29.

$$\begin{aligned}\dot{\tilde{\psi}}'_c \boldsymbol{u_a \bar{u}_k \bar{u}_l} = &\left[\frac{1}{2}\int_\Omega \left(\cancelto{0}{\dot{\tilde{N}}'_{iak}\tilde{\bar{\varepsilon}}_{il}} + \tilde{N}'_{iak}\dot{\tilde{\bar{\varepsilon}}}_{il} + \cancelto{0}{\dot{\tilde{N}}'_{ial}\tilde{\bar{\varepsilon}}_{ik}} + \tilde{N}'_{ial}\dot{\tilde{\bar{\varepsilon}}}_{ik}\right.\right.\\ &\left.\left. + \dot{\tilde{N}}_{ik}\tilde{\bar{\varepsilon}}'_{ial} + \tilde{N}_{ik}\cancelto{0}{\dot{\tilde{\bar{\varepsilon}}}'_{ial}} + \dot{\tilde{N}}_{il}\tilde{\bar{\varepsilon}}'_{iak} + \tilde{N}_{il}\cancelto{0}{\dot{\tilde{\bar{\varepsilon}}}'_{iak}}\right) d\Omega\right] u_a \bar{u}_k \bar{u}_l\\ = &\left[\frac{1}{2}\int_\Omega \left(\tilde{N}'_{iak}\dot{\tilde{\bar{\varepsilon}}}_{il} + \tilde{N}'_{ial}\dot{\tilde{\bar{\varepsilon}}}_{ik} + \dot{\tilde{N}}_{ik}\tilde{\bar{\varepsilon}}'_{ial} + \dot{\tilde{N}}_{il}\tilde{\bar{\varepsilon}}'_{iak}\right) d\Omega\right] u_a \bar{u}_k \bar{u}_l\end{aligned} \tag{6.28}$$

$$\ddot{\tilde{\psi}}'_c \boldsymbol{u_a \bar{u}_k \bar{u}_l} = \boldsymbol{0} \tag{6.29}$$

From Equation 6.21 the first derivative with respect to the imperfect shape ($\bar{\boldsymbol{u}}$) is equal to Equation 6.30.

$$\begin{aligned}\tilde{\psi}''_c \boldsymbol{u_a u_b \bar{u}_k} = &\left[\frac{1}{2}\int_\Omega \left(\tilde{\tilde{N}}'_{iak}\bar{\varepsilon}'_{ib} + \bar{N}'_{ia}\tilde{\bar{\varepsilon}}'_{ibk} + \tilde{\tilde{N}}'_{ibk}\bar{\varepsilon}'_{ia} + \bar{N}'_{ib}\tilde{\bar{\varepsilon}}'_{iak} + \cancelto{0}{\tilde{N}''_{iabk}\bar{\varepsilon}_i} + N''_{iab}\tilde{\bar{\varepsilon}}_{ik} + \cancelto{0}{\tilde{N}'_{iak}\bar{\varepsilon}'_{ib}}\right.\right.\\ &+ N'_{ia}\tilde{\bar{\varepsilon}}'_{ibk} + \cancelto{0}{\tilde{N}'_{ibk}\bar{\varepsilon}'_{ia}} + N'_{ib}\tilde{\bar{\varepsilon}}'_{iak} + \tilde{\tilde{N}}'_{iak}\varepsilon'_{ib} + \bar{N}'_{ia}\cancelto{0}{\tilde{\bar{\varepsilon}}'_{ibk}} + \tilde{\tilde{N}}'_{ibk}\varepsilon'_{ia} + \bar{N}'_{ib}\cancelto{0}{\tilde{\bar{\varepsilon}}'_{iak}}\\ &\left.\left.+\tilde{\tilde{N}}_{ik}\varepsilon''_{iab} + \bar{N}_i\cancelto{0}{\tilde{\bar{\varepsilon}}''_{iabk}} + \tilde{\tilde{M}}'_{iak}\kappa'_{ib} + \bar{M}'_{ia}\cancelto{0}{\tilde{\kappa}'_{ibk}} + \tilde{\tilde{M}}'_{ibk}\kappa'_{ia} + \bar{M}'_{ib}\cancelto{0}{\tilde{\kappa}'_{iak}}\right) d\Omega\right] u_a u_b \bar{u}_k\\ = &\left[\frac{1}{2}\int_\Omega \left(\tilde{\tilde{N}}'_{iak}\bar{\varepsilon}'_{ib} + \bar{N}'_{ia}\tilde{\bar{\varepsilon}}'_{ibk} + \tilde{\tilde{N}}'_{ibk}\bar{\varepsilon}'_{ia} + \bar{N}'_{ib}\tilde{\bar{\varepsilon}}'_{iak} + N''_{iab}\tilde{\bar{\varepsilon}}_{ik} + N'_{ia}\tilde{\bar{\varepsilon}}'_{ibk}\right.\right.\\ &\left.\left. + N'_{ib}\tilde{\bar{\varepsilon}}'_{iak} + \tilde{\tilde{N}}'_{iak}\varepsilon'_{ib} + + \tilde{\tilde{N}}'_{ibk}\varepsilon'_{ia} + \tilde{\tilde{N}}_{ik}\varepsilon''_{iab} + \tilde{\tilde{M}}'_{iak}\kappa'_{ib} + \tilde{\tilde{M}}'_{ibk}\kappa'_{ia}\right) d\Omega\right] u_a u_b \bar{u}_k\end{aligned} \tag{6.30}$$

Equation 6.30 can be used to compute the first and second derivative to λ, as shown in Equation 6.31 and 6.32.

$$\begin{aligned}\dot{\tilde{\psi}}''_c \boldsymbol{u_a u_b \bar{u}_k} = &\left[\frac{1}{2}\int_\Omega \left(\cancelto{0}{\dot{\tilde{\tilde{N}}}'_{iak}\bar{\varepsilon}'_{ib}} + \tilde{\tilde{N}}'_{iak}\cancelto{0}{\dot{\bar{\varepsilon}}'_{ib}} + \cancelto{0}{\dot{\bar{N}}'_{ia}\tilde{\bar{\varepsilon}}'_{ibk}} + \bar{N}'_{ia}\cancelto{0}{\dot{\tilde{\bar{\varepsilon}}}'_{ibk}} + \cancelto{0}{\dot{\tilde{\tilde{N}}}'_{ibk}\bar{\varepsilon}'_{ia}} + \tilde{\tilde{N}}'_{ibk}\cancelto{0}{\dot{\bar{\varepsilon}}'_{ia}} + \cancelto{0}{\dot{\bar{N}}'_{ib}\tilde{\bar{\varepsilon}}'_{iak}}\right.\right.\\ &+ \bar{N}'_{ib}\cancelto{0}{\dot{\tilde{\bar{\varepsilon}}}'_{iak}} + \cancelto{0}{\dot{\bar{N}}''_{iab}\tilde{\bar{\varepsilon}}_{ik}} + N''_{iab}\dot{\tilde{\bar{\varepsilon}}}_{ik} + \cancelto{0}{\dot{\bar{N}}'_{ia}\tilde{\bar{\varepsilon}}'_{ibk}} + N'_{ia}\dot{\tilde{\bar{\varepsilon}}}'_{ibk} + \cancelto{0}{\dot{\bar{N}}'_{ib}\tilde{\bar{\varepsilon}}'_{iak}} + N'_{ib}\cancelto{0}{\dot{\tilde{\bar{\varepsilon}}}'_{iak}}\\ &+ \cancelto{0}{\dot{\tilde{\tilde{N}}}'_{iak}\varepsilon'_{ib}} + \tilde{\tilde{N}}'_{iak}\dot{\varepsilon}'_{ib} + \cancelto{0}{\dot{\tilde{\tilde{N}}}'_{ibk}\varepsilon'_{ia}} + \tilde{\tilde{N}}'_{ibk}\dot{\varepsilon}'_{ia} + \dot{\tilde{\tilde{N}}}_{ik}\varepsilon''_{iab} + \tilde{\tilde{N}}_{ik}\cancelto{0}{\dot{\varepsilon}''_{iab}} + \cancelto{0}{\dot{\tilde{\tilde{M}}}'_{iak}\kappa'_{ib}}\\ &\left.\left.+\tilde{\tilde{M}}'_{iak}\cancelto{0}{\dot{\kappa}'_{ib}} + \cancelto{0}{\dot{\tilde{\tilde{M}}}'_{ibk}\kappa'_{ia}} + \tilde{\tilde{M}}'_{ibk}\cancelto{0}{\dot{\kappa}'_{ia}}\right) d\Omega\right] u_a u_b \bar{u}_k\\ = &\left[\frac{1}{2}\int_\Omega \left(N''_{iab}\dot{\tilde{\bar{\varepsilon}}}_{ik} + \tilde{N}'_{iak}\dot{\varepsilon}'_{ib} + \tilde{N}'_{ibk}\dot{\varepsilon}'_{ia} + \dot{\tilde{N}}_{ik}\varepsilon''_{iab}\right) d\Omega\right] u_a u_b \bar{u}_k\end{aligned} \tag{6.31}$$

$$\ddot{\tilde{\psi}}''_c \boldsymbol{u_a u_b \bar{u}_k} = \boldsymbol{0} \tag{6.32}$$

From Equation 6.27, the second derivative with respect to the displacement to form a fourth-order tensor equal to Equation 6.33. Alternatively, Equation 6.30 could also have been used as an initial starting point to compute Equation 6.33 and the result would have been the same.

$$\begin{aligned}\tilde{\tilde{\psi}}_c''\boldsymbol{u_a u_b \bar{u}_k \bar{u}_l} = \Bigg[\frac{1}{2}\int_\Omega \Bigg(&\cancelto{0}{\tilde{\tilde{N}}_{iabk}''\tilde{\tilde{\varepsilon}}_{il}} + \tilde{\tilde{N}}_{iak}'\tilde{\tilde{\varepsilon}}_{ibl}' + \cancelto{0}{\tilde{\tilde{N}}_{iabl}''\tilde{\tilde{\varepsilon}}_{ik}} + \tilde{\tilde{N}}_{ial}'\tilde{\tilde{\varepsilon}}_{ibk}' \\ &+\tilde{\tilde{N}}_{ibk}'\tilde{\tilde{\varepsilon}}_{ial}' + \tilde{\tilde{N}}_{ik}\cancelto{0}{\tilde{\tilde{\varepsilon}}_{iabl}''} + \tilde{\tilde{N}}_{ibl}'\tilde{\tilde{\varepsilon}}_{iak}' + \tilde{\tilde{N}}_{il}\cancelto{0}{\tilde{\tilde{\varepsilon}}_{iabk}''}\Bigg) d\Omega\Bigg] u_a u_b \bar{u}_k \bar{u}_l \\ = \Bigg[\frac{1}{2}\int_\Omega &\left(\tilde{\tilde{N}}_{iak}'\tilde{\tilde{\varepsilon}}_{ibl}' + \tilde{\tilde{N}}_{ial}'\tilde{\tilde{\varepsilon}}_{ibk}' + \tilde{\tilde{N}}_{ibk}'\tilde{\tilde{\varepsilon}}_{ial}' + \tilde{\tilde{N}}_{ibl}'\tilde{\tilde{\varepsilon}}_{iak}'\right) d\Omega\Bigg] u_a u_b \bar{u}_k \bar{u}_l\end{aligned} \tag{6.33}$$

$$\dot{\tilde{\tilde{\psi}}}_c''\boldsymbol{u_a u_b \bar{u}_k \bar{u}_l} = \boldsymbol{0} \tag{6.34}$$

Finally, the four-order tensor presented in Equation 6.35, can be derived from Equation 6.22.

$$\begin{aligned}\tilde{\psi}_c'''\boldsymbol{u_a u_b u_c \bar{u}_k} = \Bigg[\frac{1}{2}\int_\Omega \Bigg(&\cancelto{0}{\tilde{\tilde{N}}_{iabk}''\tilde{\tilde{\varepsilon}}_{ic}'} + N_{iab}''\tilde{\tilde{\varepsilon}}_{ick}' + \cancelto{0}{\tilde{\tilde{N}}_{iack}''\tilde{\tilde{\varepsilon}}_{ib}'} + N_{iac}''\tilde{\tilde{\varepsilon}}_{ibk}' + \cancelto{0}{\tilde{\tilde{N}}_{ibck}''\tilde{\tilde{\varepsilon}}_{ia}'} + N_{ibc}''\tilde{\tilde{\varepsilon}}_{iak}' \\ &+\tilde{\tilde{N}}_{iak}'\varepsilon_{ibc}'' + \bar{N}_{ia}'\cancelto{0}{\tilde{\tilde{\varepsilon}}_{ibck}''} + \tilde{\tilde{N}}_{ibk}'\varepsilon_{iac}'' + \bar{N}_{ib}'\cancelto{0}{\tilde{\tilde{\varepsilon}}_{iack}''} + \tilde{\tilde{N}}_{ick}'\varepsilon_{iab}'' + \bar{N}_{ic}'\cancelto{0}{\tilde{\tilde{\varepsilon}}_{iabk}''}\Bigg) d\Omega\Bigg] u_a u_b u_c \bar{u}_k \\ = \Bigg[\frac{1}{2}\int_\Omega &\left(N_{iab}''\tilde{\tilde{\varepsilon}}_{ick}' + N_{iac}''\tilde{\tilde{\varepsilon}}_{ibk}' + N_{ibc}''\tilde{\tilde{\varepsilon}}_{iak}' + \tilde{\tilde{N}}_{iak}'\varepsilon_{ibc}'' + \tilde{\tilde{N}}_{ibk}'\varepsilon_{iac}'' + \tilde{\tilde{N}}_{ick}'\varepsilon_{iab}''\right) d\Omega\Bigg] u_a u_b u_c \bar{u}_k\end{aligned} \tag{6.35}$$

The higher-order derivatives are equal to zero, as shown below, concluding the derivation of the imperfect functional derivatives.

$$\dot{\tilde{\psi}}_c'''\boldsymbol{u_a u_b u_c \bar{u}_k} = \boldsymbol{0} \tag{6.36}$$

$$\tilde{\tilde{\psi}}_c'''\boldsymbol{u_a u_b u_c \bar{u}_k \bar{u}_l} = \boldsymbol{0} \tag{6.37}$$

$$\dot{\tilde{\tilde{\psi}}}_c'''\boldsymbol{u_a u_b u_c \bar{u}_k \bar{u}_l} = \boldsymbol{0} \tag{6.38}$$

6.6. Functional Derivatives for Linear Pre-buckling

The assumption of linear pre-buckling also impacts the functional derivatives. The final expression for both the perfect and imperfect functional derivatives can be found in section A.3. If linear pre-buckling is assumed, the perfect second-order derivative (ϕ_c'') equals the constitutive stiffness matrix of the system [18, 22].

6.7. Conclusion Functional Derivatives

This concludes the derivation of all functional derivatives for an imperfect plate utilising Donnell kinematics. A short overview of the non-zero derivatives for each solution possibility is presented in Table 6.2. A total of four solution possibilities were defined based on two different assumptions. The first assumption is based on which approach is taken to derive the expansion of the potential energy and boils down to if the non-linear terms of the imperfect structure are taken into consideration or assumed equal to zero. The second assumption depends on whether the pre-buckling is assumed to linear or non-linear. These functional derivatives are the only terms that remain in the expansion of the total potential energy and the other terms cancel to zero.

This derivation is specific for an imperfect plate using Donnell Kinematics. For any other structure or kinematic relationship the functional derivatives would have to be reevaluated.

	Functional Derivatives	
	Perfect	*Imperfect*
PL	ϕ_c'', ϕ_c''', ϕ_c^{iv}, $\dot{\phi}_c''$	ψ_c', ψ_c'', ψ_c''', $\tilde{\psi}_c'$, $\dot{\tilde{\psi}}_c'$, $\tilde{\psi}_c''$, $\tilde{\psi}_c'''$
BL	ϕ_c'', ϕ_c''', ϕ_c^{iv}, $\dot{\phi}_c''$	ψ_c', ψ_c'', ψ_c''', $\tilde{\psi}_c'$, $\dot{\tilde{\psi}}_c'$, $\tilde{\psi}_c''$, $\tilde{\psi}_c'''$, $\tilde{\tilde{\psi}}_c''$
PN	ϕ_c'', ϕ_c''', ϕ_c^{iv}, $\dot{\phi}_c''$, $\ddot{\phi}_c''$, $\dot{\phi}_c'''$	ψ_c', ψ_c'', ψ''', $\tilde{\psi}_c'$, $\dot{\tilde{\psi}}_c'$, $\ddot{\tilde{\psi}}_c'$, $\tilde{\psi}_c''$, $\dot{\tilde{\psi}}_c''$, $\tilde{\psi}_c'''$
BN	ϕ_c'', ϕ_c''', ϕ_c^{iv}, $\dot{\phi}_c''$, $\ddot{\phi}_c''$, $\dot{\phi}_c'''$	ψ_c', ψ_c'', ψ''', $\tilde{\psi}_c'$, $\dot{\tilde{\psi}}_c'$, $\ddot{\tilde{\psi}}_c'$, $\tilde{\tilde{\psi}}_c'$, $\dot{\tilde{\tilde{\psi}}}_c'$, $\tilde{\psi}_c''$, $\dot{\tilde{\psi}}_c''$, $\tilde{\tilde{\psi}}_c''$, $\tilde{\psi}_c'''$

Table 6.2: Overview of non-zero functional derivatives for each solution possibility.

7

Asymptotic Analysis

The final step for including imperfections in the displacement-based Koiter methodology is to derive expressions for the initial post-buckling characteristics. There are two different possibilities to formulate these properties. The first approach is similar to the perfect methodology and the goal is to find an expression for a_I and b_I that also includes imperfections within this term. This approach is presented in detail in section 7.1. On the other hand, the alternative solution methodology assumes that the initial post-buckling coefficients are derived from the perfect structure and that the imperfection sensitivity of a structure can be measured by introducing two new coefficients, α and β, which are also referred to as the imperfection form factors. A detailed explanation of this methodology can be found in section 7.2.

7.1. Initial Imperfect Post-buckling Coefficients

The single mode asymptotic expansions for the load parameters and the displacement field are incorporated in either possible expansion of the total potential energy, previously derived in chapter 6. After performing the substitution, the brackets are expanded and terms are grouped according to their powers of ξ, up to ξ^6 to find the initial post-buckling terms a_I and b_I to satisfy the equilibrium condition. The asymptotic expansions are presented in Equation 4.37 and 4.38 and repeated below for convenience.

$$\lambda - \lambda_c = a_I \lambda_c \xi + b_I \lambda_c \xi^2 \tag{4.37}$$

$$\boldsymbol{u} - \boldsymbol{u_c} = \boldsymbol{v} = \xi \boldsymbol{u_I} + \xi^2 \boldsymbol{u_{II}} + \xi^3 \boldsymbol{u_{III}} \tag{4.38}$$

The objective is to find an expression that combines the perfect post-buckling coefficients with a correction term for the imperfections. This correction term should be dependent on the imperfect functional derivatives, similar to what is presented in Equation 7.1 and 7.2. The aim of finding this solution is to immediately observe the effect of the imperfection. It also serves as a verification for when the imperfection amplitude is set to zero, the methodology including imperfections should yield the same post-buckling coefficients as the perfect methodology. It is expected that the first post-buckling coefficient (a_I) will change from a zero value to a non-zero value with the inclusion of imperfections, while the second post-buckling coefficient will decrease due to the imperfection incorporated into the structure.

$$a_{I,imperfect} = a_{I,perfect} + constant(\psi^{(n)}, \dot{\psi}^{(n)}, \ddot{\psi}^{(n)}) \tag{7.1}$$

$$b_{I,imperfect} = b_{I,perfect} + constant(\psi^{(n)}, \dot{\psi}^{(n)}, \ddot{\psi}^{(n)}) \tag{7.2}$$

The expressions for the perfect initial post-buckling coefficients are also repeated for convenience. The first coefficient remains the same, even if the pre-buckling is assumed to be linear. The second post-buckling coefficient changes to Equation 7.3.

$$a_I = -\frac{1}{2\lambda_c} \frac{\boldsymbol{u_I^3} \phi_c'''}{\boldsymbol{u_I^2} \dot{\phi}_c''} \tag{4.40}$$

$$b_I = -\left(\frac{1}{6}\boldsymbol{u_I}^4\phi_c^{iv} + \frac{1}{2}a_I\lambda_c\boldsymbol{u_I}^3\dot{\phi}_c''' + \frac{1}{2}a_I^2\lambda_c^2\boldsymbol{u_I}^2\ddot{\phi}_c'' + \boldsymbol{u_I}^2\boldsymbol{u_{II}}\phi_c'''\right) / \left(\lambda_c\boldsymbol{u_I}^2\dot{\phi}_c''\right) \tag{4.41}$$

$$b_{I,linear} = -\left(\frac{1}{6}\boldsymbol{u_I}^4\phi_c^{iv} + \boldsymbol{u_I}^2\boldsymbol{u_{II}}\phi_c'''\right) / \left(\lambda_c\boldsymbol{u_I}^2\dot{\phi}_c''\right) \tag{7.3}$$

This solution approach of substituting the asymptotic expansions into the total potential energy and finding the unknowns such that they assure the equilibrium condition is done for each of the four solution possibilities and concludes how effective each approach is at determining the initial post-buckling characteristics.

7.1.1. Option 1: PL

After substituting the asymptotic expansions into the reduced expansion of the total potential energy as formulated by Pignataro, Equation 7.4 can be found. The underlined terms indicate all the imperfect terms. When the imperfection amplitude is set to zero all underlined terms disappear, and the remaining equation matches the one obtained for the perfect case, as presented in Equation B.2. This shows that the formulation of the perfect terms is correct.

$$\begin{aligned}
&\xi\left(\underline{\bar{\xi}\hat{\boldsymbol{u}}\dot{\tilde{\psi}}_c'a_I\lambda_c + \bar{\xi}\hat{\boldsymbol{u}}\tilde{\psi}_c''\boldsymbol{u}_I} + \phi_c''\boldsymbol{u}_I\right)\delta\boldsymbol{u}\\
+\xi^2&\left(\underline{\bar{\xi}\hat{\boldsymbol{u}}\dot{\tilde{\psi}}_c'b_I\lambda_c + \frac{1}{2}\bar{\xi}\hat{\boldsymbol{u}}\tilde{\psi}_c'''\boldsymbol{u_I}^2 + \bar{\xi}\hat{\boldsymbol{u}}\tilde{\psi}_c''\boldsymbol{u}_{II}} + \dot{\phi}_c''a_I\lambda_c\boldsymbol{u}_I + \frac{1}{2}\phi_c'''\boldsymbol{u}_I^2 + \phi_c''\boldsymbol{u}_{II}\right)\delta\boldsymbol{u}\\
+\xi^3&\left(\underline{\bar{\xi}\hat{\boldsymbol{u}}\tilde{\psi}_c'''\boldsymbol{u_I}\boldsymbol{u_{II}}} + \dot{\phi}_c''a_I\lambda_c\boldsymbol{u}_{II} + \dot{\phi}_c''b_I\lambda_c\boldsymbol{u}_I + \phi_c'''\boldsymbol{u}_I\boldsymbol{u}_{II} + \frac{1}{6}\phi_c^{iv}\boldsymbol{u}_I^3\right)\delta\boldsymbol{u}\\
+\xi^4&\left(\underline{\frac{1}{2}\bar{\xi}\hat{\boldsymbol{u}}\tilde{\psi}_c'''\boldsymbol{u_{II}}^2} + \dot{\phi}_c''b_I\lambda_c\boldsymbol{u}_{II} + \frac{1}{2}\phi_c'''\boldsymbol{u}_{II}^2 + \frac{1}{2}\phi_c^{iv}\boldsymbol{u}_I^2\boldsymbol{u}_{II}\right)\delta\boldsymbol{u}\\
&+\frac{1}{2}\xi^5\phi_c^{iv}\boldsymbol{u}_I\boldsymbol{u}_{II}^2\delta\boldsymbol{u} + \frac{1}{6}\xi^6\phi_c^{iv}\boldsymbol{u}_{II}^3\delta\boldsymbol{u} + \underline{\bar{\xi}\hat{\boldsymbol{u}}\tilde{\psi}_c'\delta\boldsymbol{u}} = 0
\end{aligned} \tag{7.4}$$

It is possible to derive a_I from the expression multiplied by ξ, according to Equation 7.5 if one assumes $\delta\boldsymbol{u} = \boldsymbol{u}_I$. However, it is problematic that the first post-buckling coefficient is not derived from the terms related to ξ^2. If the imperfection amplitude ($\bar{\xi}$) is set to zero in the methodology including imperfections it does not equal the coefficient derived for the methodology without imperfections, given in Equation 4.40. This inconsistency indicates that this specific approach never yields realistic post-buckling coefficients.

$$a_I = \frac{\bar{\xi}\hat{\boldsymbol{u}}\tilde{\psi}_c''\boldsymbol{u}_I^2 + \phi_c''\boldsymbol{u}_I^2}{-\bar{\xi}\hat{\boldsymbol{u}}\dot{\tilde{\psi}}_c'\lambda_c\boldsymbol{u}_I} \tag{7.5}$$

If the terms related to ξ^2 are inspected to overcome this irregularity, it is evident that this expression is dependent on three unknowns, namely the first and the second initial post-buckling coefficients (a_I and b_I) and the second order displacement-field ($\boldsymbol{u}_{II}$). The arbitrary value $\delta\boldsymbol{u} = \boldsymbol{u}_I$ can be used resulting in the first-order displacement field being orthogonal to the second-order displacement field. Due to this orthogonality the terms $\bar{\xi}\hat{\boldsymbol{u}}\tilde{\psi}_c''\boldsymbol{u}_I\boldsymbol{u}_{II}$ and $\phi_c''\boldsymbol{u}_I\boldsymbol{u}_{II}$ equal zero.

The terms multiplied by ξ^2 that remain after the simplification of the orthogonality between the first and second-order displacement field are presented in Equation 7.6. This formulation is dependent on two unknowns and therefore impossible to get a closed expression for either of the two, but it is possible to find a formulation for the first-post-buckling coefficient that relies on the second coefficient given by Equation 7.7.

$$\xi^2\left(\bar{\xi}\hat{\boldsymbol{u}}\dot{\tilde{\psi}}_c'b_I\lambda_c\boldsymbol{u}_I + \frac{1}{2}\bar{\xi}\hat{\boldsymbol{u}}\tilde{\psi}_c'''\boldsymbol{u_I}^3 + \dot{\phi}_c''a_I\lambda_c\boldsymbol{u}_I^2 + \frac{1}{2}\phi_c'''\boldsymbol{u}_I^3\right) \tag{7.6}$$

$$a_I = \frac{\bar{\xi}\hat{\boldsymbol{u}}\dot{\tilde{\psi}}_c'b_I\lambda_c\boldsymbol{u}_I + \frac{1}{2}\bar{\xi}\hat{\boldsymbol{u}}\tilde{\psi}_c'''\boldsymbol{u_I}^3 + \frac{1}{2}\phi_c'''\boldsymbol{u}_I^3}{\dot{\phi}_c''\lambda_c\boldsymbol{u}_I^2} \tag{7.7}$$

This expression for b_I can be found from the terms multiplied with ξ^3. The assumption that $\delta\boldsymbol{u} = \boldsymbol{u}_I$ is still valid and the terms $\bar{\xi}\hat{\boldsymbol{u}}\tilde{\psi}_c'''\boldsymbol{u_I}^2\boldsymbol{u_{II}}$ and $\hat{\boldsymbol{u}}\dot{\phi}_c''a_I\lambda_c\boldsymbol{u}_I\boldsymbol{u}_{II}$ equal zero due to the orthogonality between the two displacement fields, however, the term $\phi_c'''\boldsymbol{u}_I^2\boldsymbol{u}_{II}$ is not equivalent to zero. The remaining terms multiplied by ξ^3 are presented in Equation 7.8 and this expression would yield the same formulation for the second post-buckling coefficient as given in Equation 7.3.

$$\xi^3\left(\dot{\phi}_c''b_I\lambda_c\boldsymbol{u}_I^2 + \phi_c'''\boldsymbol{u}_I^2\boldsymbol{u}_{II} + \frac{1}{6}\phi_c^{iv}\boldsymbol{u}_I^4\right) \tag{7.8}$$

Equation 7.8 cannot be used to derive b_I since the second-order displacement field is still unknown. Unfortunately, this cannot be found from the terms corresponding to ξ^4 because it contains the unknown b_I. It is not possible with the current attempts to rewrite Equation 7.4 to find a closed formulation for $\boldsymbol{u_{II}}$. Since the second-order displacement field remains unknown, the second post-buckling coefficient can not be found since it is dependent on this unknown displacement. Consequently, it also renders Equation 7.7 useless since a_I relies on b_I. Therefore it is concluded that this attempt to find imperfect initial post-buckling coefficients was not successful due to the fact that the expressions rely on two unknowns and was not possible to isolate one of them similar to the perfect approach.

7.1.2. Option 2: BL

Equation 7.9 arises when the asymptotic expansions are replaced within the potential energy according to Budiansky and by simplifying the procedure by assuming linear pre-buckling. If the imperfect functional derivatives, the underlined terms, are excluded from this expression it is equal to the perfect methodology presented in Equation B.2. This shows that no errors are made in the derivation of the perfect terms.

$$\begin{aligned}
&\xi\left(\underline{\frac{1}{2}\bar{\xi}^2\hat{\boldsymbol{u}}^2\tilde{\dot{\psi}}_c''\boldsymbol{u}_I + \bar{\xi}\hat{\boldsymbol{u}}\dot{\tilde{\psi}}_c'a_I\lambda_c} + \bar{\xi}\hat{\boldsymbol{u}}\tilde{\psi}_c''\boldsymbol{u}_I + \phi_c''\boldsymbol{u}_I\right)\delta\boldsymbol{u}\\
+\xi^2&\left(\underline{\frac{1}{2}\bar{\xi}^2\hat{\boldsymbol{u}}^2\tilde{\dot{\psi}}_c''\boldsymbol{u}_{II} + \bar{\xi}\hat{\boldsymbol{u}}\dot{\tilde{\psi}}_c'b_I\lambda_c + \frac{1}{2}\bar{\xi}\hat{\boldsymbol{u}}\tilde{\psi}_c'''\boldsymbol{u_I}^2 + \bar{\xi}\hat{\boldsymbol{u}}\tilde{\psi}_c''\boldsymbol{u}_{II}} + \dot{\phi}_c''a_I\lambda_c\boldsymbol{u}_I + \frac{1}{2}\phi_c'''\boldsymbol{u}_I^2 + \phi_c''\boldsymbol{u}_{II}\right)\delta\boldsymbol{u}\\
+\xi^3&\left(\underline{\bar{\xi}\hat{\boldsymbol{u}}\tilde{\psi}_c'''\boldsymbol{u_I}\boldsymbol{u_{II}}} + \dot{\phi}_c''a_I\lambda_c\boldsymbol{u}_{II} + \dot{\phi}_c''b_I\lambda_c\boldsymbol{u}_I + \phi_c'''\boldsymbol{u}_I\boldsymbol{u}_{II} + \frac{1}{6}\phi_c^{iv}\boldsymbol{u}_I^3\right)\delta\boldsymbol{u}\\
+\xi^4&\left(\underline{\frac{1}{2}\bar{\xi}\hat{\boldsymbol{u}}\tilde{\psi}_c'''\boldsymbol{u_{II}}^2} + \dot{\phi}_c''b_I\lambda_c\boldsymbol{u}_{II} + \frac{1}{2}\phi_c'''\boldsymbol{u}_{II}^2 + \frac{1}{2}\phi_c^{iv}\boldsymbol{u}_I^2\boldsymbol{u}_{II}\right)\delta\boldsymbol{u}\\
&+\frac{1}{2}\xi^5\phi_c^{iv}\boldsymbol{u}_I\boldsymbol{u}_{II}^2\delta\boldsymbol{u} + \frac{1}{6}\xi^6\phi_c^{iv}\boldsymbol{u}_{II}^3\delta\boldsymbol{u} + \underline{\bar{\xi}\hat{\boldsymbol{u}}\tilde{\dot{\psi}}_c'\delta\boldsymbol{u}} = 0
\end{aligned} \tag{7.9}$$

An expression for a_I can be derived from the terms multiplied by ξ and is presented in Equation 7.10. The same issue as for the PL solution approach occurs and this expression for a_I is not derived from the terms multiplied by ξ^2. If the imperfection amplitude is set to zero in this expression it would not match the expression of the perfect post-buckling coefficient presented in Equation 4.40. This difference indicates that Equation 7.10 cannot be correct.

$$a_I = \frac{\frac{1}{2}\bar{\xi}^2\hat{\boldsymbol{u}}^2\tilde{\dot{\psi}}_c''\boldsymbol{u}_I^2 + \bar{\xi}\hat{\boldsymbol{u}}\tilde{\psi}_c''\boldsymbol{u}_I^2 + \phi_c''\boldsymbol{u}_I^2}{-\bar{\xi}\hat{\boldsymbol{u}}\dot{\tilde{\psi}}_c'\lambda_c\boldsymbol{u}_I} \tag{7.10}$$

The terms related to ξ^2 are dependent on three unknowns, the first and the second initial post-buckling coefficients (a_I and b_I) and the second order displacement-field ($\boldsymbol{u}_{II}$). It is assumed that $\delta\boldsymbol{u} = \boldsymbol{u}_I$ and that the first-order displacement field is orthogonal to the second-order displacement field. As a consequence the terms $\frac{1}{2}\bar{\xi}^2\hat{\boldsymbol{u}}^2\tilde{\dot{\psi}}_c''\boldsymbol{u}_I\boldsymbol{u}_{II}$, $\bar{\xi}\hat{\boldsymbol{u}}\tilde{\psi}_c''\boldsymbol{u}_I\boldsymbol{u}_{II}$ and $\phi_c''\boldsymbol{u}_I\boldsymbol{u}_{II}$ equate to zero. The terms that remain are equal to the PL method and presented in Equation 7.6. Since the expression is equal, the formulation for a_I remains the same, which is provided in Equation 7.7. The first buckling coefficient stays dependent on the second coefficient.

The terms multiplied by ξ^3 up to ξ^6 in equilibrium equation Equation 7.9 are equal to the PL equilibrium equation presented in Equation 7.4. As the two equilibriums are equal, the same conclusion can be made. It is not possible to formulate an expression for b_I that does not rely on the second-order

displacement field. The second-order displacement cannot be found since it requires one of the post-buckling coefficients to be known. Therefore, it must be concluded that with the current attempts, it was not possible to derive expressions for the imperfect post-buckling coefficients for the BL solution approach.

7.1.3. Option 3 and 4

Since it was not possible to derive an expression for the post-buckling coefficients even with the simplification of including linear pre-buckling it was decided to not attempt deriving an expression for the coefficients for options 3 and 4 since these rely on non-linear pre-buckling. The derivation for both equations is presented in Appendix C.

7.1.4. Conclusion Initial Imperfect Post-buckling Coefficients

It was not possible to derive expressions for a_I and b_I for the case of linear pre-buckling that was able to incorporate the effect of the imperfections with the current procedure. For both the PL and the BL approach an expression for a_I could be found from the terms multiplied by ξ however, this was disregarded as it led to an inconsistency between the perfect and the imperfect displacement-based Koiter methodology. The term multiplied with ξ^2 and higher powers did not yield satisfying results for deriving an expression for the coefficients.

Even if one were successful in finding the initial post-buckling coefficients, these results would not have been useful, because a plate with an initial imperfection no longer has a bifurcation point, but instead a limit load, as depicted in Figure 2.1. The current analysis is performed around the bifurcation point, but the structure would have changed significantly from the perfect configuration, making this bifurcation point no longer relevant. Hence, the information gained by deriving the post-buckling coefficients would no longer be representative of the physical situation the plate is experiencing.

Since the attempts to find the coefficient with linear pre-buckling were unsuccessful, the case of non-linear pre-buckling was not thoroughly analyzed as this was deemed ineffective. However, if this was attempted and one was successful in finding the initial post-buckling coefficients, these results would also represent unrealistic behaviour. Since the pre-buckling is no longer linear, the stiffness of the structure would change before it buckles, indicating that the coefficients would have to be reevaluated multiple times, which would be computationally inefficient, and therefore would defeat the purpose of the Koiter methodology.

The only case where the displacement-based Koiter methodology of finding imperfect initial post-buckling coefficients might still be relevant is for a cylinder with axisymmetric imperfections and linear pre-buckling. An axisymmetric imperfection is constant along the circumference of the cylinder. Such cylinders have a bifurcation point despite the inclusion of an imperfection. Hence, one could revisit this specific methodology and derive expressions for the post-buckling coefficients. However, this is such a unique situation that this approach of finding imperfect post-buckling coefficients a_I and b_I should not be continued.

This conclusion disproves the first hypothesis made about the derivation of the initial post-buckling coefficients, which is presented below. With the current approach, it was not possible to find initial post-buckling coefficients. Besides the fact that this attempt was unsuccessful at finding formulation, the idea behind this methodology was not sound. Due to the imperfections, there is no longer a bifurcation point and thus the initial post-buckling coefficients no longer reflect reality as the plate would have buckled sooner.

H2: Hypothesis on the derivations of the initial post-buckling properties
H2.1 Initial imperfect post-buckling coefficients (a_I and b_I) can be derived by means of the displacement-based Koiter methodology.

7.1.5. Comparison Work of Budiansky

As previously noted, the initial imperfect post-buckling coefficients are only useful for the specific scenario of a cylinder with an axisymmetric imperfection, as this structure still has a bifurcation point. Budiansky [4] was able to derive post-buckling coefficients and therefore some of the differences between Budiansky and the current research are highlighted.

The derivation for the total potential energy remains exactly equal, however, the imperfection amplitude is assumed to depend on the scalar parameter according to the relationship presented in Equation 7.11.

$$\bar{\xi} = \alpha \xi^{\gamma} \tag{7.11}$$

Both asymptotic expansions are substituted into the total potential energy and the assumption that the imperfection amplitude is dependent on the scalar parameter according to Equation 7.11 is applied where $\gamma = 2$. The emerging equation is regrouped according to the power of ξ.

The terms multiplied by ξ^2 are presented in Equation 7.12. An expression for a_I can be formulated according to Equation 7.13 where it is assumed that $\delta \boldsymbol{u} = \boldsymbol{u}_I$. It is evident that this expression for the initial post-buckling coefficient is dependent on the perfect coefficient and a correcting term dependent on the imperfection. This expression for a_I is used to reconstruct the load path in the work of Budiansky according to Equation 7.14, where α can be found by rewriting Equation 7.11.

$$\xi^2 \left(\alpha \hat{\boldsymbol{u}} \tilde{\psi}_c' + \frac{1}{2} \phi_c''' \boldsymbol{u}_{\boldsymbol{I}}^2 + \phi_c'' \boldsymbol{u}_{\boldsymbol{II}} + \dot{\phi}_c'' a_I \lambda_c \boldsymbol{u}_{\boldsymbol{I}} \right) \delta \boldsymbol{u} \tag{7.12}$$

$$a_I = -\frac{1}{2\lambda_c} \frac{\boldsymbol{u}_{\boldsymbol{I}}^3 \phi_c'''}{\boldsymbol{u}_{\boldsymbol{I}}^2 \dot{\phi}_c''} - \alpha \frac{\hat{\boldsymbol{u}} \tilde{\psi}_c' \boldsymbol{u}_I}{\dot{\phi}_c'' \lambda_c \boldsymbol{u}_I^2} = a_{I,perfect} - \alpha a_{I,imperfect} \tag{7.13}$$

$$\lambda \approx \lambda_c + a_{I,perfect} \xi - (\alpha a_{I,imperfect}) \, \xi \tag{7.14}$$

If the initial structure without imperfection is symmetric the perfect initial post-buckling coefficient ($a_{I,perfect}$) is equal to zero and thus Equation 7.14 cannot be used to reconstruct the load. An expression for the second initial imperfect post-buckling coefficient is created to define the load again. To formulate an expression for b_I, it is assumed that $\gamma = 3$. The emerging expression for the second coefficient is presented in Equation 7.15, and clearly consists of the perfect coefficient adjusted by a term that relies on the imperfect functional derivatives. The coefficient α can be found by rewriting Equation 7.11.

$$\begin{aligned} b_I = &- \left(\frac{1}{6} \boldsymbol{u}_{\boldsymbol{I}}^4 \phi_c^{iv} + \frac{1}{2} a_I \lambda_c \boldsymbol{u}_{\boldsymbol{I}}^3 \dot{\phi}_c''' + \frac{1}{2} a_I^2 \lambda_c^2 \boldsymbol{u}_{\boldsymbol{I}}^2 \ddot{\phi}_c'' + \boldsymbol{u}_{\boldsymbol{I}}^2 \boldsymbol{u}_{\boldsymbol{II}} \phi_c''' \right) / \left(\lambda_c \boldsymbol{u}_{\boldsymbol{I}}^2 \dot{\phi}_c'' \right) - \alpha \lambda_c \frac{\hat{\boldsymbol{u}} \tilde{\psi}_c' \boldsymbol{u}_I}{\dot{\phi}_c'' \lambda_c \boldsymbol{u}_I^2} \\ &= b_{I,perfect} - -\alpha b_{I,imperfect} \end{aligned} \tag{7.15}$$

The main difference between Budiansky and the current work is that Budiansky simplifies the procedure by assuming that the imperfection amplitude is dependent on ξ. If this assumption is made the current work could achieve the same conclusion. The issue with Budiansky is that $\gamma = 2$ for the computation of a_I, whereas it is equal to three to compute b_I, therefore both expressions cannot be used at the same time due to the different assumptions. The goal of this thesis was to compute both initial post-buckling coefficients and thus the formulations presented by Budiansky cannot be used directly in the current methodology of this thesis.

However, the assumption that the imperfection amplitude relies on the load parameter could be useful and the current approach could be reevaluated for $\bar{\xi} = \alpha \xi^2$. The expression for a_I would remain equal to Equation 7.13, but the expression for the second initial post-buckling coefficient b_I should be computed as well as the second-order displacement field. It was decided not to pursue this path since formulating these coefficients would only apply to the specific scenario of a cylinder with axisymmetric imperfection and was not deemed useful within the scope of this thesis.

7.2. Imperfection Form Factors

A more conventional approach to determining the initial post-buckling characteristics of a structure involves using the single-mode asymptotic expansion for the load parameter including additional terms that relate to the presence of imperfections. This expansion is given by Equation 7.16 [19, 46, 47, 44], compared to the perfect asymptotic expansion presented in Equation 4.37. In the imperfect load expansion, the parameters α and β are known as imperfection form factors. The coefficients are not

unique for each imperfection shape but depend on how the imperfection is normalised. To better quantify the sensitivity to imperfections, the term $\frac{\beta}{\alpha}$ is preferred over just the numerical values of α or β. A higher value of this ratio corresponds to a lower sensitivity to imperfections, as visually presented in Figure 7.1.

$$\xi\left(\lambda-\lambda_c\right)=a_I\lambda_c\xi^2+b_I\lambda_c\xi^3-\alpha\lambda_c\bar{\xi}-\beta\left(\lambda-\lambda_c\right)\bar{\xi}+\ldots \tag{7.16}$$

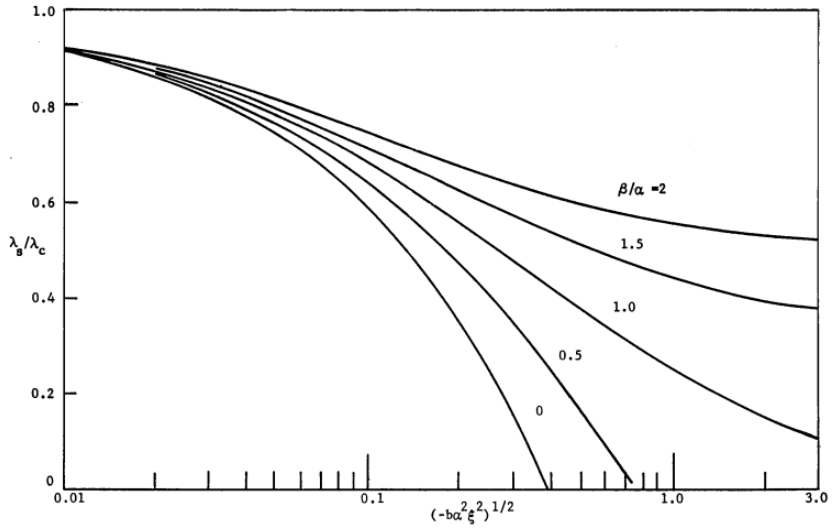

Figure 7.1: The influence of $\frac{\beta}{\alpha}$ on the buckling load [48].

For the imperfect asymptotic expansion, given by Equation 7.16, the post-buckling coefficients a_I and b_I correspond to the perfect structure. These coefficients were previously calculated using the displacement-based Koiter method by Castro and Jansen [18, 22], and the full derivation can be found in chapter 4. Additionally, the first and second-order displacement fields can be determined based on the perfect structure as demonstrated in the same chapter. Hence, the goal of the asymptotic analysis herein performed is to establish relations using the displacement-based Koiter method for the imperfection form factors α and β.

First, the imperfect asymptotic expansion can be simplified to Equation 7.17, if the assumption linear pre-buckling is taken into account, it turns out that α is equal to β [19, 46]. Furthermore, if one also assumes that the imperfection shape is equal to the first normalized buckling mode, then $\alpha=\beta=1$. The buckling modes are normalized with respect to the thickness of the plate, and consequently the imperfection shape as well if one makes this assumption about the imperfection shape.

$$\xi\left(\lambda-\lambda_c\right)=a_I\lambda_c\xi^2+b_I\lambda_c\xi^3-\alpha\lambda\bar{\xi} \tag{7.17}$$

The response of an imperfect plate with $\alpha=\beta=1$ is visually presented in Figure 7.2. It was decided to take $a_I=0$ and $b_I=0.1717$ which are the coefficients derived by Castro and Jansen [18] with the following material properties:

$$E_1=80GPa, E2=8GPa, \frac{G_{12}}{E_2}=0.6, \nu_{12}=0.12$$

The plate itself had a height and width of $0.1m$ and a thickness equal to $0.1m$. The stacking sequence is$[0/90/90/0]$. As expected, the bifurcation point is no longer visible for imperfect plates and it is replaced with a limit point. As the imperfection amplitude grows the limit point is less significant. This figure also clearly indicates that an imperfect plate is still capable of sustaining loads after buckling, as expected due to the positive value of b_I.

The issue with this simplification is that it only works for the scenario where the imperfection shape is equal to the buckling mode. From the literature review, it became clear that the buckling mode is not a realistic imperfection shape and therefore the goal is to expand the displacement-based Koiter methodology to include a general imperfection shape. Initially, it is attempted for linear pre-buckling as

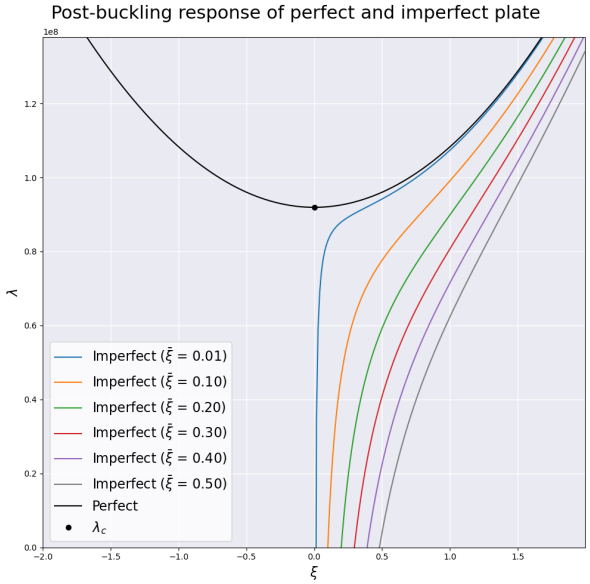

Figure 7.2: Initial post-buckling response of perfect and imperfect plate, where $\alpha = \beta = 1$ and $a_I = 0$ and $b_I = 0.1717$

only one imperfection form factor needs to be derived. The goal is to formulate an expression for α and β for a more general imperfection shape than just the buckling mode.

To achieve this objective, the following methodology is used. Initially, only the asymptotic expansion for the displacement, given by Equation 4.38, is substituted into the total potential energy. This ensures the appearance of the term $\xi\,(\lambda - \lambda_c)$ in the formulation, which can then be replaced with the imperfect expansion for the load, given by either Equation 7.16 or 7.17. The entire equation is expanded and grouped according to powers of ξ, ξ^2, $\bar{\xi}$, and $\bar{\xi}\xi$, with the intention of deriving expressions for α and β.

This solution approach is performed for the four solution possibilities. For the two possibilities involving the assumption of linear pre-buckling, an additional verification check arises. If the imperfection shape is set equal to the first buckling mode, the methodology should result in α equating to 1. If this is not the case, it indicates that a mistake was made along the way.

7.2.1. Option 1: PL

Upon substituting the expansion for the displacement, Equation 4.4, into the total potential energy formulated by Pignataro, the term $\xi\,(\lambda - \lambda_c)$ arises. The expansion for the load parameter with the assumption linear pre-buckling, provided in Equation 7.17, is replaced and regrouped to find Equation 7.18.

$$
\begin{aligned}
&\xi\phi_c''\boldsymbol{u}_I\delta\boldsymbol{u} + \underline{\bar{\xi}\left(-\dot{\phi}_c''\alpha\lambda\boldsymbol{u}_I + (\lambda-\lambda_c)\,\hat{\boldsymbol{u}}\dot{\tilde{\psi}}_c' + \hat{\boldsymbol{u}}\tilde{\psi}_c'\right)\delta\boldsymbol{u}} + \underline{\xi\bar{\xi}\left(-\dot{\phi}_c''\alpha\lambda\boldsymbol{u}_{II} + \hat{\boldsymbol{u}}\tilde{\psi}_c''\boldsymbol{u}_I\right)\delta\boldsymbol{u}} \\
&+\xi^2\left(\dot{\phi}_c''a_I\lambda_c\boldsymbol{u}_I + \frac{1}{2}\phi_c'''\boldsymbol{u}_I^2 + \phi_c''\boldsymbol{u}_{II}\right)\delta\boldsymbol{u} + \underline{\xi^2\bar{\xi}\left(\hat{\boldsymbol{u}}\tilde{\psi}_c''\boldsymbol{u}_{II} + \frac{1}{2}\hat{\boldsymbol{u}}\tilde{\psi}_c'''\boldsymbol{u}_I^2\right)\delta\boldsymbol{u}} \\
&+\xi^3\left(\dot{\phi}_c''a_I\lambda_c\boldsymbol{u}_{II} + \dot{\phi}_c''b_I\lambda_c\boldsymbol{u}_I + \phi_c'''\boldsymbol{u}_I\boldsymbol{u}_{II} + \frac{1}{6}\phi_c^{iv}\boldsymbol{u}_I^3\right)\delta\boldsymbol{u} + \underline{\xi^3\bar{\xi}\hat{\boldsymbol{u}}\tilde{\psi}_c'''\boldsymbol{u}_I\boldsymbol{u}_{II}\delta\boldsymbol{u}} \\
&+\xi^4\left(\dot{\phi}_c''b_I\lambda_c\boldsymbol{u}_{II} + \frac{1}{2}\phi_c'''\boldsymbol{u}_{II}^2 + \frac{1}{2}\phi_c^{iv}\boldsymbol{u}_I^2\boldsymbol{u}_{II}\right)\delta\boldsymbol{u} + \underline{\frac{1}{2}\xi^4\bar{\xi}\hat{\boldsymbol{u}}\tilde{\psi}_c'''\boldsymbol{u}_{II}^2\delta\boldsymbol{u}} \\
&+\frac{1}{2}\xi^5\phi_c^{iv}\boldsymbol{u}_I\boldsymbol{u}_{II}^2\delta\boldsymbol{u} + \frac{1}{6}\xi^6\phi_c^{iv}\boldsymbol{u}_{II}^3\delta\boldsymbol{u} = 0
\end{aligned}
\tag{7.18}
$$

The term multiplied by $\bar{\xi}$ can be used to derive an expression for $\alpha\lambda$. If the term $(\lambda - \lambda_c)$ is disregarded similar to what is presented by Arbocz in [44], Equation 7.19 emerges.

$$\alpha\lambda = \frac{\hat{\boldsymbol{u}}\tilde{\psi}_c'\boldsymbol{u}_I}{\dot{\phi}_c''\boldsymbol{u}_I^2} \tag{7.19}$$

Equation 7.19 is computed for a square plate with the properties previously mentioned. The finite element implementation of the displacement-based Koiter methodology is described in detail in section 4.4. The imperfection shape is initially assumed to be equal to the scaled first buckling mode and it turns out $\alpha\lambda$ is equal to $1 \cdot \lambda_c$. This is exactly as was hypothesized since the imperfection shape is set equal to the buckling mode. The load and displacement expansions are performed in the vicinity of the bifurcation point (λ_c) and thus it makes sense that the value $\alpha\lambda$ is computed instead of solely α and most accurate around this bifurcation point. If one compares the initial post-buckling response of the displacement-based Koiter methodology with the initial assumption that $\alpha = \beta = 1$, it is clear that both responses are equal, as visually depicted in Figure 7.3.

The initial post-buckling response is also plotted for the first four buckling modes and this is presented in Figure 7.4. It is visible that the first buckling mode is the most significant and has the lowest bifurcation point. The displacement-based Koiter approach including imperfection shows the typical post-buckling characteristics that are also visible in literature. Both Figure 7.3 and 7.4 indicate that the displacement-based Koiter methodology is capable of determining the initial post-buckling characteristics.

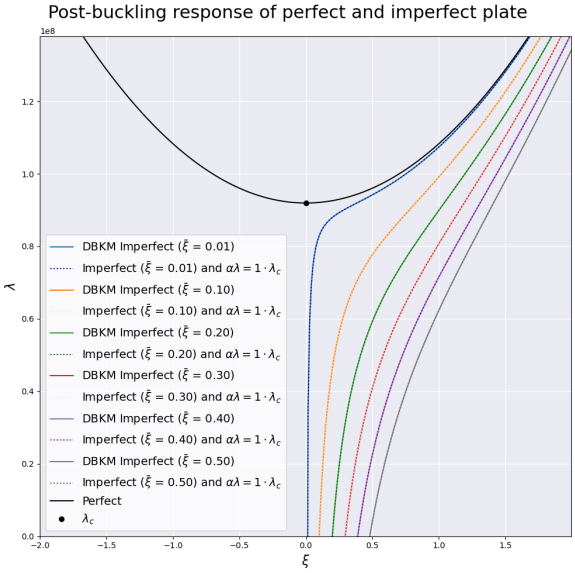

Figure 7.3: Comparison between the initial post-buckling responses of an imperfect plate where $\alpha = \beta = 1$ and $a_I = 0$ and $b_I = 0.1717$ and the displacement-based Koiter methodology (DBKM) where $\hat{u} = u_I$.

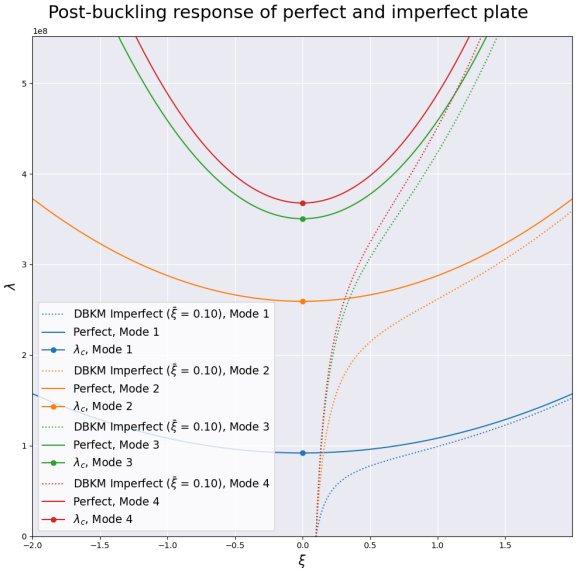

Figure 7.4: Initial post-buckling response of an imperfect plate for different buckling modes computed by the displacement-based Koiter methodology (DBKM), where $\hat{u} = u_I$.

This initial verification that the results are as expected for an imperfection shape equal to the buckling modes is positive, however, this verification step alone is not sufficient to accept that the method is without flaws. The model should be compared to literature that computes the imperfection form factors for different imperfection shapes to validate the inclusion of imperfections in the displacement-based Koiter methodology. Unfortunately, it was not possible to conduct more verification and validation within the time frame of this research, but an overview of the proceeding steps can be found in the recommendations in chapter 9.

7.2.2. Option 2: BL

The expansion of the displacement, Equation 4.4, is substituted into the total potential energy formulated by Budiansky. Afterwards, the expansion for the load parameter with the assumption of linear pre-buckling, as given in Equation 7.17, is inserted into this formulation and subsequently regrouped to obtain Equation 7.20.

$$
\begin{aligned}
&\xi\phi_c''\boldsymbol{u}_I\delta\boldsymbol{u} + \underline{\bar{\xi}\left(-\dot{\phi}_c''\alpha\lambda\boldsymbol{u}_I + (\lambda-\lambda_c)\,\hat{\boldsymbol{u}}\dot{\tilde{\psi}}_c' + \hat{\boldsymbol{u}}\tilde{\psi}_c'\right)\delta\boldsymbol{u}} + \underline{\xi\bar{\xi}\left(-\dot{\phi}_c''\alpha\lambda\boldsymbol{u}_{II} + \hat{\boldsymbol{u}}\tilde{\psi}_c''\boldsymbol{u}_I\right)\delta\boldsymbol{u}} \\
&+\xi^2\left(\dot{\phi}_c''a_I\lambda_c\boldsymbol{u}_I + \frac{1}{2}\phi_c'''\boldsymbol{u}_I^2 + \phi_c''\boldsymbol{u}_{II}\right)\delta\boldsymbol{u} + \underline{\xi^2\bar{\xi}\left(\hat{\boldsymbol{u}}\tilde{\psi}_c''\boldsymbol{u}_{II} + \frac{1}{2}\hat{\boldsymbol{u}}\tilde{\psi}_c'''\boldsymbol{u}_I^2\right)\delta\boldsymbol{u}} + \underline{\frac{1}{2}\xi\bar{\xi}^2\hat{\boldsymbol{u}}^2\tilde{\psi}_c''\boldsymbol{u}_I\delta\boldsymbol{u}} \\
&+\underline{\frac{1}{2}\xi^2\bar{\xi}^2\hat{\boldsymbol{u}}^2\tilde{\psi}_c''\boldsymbol{u}_{II}\delta\boldsymbol{u}} + \xi^3\left(\dot{\phi}_c''a_I\lambda_c\boldsymbol{u}_{II} + \dot{\phi}_c''b_I\lambda_c\boldsymbol{u}_I + \phi_c'''\boldsymbol{u}_I\boldsymbol{u}_{II} + \frac{1}{6}\phi_c^{iv}\boldsymbol{u}_I^3\right)\delta\boldsymbol{u} \\
&+\underline{\xi^3\bar{\xi}\hat{\boldsymbol{u}}\tilde{\psi}_c'''\boldsymbol{u}_I\boldsymbol{u}_{II}\delta\boldsymbol{u}} + \xi^4\left(\dot{\phi}_c''b_I\lambda_c\boldsymbol{u}_{II} + \frac{1}{2}\phi_c'''\boldsymbol{u}_{II}^2 + \frac{1}{2}\phi_c^{iv}\boldsymbol{u}_I^2\boldsymbol{u}_{II}\right)\delta\boldsymbol{u} + \underline{\frac{1}{2}\xi^4\bar{\xi}\hat{\boldsymbol{u}}\tilde{\psi}_c'''\boldsymbol{u}_{II}^2\delta\boldsymbol{u}} \\
&+\frac{1}{2}\xi^5\phi_c^{iv}\boldsymbol{u}_I\boldsymbol{u}_{II}^2\delta\boldsymbol{u} + \frac{1}{6}\xi^6\phi_c^{iv}\boldsymbol{u}_{II}^3\delta\boldsymbol{u} = 0
\end{aligned}
\tag{7.20}
$$

The term multiplied by $\bar{\xi}$ can be used to formulate an expression for $\alpha\lambda$. The term $\bar{\xi}$ is precisely equal to what is presented in Equation 7.18 and therefore it can be concluded that the expression for the imperfect form factor is also equal and given by Equation 7.19. Preliminary results show that this formulation of the imperfection form factors is correct. The fact that both BL and PL conclude the same post-buckling coefficient indicates that the different approaches to expanding the total potential energy do not influence the initial post-buckling coefficients for the case of linear pre-buckling.

7.2.3. Option 3 and 4

The remaining two solution possibilities do not rely on the simplification of linear pre-buckling, complicating the solution approach significantly. The derivation of both equilibrium equations can be found in Appendix C. Due to the increased complexity of deriving the form factors α and β it was not possible to do this within the time frame of this research.

7.2.4. Conclusion Imperfection Form Factors

The effect of including imperfection form factors in the load expansion yields initial positive results. There is an indication that imperfections can successfully be included in the displacement-based Koiter methodology. If the imperfection shape is set equal to the buckling mode, the displacement-based Koiter methodology concludes that $\alpha\lambda$ is equal to $1 \cdot \lambda_c$, in line with what literature also predicts. However, this initial verification is not sufficient to accept that the methodology is without flaws. A detailed overview of recommendations for future work is presented in chapter 9.

Besides the preliminary conclusion that it might be possible to include imperfections within the displacement-based Koiter methodology, a conclusion can be made about the two different approaches to expanding the total potential energy. The expression for $\alpha\lambda$ is computed from the terms related to $\bar{\xi}$ therefore it makes no difference which of the two approaches is used. Budiansky includes the non-linear terms of the imperfection functional derivatives ($\tilde{\tilde{\psi}}^{(n)}$, $\dot{\tilde{\tilde{\psi}}}^{(n)}$ and $\ddot{\tilde{\tilde{\psi}}}^{(n)}$), but these terms are multiplied by $\bar{\xi}^2$ and hence do not influence $\alpha\lambda$.

7.3. Conclusion Asymptotic Analysis

The goal of the asymptotic analysis is to derive expressions for the initial post-buckling characteristics and conclude that imperfections can successfully be included in the displacement-based Koiter methodology. Two different approaches to deriving these expressions were analyzed.

First of all, the less traditional approach of finding imperfect initial post-buckling coefficients did not yield satisfying results. With the current approach, it was not possible to derive expressions for a_I and b_I. On top of the unsuccessful attempts, it was reflected that this approach would result in unrealistic coefficients. Due to the introduction of an imperfection to the plate, it no longer has a bifurcation point and hence performing the asymptotic around the known bifurcation point is not correct. Therefore it is concluded that this path of determining the initial post-buckling characteristics by means of imperfect coefficients should be not continued.

On the other hand, the attempts to define the initial post-buckling properties utilising the imperfection form factors were more successful. Preliminary results show that it is possible to include imperfection within the displacement-based Koiter methodology. The results are correct for an initial test case, but more verification and validation should be done to confirm that the approach is correct.

With all the results presented it is possible to reflect on the hypotheses made at the start of this thesis. The initial hypotheses are repeated for convenience.

H1: Hypothesis on the assumption linear pre-buckling

The assumption of linear pre-buckling simplifies the procedure of finding the initial post-buckling coefficients by means of the displacement-based Koiter methodology, but the results are less accurate.

H2: Hypothesis on the derivations of the initial post-buckling properties

H2.1 Initial imperfect post-buckling coefficients (a_I and b_I) can be derived by means of the displacement-based Koiter methodology.

H2.2 The initial imperfect post-buckling coefficients (a_I and b_I) are more efficient in predicting the post-buckling behaviour of a structure, compared to the imperfect form factors.

H1 cannot be disproved or said to be correct since the attempts of non-linear pre-buckling were not done due to the lack of results for a plate with linear pre-buckling. For non-linear pre-buckling, it is more complicated to find formulations for the imperfection form factors (α and β) since now two coefficients have to be found instead of just one for the case of linear pre-buckling. However, no statement can be made if the results are more accurate.

H2.1 was previously said to be invalid in the conclusion of the initial imperfect post-buckling coefficients. The coefficients cannot be derived with the current approach. Moreover, the idea of finding imperfect coefficients should not be continued to due the fact that imperfect structures no longer have a bifurcation point.

H2.2 is rejected due to the inability to find imperfect post-buckling coefficients. It was concluded that this approach to define the initial post-buckling properties was not correct and should not be continued, therefore it will never be more efficient than finding the imperfect form factors. Note that is assumed that the displacement-based Koiter approach of defining the imperfection form factors is extensively verified and validated and proven to be accurate, which it is currently not.

8

Conclusion

This research aimed to include imperfections in the displacement-based Koiter methodology and to develop an easily implementable and computationally efficient approach. This novel approach should be suitable for recurring processes such as sensitivity studies, ultimately leading to the creation of design guidelines for imperfection-insensitive cylinders. These cylinders are more weight-efficient compared to cylinders sensitive to imperfections and therefore ideal for aerospace applications, such as the outer shells of rockets.

To demonstrate the incorporation of imperfections within the displacement-based Koiter methodology, it was decided to apply the approach first to a plate with an imperfection utilising the single-mode expansion and Donnell-type kinematics. In order to achieve this goal, three steps are identified to include imperfections within the displacement-based methodology. First of all the total potential energy of an imperfect structure is expanded by performing three Taylor expansions. Two possibilities arise for this expansion, one formulation set up by Budiansky and another one derived by Pignataro. Following this, the functional derivatives are derived utilising the Donnell kinematics by means of Frechét derivatives. One can simplify this procedure by assuming that the pre-buckling is linear resulting in the out-of-plane rotations to be equal to zero, alternatively, one can disregard this assumption and have supposedly more accurate but consequently also more functional derivatives. A total of four solution possibilities arise due to the two assumptions related to the expansion of the total potential energy and the pre-buckling behaviour. The last step is to perform an asymptotic analysis.

Each of these four solution opportunities is used to derive the initial post-buckling characteristics of an imperfect plate. The initial idea was to formulate expressions for imperfect initial post-buckling coefficients. This approach did not yield satisfying results and it was decided not to continue this path of finding imperfect coefficients. This decision was backed up due to the fact that imperfect structures no longer have a bifurcation point and therefore it does not make sense to perform an asymptotic expansion in the vicinity of this critical load.

A more successful attempt was to evaluate the initial post-buckling characteristics by means of imperfection form factors. Two new coefficients are introduced in the load expansion for which expressions should be found. For the case of linear pre-buckling, it was possible to derive an expression for $\alpha\lambda$. The first preliminary results show that this derivation was correct, but more cases should be evaluated before it is concluded that the inclusion of imperfections was done correctly for the displacement-based Koiter methodology. Besides the promising results, it was also shown that it did not matter whether the formulation of Pignataro or Budiansky was used to expand the total potential energy since both obtained the same expression for $\alpha\lambda$.

Therefore, the goal of including imperfections in the displacement-based Koiter methodology is not completed yet. The first attempt to find imperfect post-buckling coefficients was not successful and should not be revisited. The preliminary results for deriving imperfection form factors are promising, however, it is too soon to conclude that this approach for including imperfections in the displacement-based Koiter approach is correct without further verification of the model.

9

Recommendations

The objective of including imperfection in the displacement-based Koiter methodology was not achieved yet and therefore several recommendations for future research are presented in this chapter such that this goal becomes attainable.

The displacement-based Koiter approach of finding imperfection form factors needs to be verified and validated thoroughly before it can be concluded that imperfections have been incorporated successfully. The most simple way to verify the inclusion of imperfections within the displacement-based approach is to compare its results to work presented in the work of Rahman [19] and Tiso [43]. Both researchers are focused on implementing the Koiter approach within finite element simulations, but there are no examples of imperfect plates presented in their work. The methodology of deriving the imperfection form factors presented in both is implemented in the finite element software DIANA. Therefore it is possible to create the missing data on imperfect plates. A reference plate with several different imperfection shapes should be modelled in DIANA as well as the current displacement-based approach and the results of the imperfection form factors should be compared. The coefficients are expected to be exactly equal since both methodologies utilize the Koiter approach. One should pay attention to the scaling of the imperfection shapes as this influences the imperfection factors and could be a potential source for differences.

Another possible verification is to recompute the displacement field and observe the effect of the initial imperfection. The displacement field can easily be reconstructed by finding the scalar parameter ξ for each different load parameter. This ξ needs to be substituted back in $\boldsymbol{u} - \boldsymbol{u_c} = \boldsymbol{v} = \xi \boldsymbol{u_I} + \xi^2 \boldsymbol{u_{II}} + \xi^3 \boldsymbol{u_{III}}$ to the displacement. The out-of-plane displacement of a given node can be compared to the same out-of-plane displacement computed by FE simulation of an imperfect plate to verify that the inclusion of imperfections in the displacement-based Koiter methodology is correct.

Once the inclusion of imperfections in the displacement-based methodology has been proven to work it opens up many possibilities. The method can be expanded from single mode to multi-mode to find the post-buckling characteristics when multiple buckling modes interact which is often the case for cylinders. The kinematics can be extended from Donnell to Sanders' to include more non-linear terms that are more accurate for cylindrical shells as it captures the non-linear behaviour of the initial post-buckling better than Donnell's [22]. The Sanders kinematics including initial imperfections is presented in Equation 9.1 and 9.2 [49]. When deriving the functional derivatives for a cylinder assuming linear pre-buckling, it is no longer true that the out-of-plane displacement is equal to zero, as in the case of a plate.

$$\boldsymbol{\varepsilon} = \begin{Bmatrix} \varepsilon_{xx} \\ \varepsilon_{yy} \\ \gamma_{xy} \end{Bmatrix} = \begin{Bmatrix} \frac{\partial u}{\partial x} + \frac{\partial w^0}{\partial x}\frac{\partial w}{\partial x} + \frac{1}{2}\left(\frac{\partial w}{\partial x}\right)^2 \\ \frac{\partial v}{\partial y} + \frac{w}{r} + \frac{\partial w^0}{\partial y}\frac{\partial w}{\partial y} + \frac{1}{2}\left(\frac{\partial w}{\partial y}\right)^2 \frac{v^2}{2r^2} - \frac{v}{r}\frac{\partial w}{\partial y} - \frac{v}{r}\frac{\partial w^0}{\partial y} \\ \frac{\partial u}{\partial y} + \frac{\partial v}{\partial x} + \frac{\partial w}{\partial x}\frac{\partial w}{\partial y} + \frac{\partial w^0}{\partial x}\frac{\partial w}{\partial y} + \frac{\partial w^0}{\partial y}\frac{\partial w}{\partial x} - \frac{v}{r}\frac{\partial w}{\partial x} - \frac{v}{r}\frac{\partial w^0}{\partial x} \end{Bmatrix} \tag{9.1}$$

$$\boldsymbol{\kappa} = \left\{ \begin{array}{c} \kappa_{xx} \\ \kappa_{yy} \\ \kappa_{xy} \end{array} \right\} = \left\{ \begin{array}{c} -\frac{\partial^2 w}{\partial x^2} \\ -\frac{\partial^2 w}{\partial y^2} + \frac{1}{r}\frac{\partial v}{\partial y} \\ -2\frac{\partial^2 w}{\partial x \partial y} + \frac{1}{r}\frac{\partial v}{\partial x} \end{array} \right\} \tag{9.2}$$

Finally, the methodology relying on the imperfect form factors is based on the perfect post-buckling coefficients. Cylinders are known to have a negative second post-buckling coefficient and therefore cannot sustain loads after buckling. Optimisation algorithms are recommended in combination with the Koiter methodology to find cylinders with a positive buckling slope. This will be similar to the research conducted by Santos and Castro. [40], but the topic could be more explored to establish guidelines for composite cylinders with positive b-factors. This research did not include the manufacturing limitation that shearing can only initiate from a zero-degree angle. It would be interesting to explore if cylinders with a positive b-factor can still be achieved if the true manufacturing capabilities of CTS are considered. Moreover, the research by Santos and Castro was explicitly done with CTS in mind, however, other VA manufacturing techniques could be explored since it was evident from the literature review that AFP and TFP also showed promising results.

In addition to suggesting necessary implementations, it is also important to discourage certain practices. The methodology of finding initial imperfect post-buckling coefficients should not be done again. No time and effort should be put into revisiting this methodology and finding the correct coefficients. These coefficients would only be applicable for a cylinder with an axisymmetric imperfection and this specific scenario is not broad enough that is it deemed useful for practical application.

References

[1] M. Kaufmann, D. Zenkert, and C. Mattei. “Cost optimization of composite aircraft structures including variable laminate qualities”. In: *Composites Science and Technology* 68.13 (Oct. 2008), pp. 2748–2754. ISSN: 0266-3538. DOI: 10.1016/J.COMPSCITECH.2008.05.024.

[2] J. H. Saleh, D. E. Hastings, and D. J. Newman. “Spacecraft Design Lifetime”. In: *JOURNAL OF SPACECRAFT AND ROCKETS* 39.2 (). DOI: 10.2514/2.3806. URL: http://arc.aiaa.org.

[3] W. H. Tsai, Y. C. Chang, S. J. Lin, H. C. Chen, and P. Y. Chu. “A green approach to the weight reduction of aircraft cabins”. In: *Journal of Air Transport Management* 40 (Aug. 2014), pp. 65–77. ISSN: 0969-6997. DOI: 10.1016/J.JAIRTRAMAN.2014.06.004.

[4] B. Budiansky. “Theory of Buckling and Post-Buckling Behavior of Elastic Structures”. In: *Advances in Applied Mechanics* 14.C (1974), pp. 1–65. ISSN: 00652156. DOI: 10.1016/S0065-2156(08)70030-9. URL: https://linkinghub.elsevier.com/retrieve/pii/S0065215608700309%20http://linkinghub.elsevier.com/retrieve/pii/S0065215608700309.

[5] P. Mandal and C. R. Calladine. “Buckling of thin cylindrical shells under axial compression”. In: *International Journal of Solids and Structures* 37.33 (Aug. 2000), pp. 4509–4525. ISSN: 0020-7683. DOI: 10.1016/S0020-7683(99)00160-2.

[6] M. Wilburger. *Buckling of Thin-Walled Circular Cylinders*. Tech. rep. National Aeronautics and Space Administration, 2020.

[7] W. T. Koiter. “A Translation of The Stability of Elastic Equilibrium”. PhD thesis. Delft University f Technology, Nov. 1945.

[8] T. v. Karman and H.-S. Tsien. “The Buckling of Thin Cylindrical Shells Under Axial Compression”. In: *Journal of the Aeronautical Sciences* 8.8 (Aug. 1941), pp. 303–312. DOI: 10.2514/8.10722. URL: https://arc.aiaa.org/doi/pdf/10.2514/8.10722.

[9] L. H. Donnell and C. C. Wan. “Effect of Imperfections on Buckling of Th in Cylinders and Columns Under Axial Compression”. In: *Journal of Applied Mechanics* 17.1 (1950), pp. 73–83. URL: http://asmedigitalcollection.asme.org/appliedmechanics/article-pdf/17/1/73/6746531/73_1.pdf.

[10] S. G. P. Castro. “Semi-Analytical Tools for the Analysis of Laminated Composite Cylindrical and Conical Imperfect Shells under Various Loading and Boundary Conditions”. PhD thesis. Clausthal University of Technology, Dec. 2014.

[11] C. Hühne, R. Rolfes, E. Breitbach, and J. Teßmer. “Robust design of composite cylindrical shells under axial compression — Simulation and validation”. In: *Thin-Walled Structures* 46.7-9 (July 2008), pp. 947–962. ISSN: 0263-8231. DOI: 10.1016/J.TWS.2008.01.043.

[12] S. G. Castro, R. Zimmermann, M. A. Arbelo, R. Khakimova, M. W. Hilburger, and R. Degenhardt. “Geometric imperfections and lower-bound methods used to calculate knock-down factors for axially compressed composite cylindrical shells”. In: *Thin-Walled Structures* 74 (Jan. 2014), pp. 118–132. ISSN: 0263-8231. DOI: 10.1016/J.TWS.2013.08.011.

[13] H. N. Wagner, C. Hühne, and S. Niemann. “Robust knockdown factors for the design of axially loaded cylindrical and conical composite shells – Development and Validation”. In: *Composite Structures* 173 (Aug. 2017), pp. 281–303. ISSN: 0263-8223. DOI: 10.1016/J.COMPSTRUCT.2017.02.031.

[14] R. Khakimova, C. J. Warren, R. Zimmermann, S. G. Castro, M. A. Arbelo, and R. Degenhardt. “The single perturbation load approach applied to imperfection sensitive conical composite structures”. In: *Thin-Walled Structures* 84 (Nov. 2014), pp. 369–377. ISSN: 0263-8231. DOI: 10.1016/J.TWS.2014.07.005.

[15] S. G. Castro, R. Zimmermann, M. A. Arbelo, and R. Degenhardt. “Exploring the constancy of the global buckling load after a critical geometric imperfection level in thin-walled cylindrical shells for less conservative knock-down factors”. In: *Thin-Walled Structures* 72 (Nov. 2013), pp. 76–87. ISSN: 0263-8231. DOI: 10.1016/J.TWS.2013.06.016.

[16] L. Friedrich and K. U. Schröder. “Discrepancy between boundary conditions and load introduction of full-scale built-in and sub-scale experimental shell structures of space launcher vehicles”. In: *Thin-Walled Structures* 98 (Jan. 2016), pp. 403–415. ISSN: 0263-8231. DOI: 10.1016/J.TWS.2015.10.007.

[17] B. Kriegesmann, E. L. Jansen, and R. Rolfes. “Design of cylindrical shells using the Single Perturbation Load Approach – Potentials and application limits”. In: *Thin-Walled Structures* 108 (Nov. 2016), pp. 369–380. ISSN: 0263-8231. DOI: 10.1016/J.TWS.2016.09.005.

[18] S. G. P. Castro and E. L. Jansen. “Displacement-based formulation of Koiter’s method: application tomulti-modal post-buckling finite element analysis of plates”. In: *Thin-Walled Structures* 159 (Feb. 2021), p. 107217. DOI: 10.1016/j.tws.2020.107217.

[19] T. Rahman. “A perturbation approach for geometrically nonlinear structural analysis using a general purpose finite element code”. PhD thesis. Delft University of Technology, 2009. ISBN: 9789090249513. URL: http://resolver.tudelft.nl/uuid:80e11dbd-90be-44f1-bb36-049503a265bd.

[20] D. Magisano, L. Leonetti, and G. Garcea. “Koiter asymptotic analysis of multilayered composite structures using mixed solid-shell finite elements”. In: *Composite Structures* 154 (Oct. 2016), pp. 296–308. ISSN: 0263-8223. DOI: 10.1016/J.COMPSTRUCT.2016.07.046.

[21] J. Yan. “Finite Element Implementation of Koiter’s Initial Post-buckling Analysis”. PhD thesis. Nottingham: University of Nottingham.

[22] S. G. Castro and E. L. Jansen. “Displacement-based multi-modal formulation of Koiter’s method applied to cylindrical shells”. In: *AIAA Science and Technology Forum and Exposition, AIAA SciTech Forum 2022*. American Institute of Aeronautics and Astronautics Inc, AIAA, 2022. ISBN: 9781624106316. DOI: 10.2514/6.2022-0256.

[23] J. Arbocz. “The Imperfection Data Bank, a Mean to Obtain Realistic Buckling Loads”. In: *Buckling of Shells, Proceedings of the State-of-the-Art Colloquium*. Springer Verlag, 1982, pp. 535–567. ISBN: 3540117857. DOI: 10.1007/978-3-642-49334-8{_}19/COVER. URL: https://link.springer.com/chapter/10.1007/978-3-642-49334-8_19.

[24] T. Weller and J. Singer. “Experimental Studies on the Buckling Under Axial Compression of Integrally Stringer-Stiffened Circular Cylindrical Shells”. In: *Journal of Applied Mechanics* 44.4 (Dec. 1977), pp. 721–730. ISSN: 0021-8936. DOI: 10.1115/1.3424163. URL: https://asmedigitalcollection.asme.org/appliedmechanics/article/44/4/721/387639/Experimental-Studies-on-the-Buckling-Under-Axial.

[25] S. C. White and P. M. Weaver. “Towards imperfection insensitive buckling response of shell structures-shells with plate-like post-buckled responses”. In: *The Aeronautical Journal* 120.1224 (2016), pp. 233–253. DOI: 10.1017/aer.2015.14. URL: https://www.cambridge.org/core/product/identifier/S0001924015000147/type/journal_article.

[26] H. N. Wagner, E. Petersen, R. Khakimova, and C. Hühne. “Buckling analysis of an imperfection-insensitive hybrid composite cylinder under axial compression – numerical simulation, destructive and non-destructive experimental testing”. In: *Composite Structures* 225 (Oct. 2019), p. 111152. ISSN: 0263-8223. DOI: 10.1016/J.COMPSTRUCT.2019.111152.

[27] P. Hao, B. Wang, G. Li, K. Tian, K. Du, X. Wang, and X. Tang. “Surrogate-based optimization of stiffened shells including load-carrying capacity and imperfection sensitivity”. In: *Thin-Walled Structures* 72 (Nov. 2013), pp. 164–174. ISSN: 0263-8231. DOI: 10.1016/J.TWS.2013.06.004.

[28] P. Hao, B. Wang, G. Li, Z. Meng, K. Tian, and X. Tang. “Hybrid optimization of hierarchical stiffened shells based on smeared stiffener method and finite element method”. In: *Thin-Walled Structures* 82 (Sept. 2014), pp. 46–54. ISSN: 0263-8231. DOI: 10.1016/J.TWS.2014.04.004.

[29] B. Wang, P. Hao, G. Li, J.-X. Zhang, K.-F. Du, K. Tian, X.-J. Wang, X.-H. Tang, B. Wang, P. Hao, G. Li, J.-x. Zhang, K.-f. Du, K. Tian, X.-j. Wang, and X.-h. Tang. “Optimum design of hierarchical stiffened shells for low imperfection sensitivity”. In: *Acta Mechanica Sinica 2014 30:3* 30.3 (Mar. 2014), pp. 391–402. ISSN: 1614-3116. DOI: 10.1007/S10409-014-0003-3. URL: https://link.springer.com/article/10.1007/s10409-014-0003-3.

[30] A. Catapano, M. Montemurro, J.-A. Balcou, and E. Panettieri. “Rapid Prototyping of Variable Angle-Tow Composites”. In: *Aerotecnica Missili & Spazio 2019 98:4* 98.4 (Aug. 2019), pp. 257–271. ISSN: 2524-6968. DOI: 10.1007/S42496-019-00019-0. URL: https://link.springer.com/article/10.1007/s42496-019-00019-0.

[31] Z. Wang, J. H. S. Almeida, L. St-Pierre, Z. Wang, and S. G. Castro. “Reliability-based buckling optimization with an accelerated Kriging metamodel for filament-wound variable angle tow composite cylinders”. In: *Composite Structures* 254 (Dec. 2020), p. 112821. ISSN: 0263-8223. DOI: 10.1016/J.COMPSTRUCT.2020.112821.

[32] B. C. Kim, K. Potter, and P. M. Weaver. “Continuous tow shearing for manufacturing variable angle tow composites”. In: *Composites Part A: Applied Science and Manufacturing* 43.8 (Aug. 2012), pp. 1347–1356. ISSN: 1359-835X. DOI: 10.1016/J.COMPOSITESA.2012.02.024.

[33] K. Chauncey Wu, B. K. Stanford, G. A. Hrinda, Z. Wang, R. A. Martin, and H. Alicia Kim. “Structural assessment of advanced composite tow-steered shells”. In: *54th AIAA/ASME/ASCE/AHS/ASC Structures, Structural Dynamics, and Materials Conference*. 2013, pp. 8–11. ISBN: 9781624102233. DOI: 10.2514/6.2013-1769. URL: https://arc.aiaa.org/doi/10.2514/6.2013-1769.

[34] K. C. Wu, B. Farrokh, B. K. Stanford, and P. M. Weaver. “Imperfection insensitivity analyses of advanced composite tow-steered shells”. In: *57th AIAA/ASCE/AHS/ASC Structures, Structural Dynamics, and Materials Conference*. San Diego: American Institute of Aeronautics and Astronautics Inc, AIAA, Apr. 2016. ISBN: 978-1-62410-392-6. DOI: 10.2514/6.2016-1498. URL: https://arc.aiaa.org/doi/10.2514/6.2016-1498.

[35] A. Brasington, C. Sacco, J. Halbritter, R. Wehbe, and R. Harik. “Automated fiber placement: A review of history, current technologies, and future paths forward”. In: *Composites Part C: Open Access* 6 (Oct. 2021), p. 100182. ISSN: 2666-6820. DOI: 10.1016/J.JCOMC.2021.100182.

[36] S. G. Castro, M. V. Donadon, and T. A. Guimarães. “ES-PIM applied to buckling of variable angle tow laminates”. In: *Composite Structures* 209 (Feb. 2019), pp. 67–78. ISSN: 0263-8223. DOI: 10.1016/J.COMPSTRUCT.2018.10.058.

[37] L. Vertonghen and S. G. Castro. “Modelling of fibre steered plates with coupled thickness variation from overlapping continuous tows”. In: *Composite Structures* 268 (July 2021), p. 113933. ISSN: 0263-8223. DOI: 10.1016/J.COMPSTRUCT.2021.113933.

[38] R. L. Lincoln, P. M. Weaver, A. Pirrera, and R. M. Groh. “Optimization of imperfection-insensitive continuous tow sheared rocket launch structures”. In: *AIAA Scitech 2021 Forum* (2021), pp. 1–19. DOI: 10.2514/6.2021-0202. URL: https://arc.aiaa.org/doi/abs/10.2514/6.2021-0202.

[39] R. Lincoln, P. Weaver, A. Pirrera, and R. Groh. “Imperfection-insensitive continuous tow-sheared cylinders”. In: *Composite Structures* 260 (Mar. 2021), p. 113445. ISSN: 02638223. DOI: 10.1016/j.compstruct.2020.113445. URL: https://linkinghub.elsevier.com/retrieve/pii/S0263822320333742.

[40] R. R. d. Santos and S. G. P. Castro. “Lightweight Design of Variable-Stiffness Cylinders with Reduced Imperfection Sensitivity Enabled by Continuous Tow Shearing and Machine Learning”. In: *Materials 2022, Vol. 15, Page 4117* 15.12 (June 2022), p. 4117. ISSN: 1996-1944. DOI: 10.3390/MA15124117. URL: https://www.mdpi.com/1996-1944/15/12/4117/htm%20https://www.mdpi.com/1996-1944/15/12/4117.

[41] P. Mattheij, K. Gliesche, and D. Feltin. “Tailored Fiber Placement-Mechanical Properties and Applications:” in: *http://dx.doi.org/10.1177/073168449801700901* 17.9 (Aug. 2016), pp. 774–786. ISSN: 07316844. DOI: 10.1177/073168449801700901. URL: https://journals.sagepub.com/doi/10.1177/073168449801700901.

[42] J. H. S. Almeida, L. Bittrich, E. Jansen, V. Tita, and A. Spickenheuer. “Buckling optimization of composite cylinders for axial compression: A design methodology considering a variable-axial fiber layout”. In: *Composite Structures* 222 (Aug. 2019), p. 110928. ISSN: 0263-8223. DOI: 10.1016/J.COMPSTRUCT.2019.110928.

[43] P. Tiso. “Finite element based reduction methods for static and dynamic analysis of thin-walled structures”. PhD thesis. Delft: Delft University of Technology. ISBN: 90-9021336-8. URL: https://repository.tudelft.nl/islandora/object/uuid%3A3affd8eb-8fbd-40da-aefc-48a96efe8afb.

[44] J. Arbocz and J. Hol. *ANILISA - Computational Module for Koiter’s Imperfection Sensitivity Theory*. Tech. rep. Delft: Delft University of Technology Faculty of Aeropsace Engineering, Jan. 1989, pp. 1–86.

[45] M. Pignataro. “Stability, Bifurcation and Postbuckling Analysis”. In: *Coupled Instabilities in Metal Structures* (1998), pp. 29–83. DOI: 10.1007/978-3-7091-2510-6{_}2. URL: https://link-springer-com.tudelft.idm.oclc.org/chapter/10.1007/978-3-7091-2510-6_2.

[46] G. A. Cohen. “Effect of a nonlinear prebuckling state on the postbuckling behaviorand imperfect on sensitivity of elastic structures.” In: *https://doi.org/10.2514/3.4832* 6.8 (May 1968), pp. 1616–1619. ISSN: 00011452. DOI: 10.2514/3.4832. URL: https://arc.aiaa.org/doi/10.2514/3.4832.

[47] G. Cederbaum and J. Arbocz. “Reliability of imperfection-sensitive composite shells via the Koiter-Cohen criterion”. In: *Reliability Engineering & System Safety* 56.3 (June 1997), pp. 257–263. ISSN: 0951-8320. DOI: 10.1016/S0951-8320(96)00018-X.

[48] G. Cohen. *Computer program for analysis of imperfection sensitivity of ring stiffened shells of revolution*. Tech. rep. Newport Beach, CA, United States: National Aeronautics and Space Administration, Aug. 1971, pp. 1–181.

[49] G. J. Simitses, I. Sheinman, and D. Shaw. “The accuracy of Donnell’s equations for axially-loaded, imperfect orthotropic cylinders”. In: *Computers & Structures* 20.6 (Jan. 1985), pp. 939–945. ISSN: 0045-7949. DOI: 10.1016/0045-7949(85)90013-6.

A

Derivation Functional Derivatives for Linear Pre-buckling

A.1. Strains

The kinematics with the assumption of linear pre-buckling neglect the initial out-of-place displacement (w_0), however due to the fact that $\boldsymbol{u_c} = \boldsymbol{u_0}(\lambda_c)$ is applicable all terms related to the out-of-place displacement equate to zero.

A.1.1. Perfect

The derivation of the derivatives of the perfect strain can be found in subsection 4.2.1 and only the conclusions are presented here to with the goal of removing the out-of-plane terms.

$$\boldsymbol{\varepsilon} = \begin{Bmatrix} \varepsilon_{xx} \\ \varepsilon_{yy} \\ \gamma_{xy} \end{Bmatrix} = \begin{Bmatrix} u_{,x} + \frac{1}{2}\cancel{(w_{,x})^2} \\ v_{,y} + \frac{1}{2}\cancel{(w_{,y})^2} \\ u_{,y} + v_{,x} + \cancel{w_{,x}w_{,y}} \end{Bmatrix} = \begin{Bmatrix} u_{,x} \\ v_{,y} \\ u_{,y} + v_{,x} \end{Bmatrix} \tag{A.1}$$

$$\boldsymbol{\kappa} = \begin{Bmatrix} \kappa_{xx} \\ \kappa_{yy} \\ \kappa_{xy} \end{Bmatrix} = \begin{Bmatrix} \cancel{-w_{,xx}} \\ \cancel{-w_{,yy}} \\ \cancel{-2w_{,xy}} \end{Bmatrix} = \begin{Bmatrix} 0 \\ 0 \\ 0 \end{Bmatrix} \tag{A.2}$$

$$\boldsymbol{\varepsilon}'_a = \begin{Bmatrix} S^u_{a,x} + S^w_{a,x}\cancel{w_{,x}} \\ S^v_{a,y} + S^w_{a,y}\cancel{w_{,y}} \\ S^u_{a,y} + S^v_{a,y} + S^w_{a,x}\cancel{w_{,y}} + S^w_{a,y}\cancel{w_{,x}} \end{Bmatrix} = \begin{Bmatrix} S^u_{a,x} \\ S^v_{a,y} \\ S^u_{a,y} \end{Bmatrix} \tag{A.3}$$

$$\boldsymbol{\kappa}'_a = \begin{Bmatrix} -S^w_{a,xx} \\ -S^w_{a,yy} \\ -2S^w_{a,xy} \end{Bmatrix} \tag{A.4}$$

$$\boldsymbol{\varepsilon}''_{ab} = \begin{Bmatrix} S^w_{a,x}S^w_{b,x} \\ S^w_{a,y}S^w_{b,y} \\ S^w_{a,x}S^w_{b,y} + S^w_{a,y}S^w_{b,x} \end{Bmatrix} \tag{A.5}$$

$$\dot{\boldsymbol{\varepsilon}} = \begin{Bmatrix} u_{0,x} + \lambda\cancel{w^2_{0,x}} \\ v_{0,y} + \lambda\cancel{w^2_{0,y}} \\ u_{0,y} + v_{0,x} + 2\lambda\cancel{w_{0,x}w_{0,y}} \end{Bmatrix} = \begin{Bmatrix} u_{0,x} \\ v_{0,y} \\ u_{0,y} + v_{0,x} \end{Bmatrix} \tag{A.6}$$

$$\dot{\boldsymbol{\kappa}} = \begin{Bmatrix} \cancel{-w_{0,xx}} \\ \cancel{-w_{0,yy}} \\ \cancel{-2w_{0,xy}} \end{Bmatrix} = \begin{Bmatrix} 0 \\ 0 \\ 0 \end{Bmatrix} \tag{A.7}$$

$$\ddot{\boldsymbol{\varepsilon}} = \begin{Bmatrix} \cancel{w_{0,x}^2} \\ \cancel{w_{0,y}^2} \\ \cancel{2w_{0,x}w_{0,y}} \end{Bmatrix} = \begin{Bmatrix} 0 \\ 0 \\ 0 \end{Bmatrix} \tag{A.8}$$

$$\dot{\boldsymbol{\varepsilon}}'_{\boldsymbol{a}} = \begin{Bmatrix} \cancel{w_{0,x}}S^w_{a,x} \\ \cancel{w_{0,y}}S^w_{a,y} \\ \cancel{w_{0,x}}S^w_{a,y} + \cancel{w_{0,y}}S^w_{a,x} \end{Bmatrix} = \begin{Bmatrix} 0 \\ 0 \\ 0 \end{Bmatrix} \tag{A.9}$$

A.1.2. Imperfect

The derivation of the derivatives of the perfect strain can be found in section 6.1.

$$\bar{\boldsymbol{\varepsilon}} = \begin{Bmatrix} \bar{w}_{,x}\cancel{w_{,x}} \\ \bar{w}_{,y}\cancel{w_{,y}} \\ \bar{w}_{,y}\cancel{w_{,x}} + \bar{w}_{,x}\cancel{w_{,y}} \end{Bmatrix} = \begin{Bmatrix} 0 \\ 0 \\ 0 \end{Bmatrix} \tag{A.10}$$

$$\bar{\boldsymbol{\varepsilon}}'_{\boldsymbol{a}} = \begin{Bmatrix} \cancel{\bar{w}'_{,x}}w_{,x} + S^w_{a,x}\bar{w}_{,x} \\ \cancel{\bar{w}'_{,y}}w_{,y} + S^w_{a,y}\bar{w}_{,y} \\ \cancel{\bar{w}'_{,x}}w_{,y} + S^w_{a,y}\bar{w}_{,x} + \cancel{\bar{w}'_{,y}}w_{,x} + S^w_{a,x}\bar{w}_{,y} \end{Bmatrix} = \begin{Bmatrix} S^w_{a,x}\bar{w}_{,x} \\ S^w_{a,y}\bar{w}_{,y} \\ S^w_{a,y}\bar{w}_{,x} + S^w_{a,x}\bar{w}_{,y} \end{Bmatrix} \tag{A.11}$$

$$\dot{\bar{\boldsymbol{\varepsilon}}} = \begin{Bmatrix} \bar{w}_{,x}\cancel{w_{0,x}} \\ \bar{w}_{,y}\cancel{w_{0,y}} \\ \bar{w}_{,x}\cancel{w_{0,y}} + \bar{w}_{,y}\cancel{w_{0,x}} \end{Bmatrix} = \begin{Bmatrix} 0 \\ 0 \\ 0 \end{Bmatrix} \tag{A.12}$$

$$\tilde{\bar{\boldsymbol{\varepsilon}}}_{\boldsymbol{k}} = \begin{Bmatrix} S^{\bar{w}}_{k,x}\cancel{w_{,x}} \\ S^{\bar{w}}_{k,y}\cancel{w_{,y}} \\ S^{\bar{w}}_{k,y}\cancel{w_{,x}} + S^{\bar{w}}_{k,x}\cancel{w_{,y}} \end{Bmatrix} = \begin{Bmatrix} 0 \\ 0 \\ 0 \end{Bmatrix} \tag{A.13}$$

$$\tilde{\bar{\boldsymbol{\varepsilon}}}'_{\boldsymbol{ka}} = \begin{Bmatrix} S^{\bar{w}}_{k,x}S^w_{a,x} \\ S^{\bar{w}}_{k,y}S^w_{a,y} \\ S^{\bar{w}}_{k,y}S^w_{a,x} + S^{\bar{w}}_{k,x}S^w_{a,y} \end{Bmatrix} \tag{A.14}$$

$$\dot{\tilde{\bar{\boldsymbol{\varepsilon}}}}_{\boldsymbol{k}} = \begin{Bmatrix} S^{\bar{w}}_{k,x}\cancel{w_{0,x}} \\ S^{\bar{w}}_{k,y}\cancel{w_{0,y}} \\ S^{\bar{w}}_{k,y}\cancel{w_{0,x}} + S^{\bar{w}}_{k,x}\cancel{w_{0,y}} \end{Bmatrix} = \begin{Bmatrix} 0 \\ 0 \\ 0 \end{Bmatrix} \tag{A.15}$$

A.2. Stresses

The stresses are derived directly from the strains and therefore only the non-zero stresses are presented down below. An overview of the non-zero strains is presented here.

$$\begin{matrix} \varepsilon & \bar{\varepsilon}'_a \\ \varepsilon'_a & \tilde{\bar{\varepsilon}}'_{ak} \\ \kappa'_a & \\ \varepsilon''_{ab} & \\ \dot{\varepsilon} & \end{matrix}$$

A.2.1. Perfect

$$\begin{aligned} N_i &= A_{ij}\varepsilon_j \\ M_i &= B_{ij}\varepsilon_j \end{aligned} \tag{A.16}$$

$$\begin{aligned} N'_{ia} &= A_{ij}\varepsilon'_{ja} + B_{ij}\kappa'_{ja} \\ M'_{ia} &= B_{ij}\varepsilon'_{ja} + D_{ij}\kappa'_{ja} \end{aligned} \tag{A.17}$$

$$\begin{aligned} N''_{iab} &= A_{ij}\varepsilon''_{jab} \\ M''_{iab} &= B_{ij}\varepsilon''_{jab} \end{aligned} \tag{A.18}$$

$$\begin{aligned} \dot{N}_i &= A_{ij}\dot{\varepsilon}_j \\ \dot{M}_i &= B_{ij}\dot{\varepsilon}_j \end{aligned} \tag{A.19}$$

A.2.2. Imperfect

$$\begin{aligned} \bar{N}'_{ia} &= A_{ij}\bar{\varepsilon}'_{ja} \\ \bar{M}'_{ia} &= B_{ij}\bar{\varepsilon}'_{ja} \end{aligned} \tag{A.20}$$

$$\begin{aligned} \tilde{\bar{N}}'_{ika} &= A_{ij}\tilde{\bar{\varepsilon}}'_{jka} \\ \tilde{\bar{M}}'_{ika} &= B_{ij}\tilde{\bar{\varepsilon}}'_{jka} \end{aligned} \tag{A.21}$$

A.3. Functional Derivatives

The functional derivatives for a plate with the assumption linear pre-buckling are presented down below. All the terms equal zero are crossed-out in the derivation. An overview of the non-zero terms is presented in Table A.1 which is created from the derivation presented above.

Strains		**Stresses**	
Perfect	Imperfect	Perfect	Imperfect
$\boldsymbol{\varepsilon}$	$\bar{\boldsymbol{\varepsilon}}'_{\boldsymbol{a}}$	N_i and M_i	$\bar{N}'_{ia}$ and $\bar{M}'_{ia}$
$\boldsymbol{\varepsilon}'_a$	$\tilde{\bar{\boldsymbol{\varepsilon}}}'_{\boldsymbol{ka}}$	N'_{ia} and M'_{ia}	$\tilde{\bar{N}}'_{ika}$ and $\tilde{\bar{M}}'_{ika}$
$\boldsymbol{\kappa}'_a$		N''_{iab} and M''_{iab}	
$\boldsymbol{\varepsilon}''_{ab}$		$\dot{N}_i$ and $\dot{M}_i$	
$\dot{\boldsymbol{\varepsilon}}$			

Table A.1: Overview all relevant strains and stresses for the perfect and imperfect structure with assumption linear pre-buckling

A.3.1. Perfect

The derivation of the perfect functional derivatives can be found in subsection 4.2.3.

$$\begin{aligned} \phi'_c \boldsymbol{u_a} &= \left[\frac{1}{2}\int_\Omega \left(N'_{ia}\varepsilon_i + N_i\varepsilon'_{ia} + M'_{ia}\cancelto{0}{\kappa_i} + M_i\kappa'_{ia}\right) d\Omega - \int_{\delta\Omega} \lambda\widehat{\boldsymbol{N}}^\top S^u_{ax=\ell_x} d(\delta\Omega)\right] u_a \\ &= \left[\frac{1}{2}\int_\Omega \left(N'_{ia}\varepsilon_i + N_i\varepsilon'_{ia} + M_i\kappa'_{ia}\right) d\Omega - \int_{\delta\Omega} \lambda\widehat{\boldsymbol{N}}^\top S^u_{ax=\ell_x} d(\delta\Omega)\right] u_a \end{aligned} \tag{A.22}$$

$$\begin{aligned} \phi''_c \boldsymbol{u_a u_b} &= \left[\frac{1}{2}\int_\Omega \left(N''_{iab}\varepsilon_i + N'_{ia}\varepsilon'_{ib} + N'_{ib}\varepsilon'_{ia} + N_i\varepsilon''_{iab} + M''_{iab}\cancelto{0}{\kappa_i} + M'_{ia}\kappa'_{ib} + M'_{ib}\kappa'_{ia}\right) d\Omega\right] u_a u_b \\ &= \left[\frac{1}{2}\int_\Omega \left(N''_{iab}\varepsilon_i + N'_{ia}\varepsilon'_{ib} + N'_{ib}\varepsilon'_{ia} + N_i\varepsilon''_{iab} + M'_{ia}\kappa'_{ib} + M'_{ib}\kappa'_{ia}\right) d\Omega\right] u_a u_b \end{aligned} \tag{A.23}$$

$$\begin{aligned}\phi_c'''\boldsymbol{u_a u_b u_c} = \Bigg[\frac{1}{2}\int_\Omega (&N''_{iab}\varepsilon'_{ic} + N''_{iac}\varepsilon'_{ib} + N'_{ia}\varepsilon''_{ibc} + N''_{ibc}\varepsilon'_{ia} + N'_{ib}\varepsilon''_{iac} \\ &+N'_{ic}\varepsilon''_{iab} + M''_{iab}\kappa'_{ic} + M''_{iac}\kappa'_{ib} + M''_{ibc}\kappa'_{ia})\, d\Omega\Bigg] u_a u_b u_c\end{aligned} \tag{A.24}$$

$$\begin{aligned}\phi_c^{iv}\boldsymbol{u_a u_b u_c u_d} = \Bigg[\frac{1}{2}\int_\Omega (&N''_{iab}\varepsilon''_{icd} + N''_{iac}\varepsilon''_{ibd} + N''_{iad}\varepsilon''_{ibc} \\ &+N''_{ibc}\varepsilon''_{iad} + N''_{ibd}\varepsilon''_{iac} + N''_{icd}\varepsilon''_{iab})\, d\Omega\Bigg] u_a u_b u_c u_d\end{aligned} \tag{A.25}$$

$$\begin{aligned}\dot{\phi}_c''\boldsymbol{u_a u_b} &= \left[\frac{1}{2}\int_\Omega \left(N''_{iab}\dot{\varepsilon}_i + \cancelto{0}{\dot{N}'_{ia}\varepsilon'_{ib}} + N'_{ia}\cancelto{0}{\dot{\varepsilon}'_{ib}} + \cancelto{0}{\dot{N}'_{ib}\varepsilon'_{ia}} + N'_{ib}\cancelto{0}{\dot{\varepsilon}'_{ia}} + \dot{N}_i\varepsilon''_{iab}\right.\right. \\ &\left.\left. +M''_{iab}\cancelto{0}{\dot{\kappa}_i} + \cancelto{0}{\dot{M}'_{ia}\kappa'_{ib}} + \cancelto{0}{\dot{M}'_{ib}\kappa'_{ia}}\right) d\Omega\right] u_a u_b \\ &= \left[\frac{1}{2}\int_\Omega \left(N''_{iab}\dot{\varepsilon}_i + \dot{N}_i\varepsilon''_{iab}\right) d\Omega\right] u_a u_b\end{aligned} \tag{A.26}$$

$$\begin{aligned}\ddot{\phi}_c''\boldsymbol{u_a u_b} &= \left[\frac{1}{2}\int_\Omega \left(N''_{iab}\cancelto{0}{\ddot{\varepsilon}_i} + 2\cancelto{0}{\dot{N}'_{ia}\dot{\varepsilon}'_{ib}} + 2\cancelto{0}{\dot{N}'_{ib}\dot{\varepsilon}'_{ia}} + \cancelto{0}{\ddot{N}_i}\varepsilon''_{iab}\right) d\Omega\right] u_a u_b \\ &=0\end{aligned} \tag{A.27}$$

$$\begin{aligned}\dot{\phi}_c'''\boldsymbol{u_a u_b u_c} &= \left[\frac{1}{2}\int_\Omega \left(N''_{iab}\cancelto{0}{\dot{\varepsilon}'_{ic}} + N''_{iac}\cancelto{0}{\dot{\varepsilon}'_{ib}} + \cancelto{0}{\dot{N}'_{ia}}\varepsilon''_{ibc} + N''_{ibc}\cancelto{0}{\dot{\varepsilon}'_{ia}} + \cancelto{0}{\dot{N}'_{ib}}\varepsilon''_{iac} + \cancelto{0}{\dot{N}'_{ic}}\varepsilon''_{iab}\right) d\Omega\right] u_a u_b u_c \\ &=0\end{aligned} \tag{A.28}$$

$$\ddot{\phi}_c'''\boldsymbol{u_a u_b u_c} =0 \tag{A.29}$$

$$\dot{\phi}_c^{iv}\boldsymbol{u_a u_b u_c} =0 \tag{A.30}$$

$$\ddot{\phi}_c^{iv}\boldsymbol{u_a u_b u_c} =0 \tag{A.31}$$

A.3.2. Imperfect

The derivation of the imperfect functional derivatives can be found in section 6.5.

$$\begin{aligned}\psi_c'\boldsymbol{u_a} &= \left[\frac{1}{2}\int_\Omega \left(\bar{N}'_{ia}\cancelto{0}{\bar{\varepsilon}_i} + \cancelto{0}{\bar{N}_i\bar{\varepsilon}'_{ia}} + N'_{ia}\cancelto{0}{\bar{\varepsilon}_i} + N_i\bar{\varepsilon}'_{ia} + \bar{N}'_{ia}\varepsilon_i + \cancelto{0}{\bar{N}_i\varepsilon'_{ia}} + \bar{M}'_{ia}\cancelto{0}{\kappa_i} + \cancelto{0}{\bar{M}_i\kappa'_{ia}}\right) d\Omega\right] u_a \\ &= \left[\frac{1}{2}\int_\Omega \left(N_i\bar{\varepsilon}'_{ia} + \bar{N}'_{ia}\varepsilon_i\right) d\Omega\right] u_a\end{aligned} \tag{A.32}$$

$$\begin{aligned}\psi_c''\boldsymbol{u_a u_b} &= \left[\frac{1}{2}\int_\Omega \Big(\bar N'_{ia}\bar\varepsilon'_{ib} + \bar N'_{ib}\bar\varepsilon'_{ia} + N''_{iab}\cancelto{0}{\bar\varepsilon_i} + N'_{ia}\bar\varepsilon'_{ib} + N'_{ib}\bar\varepsilon'_{ia} \right.\\ &\qquad \left. + \bar N'_{ia}\varepsilon'_{ib} + \bar N'_{ib}\varepsilon'_{ia} + \cancelto{0}{\bar N_i}\varepsilon''_{iab} + \bar M'_{ia}\kappa'_{ib} + \bar M'_{ib}\kappa'_{ia}\Big)\, d\Omega\right] u_a u_b \\ &= \left[\frac{1}{2}\int_\Omega \big(\bar N'_{ia}\bar\varepsilon'_{ib} + \bar N'_{ib}\bar\varepsilon'_{ia} + N'_{ia}\bar\varepsilon'_{ib} + N'_{ib}\bar\varepsilon'_{ia} \right.\\ &\qquad \left. + \bar N'_{ia}\varepsilon'_{ib} + \bar N'_{ib}\varepsilon'_{ia} + \bar M'_{ia}\kappa'_{ib} + \bar M'_{ib}\kappa'_{ia}\big)\, d\Omega\right] u_a u_b\end{aligned} \tag{A.33}$$

$$\psi_c'''\boldsymbol{u_a u_b u_c} = \left[\frac{1}{2}\int_\Omega \big(N''_{iab}\bar\varepsilon'_{ic} + N''_{iac}\bar\varepsilon'_{ib} + N''_{ibc}\bar\varepsilon'_{ia} + \bar N'_{ia}\varepsilon''_{ibc} + \bar N'_{ib}\varepsilon''_{iac} + \bar N'_{ic}\varepsilon''_{iab}\big)\, d\Omega\right] u_a u_b u_c \tag{A.34}$$

$$\psi_c^{iv}\boldsymbol{u_a u_b u_c u_d} = \boldsymbol{0} \tag{A.35}$$

$$\begin{aligned}\tilde\psi'_c\boldsymbol{u_a}\bar{\boldsymbol{u}}_{\boldsymbol{k}} &= \left[\frac{1}{2}\int_\Omega \Big(\tilde{\bar N}'_{iak}\cancelto{0}{\bar\varepsilon_i} + \bar N'_{ia}\cancelto{0}{\tilde{\bar\varepsilon}_{ik}} + \cancelto{0}{\tilde{\bar N}_{ik}}\bar\varepsilon'_{ia} + \cancelto{0}{\bar N_i}\tilde{\bar\varepsilon}'_{iak} + N'_{ia}\cancelto{0}{\tilde{\bar\varepsilon}_{ik}} \right.\\ &\qquad \left. + N_i\tilde{\bar\varepsilon}'_{iak} + \tilde{\bar N}'_{iak}\varepsilon_i + \cancelto{0}{\tilde{\bar N}_{ik}}\varepsilon'_{ia} + \tilde{\bar M}'_{iak}\cancelto{0}{\kappa_i} + \cancelto{0}{\tilde{\bar M}_{ik}}\kappa'_{ia}\Big)\, d\Omega\right] u_a\bar u_k \\ &= \left[\frac{1}{2}\int_\Omega \Big(N_i\tilde{\bar\varepsilon}'_{iak} + \tilde{\bar N}'_{iak}\varepsilon_i\Big)\, d\Omega\right] u_a\bar u_k\end{aligned} \tag{A.36}$$

$$\begin{aligned}\dot{\tilde\psi}'_c\boldsymbol{u_a}\bar{\boldsymbol{u}}_{\boldsymbol{k}} &= \left[\frac{1}{2}\int_\Omega \Big(\tilde{\bar N}'_{iak}\cancelto{0}{\dot{\bar\varepsilon}_i} + \bar N'_{ia}\cancelto{0}{\dot{\tilde{\bar\varepsilon}}_{ik}} + \cancelto{0}{\dot{\tilde{\bar N}}_{ik}}\bar\varepsilon'_{ia} + \cancelto{0}{\dot{\bar N}_i}\tilde{\bar\varepsilon}'_{iak} + \dot N'_{ia}\cancelto{0}{\tilde{\bar\varepsilon}_{ik}} + N'_{ia}\cancelto{0}{\dot{\tilde{\bar\varepsilon}}_{ik}} + \dot N_i\tilde{\bar\varepsilon}'_{iak} \right.\\ &\qquad \left. + \tilde{\bar N}'_{iak}\dot\varepsilon_i + \cancelto{0}{\dot{\tilde{\bar N}}_{ik}}\varepsilon'_{ia} + \cancelto{0}{\tilde{\bar N}_{ik}}\dot\varepsilon'_{ia} + \tilde{\bar M}'_{iak}\cancelto{0}{\dot\kappa_i} + \cancelto{0}{\dot{\tilde{\bar M}}_{ik}}\kappa'_{ia}\Big)\, d\Omega\right] u_a\bar u_k \\ &= \left[\frac{1}{2}\int_\Omega \Big(\dot N_i\tilde{\bar\varepsilon}'_{iak} + \tilde{\bar N}'_{iak}\dot\varepsilon_i\Big)\, d\Omega\right] u_a\bar u_k\end{aligned} \tag{A.37}$$

$$\begin{aligned}\ddot{\tilde\psi}'_c\boldsymbol{u_a}\bar{\boldsymbol{u}}_{\boldsymbol{k}} &= \left[\frac{1}{2}\int_\Omega \Big(2\cancelto{0}{\dot{\bar N}'_{ia}}\cancelto{0}{\dot{\tilde{\bar\varepsilon}}_{ik}} + \cancelto{0}{\ddot{\bar N}_i}\tilde{\bar\varepsilon}'_{iak} + \tilde{\bar N}'_{iak}\cancelto{0}{\ddot{\bar\varepsilon}_i} + \cancelto{0}{\ddot{\tilde{\bar N}}_{ik}}\cancelto{0}{\dot{\bar\varepsilon}'_{ia}}\Big)\, d\Omega\right] u_a \\ &= 0\end{aligned} \tag{A.38}$$

$$\begin{aligned}\tilde{\tilde\psi}'_c\boldsymbol{u_a}\bar{\boldsymbol{u}}_{\boldsymbol{k}}\bar{\boldsymbol{u}}_{\boldsymbol{l}} &= \left[\frac{1}{2}\int_\Omega \Big(\tilde{\bar N}'_{iak}\cancelto{0}{\tilde{\bar\varepsilon}_{il}} + \tilde{\bar N}'_{ial}\cancelto{0}{\tilde{\bar\varepsilon}_{ik}} + \cancelto{0}{\tilde{\bar N}_{ik}}\tilde{\bar\varepsilon}'_{ial} + \cancelto{0}{\tilde{\bar N}_{il}}\tilde{\bar\varepsilon}'_{iak}\Big)\, d\Omega\right] u_a\bar u_k\bar u_l \\ &= 0\end{aligned} \tag{A.39}$$

$$\begin{aligned}\dot{\tilde{\tilde\psi}}'_c\boldsymbol{u_a}\bar{\boldsymbol{u}}_{\boldsymbol{k}}\bar{\boldsymbol{u}}_{\boldsymbol{l}} &= \left[\frac{1}{2}\int_\Omega \Big(\tilde{\bar N}'_{iak}\cancelto{0}{\dot{\tilde{\bar\varepsilon}}_{il}} + \tilde{\bar N}'_{ial}\cancelto{0}{\dot{\tilde{\bar\varepsilon}}_{ik}} + \cancelto{0}{\dot{\tilde{\bar N}}_{ik}}\tilde{\bar\varepsilon}'_{ial} + \cancelto{0}{\dot{\tilde{\bar N}}_{il}}\tilde{\bar\varepsilon}'_{iak}\Big)\, d\Omega\right] u_a\bar u_k\bar u_l \\ &= 0\end{aligned} \tag{A.40}$$

$$\ddot{\tilde{\psi}}'_c \boldsymbol{u_a \bar{u}_k \bar{u}_l} = \mathbf{0} \tag{A.41}$$

$$\begin{aligned}\tilde{\psi}''_c \boldsymbol{u_a u_b \bar{u}_k} = &\left[\frac{1}{2}\int_\Omega \Big(\tilde{\bar{N}}'_{iak}\bar{\varepsilon}'_{ib} + \bar{N}'_{ia}\tilde{\bar{\varepsilon}}'_{ibk} + \tilde{\bar{N}}'_{ibk}\bar{\varepsilon}'_{ia} + \bar{N}'_{ib}\tilde{\bar{\varepsilon}}'_{iak} + \cancelto{0}{N''_{iab}\bar{\varepsilon}_{ik}} + N'_{ia}\tilde{\bar{\varepsilon}}'_{ibk}\right.\\ &\left. + N'_{ib}\tilde{\bar{\varepsilon}}'_{iak} + \tilde{\bar{N}}'_{iak}\varepsilon'_{ib} + + \tilde{\bar{N}}'_{ibk}\varepsilon'_{ia} + \tilde{\bar{N}}_{ik}\cancelto{0}{\varepsilon''_{iab}} + \tilde{\bar{M}}'_{iak}\kappa'_{ib} + \tilde{\bar{M}}'_{ibk}\kappa'_{ia}\Big)\, d\Omega\right] u_a u_b \bar{u}_k\\ &\left[\frac{1}{2}\int_\Omega \Big(\tilde{\bar{N}}'_{iak}\bar{\varepsilon}'_{ib} + \bar{N}'_{ia}\tilde{\bar{\varepsilon}}'_{ibk} + \tilde{\bar{N}}'_{ibk}\bar{\varepsilon}'_{ia} + \bar{N}'_{ib}\tilde{\bar{\varepsilon}}'_{iak} + N'_{ia}\tilde{\bar{\varepsilon}}'_{ibk}\right.\\ &\left. + N'_{ib}\tilde{\bar{\varepsilon}}'_{iak} + \tilde{\bar{N}}'_{iak}\varepsilon'_{ib} + + \tilde{\bar{N}}'_{ibk}\varepsilon'_{ia} + \tilde{\bar{M}}'_{iak}\kappa'_{ib} + \tilde{\bar{M}}'_{ibk}\kappa'_{ia}\Big)\, d\Omega\right] u_a u_b \bar{u}_k\end{aligned} \tag{A.42}$$

$$\begin{aligned}\dot{\tilde{\psi}}''_c \boldsymbol{u_a u_b \bar{u}_k} &= \left[\frac{1}{2}\int_\Omega \left(\cancelto{0}{N''_{iab}\dot{\bar{\varepsilon}}_{ik}} + \cancelto{0}{\tilde{\bar{N}}'_{iak}\dot{\varepsilon}'_{ib}} + \cancelto{0}{\tilde{\bar{N}}'_{ibk}\dot{\varepsilon}'_{ia}} + \cancelto{0}{\dot{\tilde{\bar{N}}}_{ik}\varepsilon''_{iab}}\right) d\Omega\right] u_a u_b \bar{u}_k\\ &= 0\end{aligned} \tag{A.43}$$

$$\ddot{\tilde{\psi}}''_c \boldsymbol{u_a u_b \bar{u}_k} = \mathbf{0} \tag{A.44}$$

$$\tilde{\tilde{\psi}}''_c \boldsymbol{u_a u_b \bar{u}_k \bar{u}_l} = \left[\frac{1}{2}\int_\Omega \Big(\tilde{\bar{N}}'_{iak}\tilde{\bar{\varepsilon}}'_{ibl} + \tilde{\bar{N}}'_{ial}\tilde{\bar{\varepsilon}}'_{ibk} + \tilde{\bar{N}}'_{ibk}\tilde{\bar{\varepsilon}}'_{ial} + \tilde{\bar{N}}'_{ibl}\tilde{\bar{\varepsilon}}'_{iak}\Big)\, d\Omega\right] u_a u_b \bar{u}_k \bar{u}_l \tag{A.45}$$

$$\dot{\tilde{\tilde{\psi}}}''_c \boldsymbol{u_a u_b \bar{u}_k \bar{u}_l} = \mathbf{0} \tag{A.46}$$

$$\begin{aligned}\tilde{\psi}'''_c \boldsymbol{u_a u_b u_c \bar{u}_k} = &\left[\frac{1}{2}\int_\Omega (N'''_{iab}\tilde{\bar{\varepsilon}}'_{ick} + N'''_{iac}\tilde{\bar{\varepsilon}}'_{ibk} + N'''_{ibc}\tilde{\bar{\varepsilon}}'_{iak}\right.\\ &\left. + \tilde{\bar{N}}'_{iak}\varepsilon''_{ibc} + \tilde{\bar{N}}'_{ibk}\varepsilon''_{iac} + \tilde{\bar{N}}'_{ick}\varepsilon''_{iab}\Big)\, d\Omega\right] u_a u_b u_c \bar{u}_k\end{aligned} \tag{A.47}$$

$$\dot{\tilde{\psi}}'''_c \boldsymbol{u_a u_b u_c \bar{u}_k} = \mathbf{0} \tag{A.48}$$

$$\tilde{\tilde{\psi}}'''_c \boldsymbol{u_a u_b u_c \bar{u}_k \bar{u}_l} = \mathbf{0} \tag{A.49}$$

$$\dot{\tilde{\tilde{\psi}}}'''_c \boldsymbol{u_a u_b u_c \bar{u}_k \bar{u}_l} = \mathbf{0} \tag{A.50}$$

B

Full Expansion of the Total Potential Energy

Equation B.1 arises after the asymptotic expansions are substituted into the expansion of the total potential energy for a perfect plate.

$$
\begin{aligned}
&\xi^2\Big(\frac{1}{2}\phi_c'''\boldsymbol{u_I}^2+\phi_c''\boldsymbol{u_{II}}+\dot{\phi}_c''a_I\lambda_c\boldsymbol{u_I}\Big)\,\delta\boldsymbol{u}\\
+\xi^3&\left(\frac{1}{6}\phi_c^{iv}\boldsymbol{u_I}^3+\dot{\phi}_c''a_I\lambda_c\boldsymbol{u_{II}}+\frac{1}{2}\dot{\phi}_c'''a_I\lambda_c\boldsymbol{u_I}^2+\frac{1}{2}\ddot{\phi}_c''a_I^2\lambda_c^2\boldsymbol{u_I}+\phi_c'''\boldsymbol{u_I}\boldsymbol{u_{II}}+\dot{\phi}_c''b_I\lambda_c\boldsymbol{u_I}\right)\delta\boldsymbol{u}\\
+\xi^4&\left(\frac{1}{2}\ddot{\phi}_c''a_I^2\lambda_c^2\boldsymbol{u}_{II}+\ddot{\phi}_c''a_Ib_I\lambda_c^2\boldsymbol{u}_I+\dot{\phi}_c'''a_I\lambda_c\boldsymbol{u}_I\boldsymbol{u}_{II}+\frac{1}{2}\dot{\phi}_c'''b_I\lambda_c\boldsymbol{u}_I^2+\dot{\phi}_c''b_I\lambda_c\boldsymbol{u}_{II}+\frac{1}{2}\phi_c'''\boldsymbol{u}_{II}^2\right.\\
&\left.+\frac{1}{2}\phi_c^{iv}\boldsymbol{u}_I^2\boldsymbol{u}_{II}\right)\delta\boldsymbol{u}+\\
+\xi^5&\left(\ddot{\phi}_c''a_Ib_I\lambda_c^2\boldsymbol{u}_{II}+\frac{1}{2}\ddot{\phi}_c''b_I^2\lambda_c^2\boldsymbol{u}_I+\frac{1}{2}\dot{\phi}_c'''a_I\lambda_c\boldsymbol{u}_{II}^2+\dot{\phi}_c'''b_I\lambda_c\boldsymbol{u}_I\boldsymbol{u}_{II}+\frac{1}{2}\phi_c^{iv}\boldsymbol{u}_I\boldsymbol{u}_{II}^2\right)\delta\boldsymbol{u}\\
+\xi^6&\left(\frac{1}{2}\ddot{\phi}_c''b_I^2\lambda_c^2\boldsymbol{u}_{II}+\frac{1}{2}\dot{\phi}_c'''b_I\lambda_c\boldsymbol{u}_{II}^2+\frac{1}{6}\phi_c^{iv}\boldsymbol{u}_{II}^3\right)\delta\boldsymbol{u}+\xi\phi_c''\boldsymbol{u}_I\delta\boldsymbol{u}=0
\end{aligned}
\tag{B.1}
$$

Equation B.1 can be rewritten including the assumption linear pre-buckling to Equation B.2.

$$
\begin{aligned}
&\xi^2\Big(\frac{1}{2}\phi_c'''\boldsymbol{u_I}^2+\phi_c''\boldsymbol{u_{II}}+\dot{\phi}_c''a_I\lambda_c\boldsymbol{u_I}\Big)\,\delta\boldsymbol{u}\\
+\xi^3&\left(\frac{1}{6}\phi_c^{iv}\boldsymbol{u_I}^3+\dot{\phi}_c''a_I\lambda_c\boldsymbol{u_{II}}+\frac{1}{2}\cancelto{0}{\dot{\phi}_c'''}a_I\lambda_c\boldsymbol{u_I}^2+\frac{1}{2}\cancelto{0}{\ddot{\phi}_c''}a_I^2\lambda_c^2\boldsymbol{u_I}+\phi_c'''\boldsymbol{u_I}\boldsymbol{u_{II}}+\dot{\phi}_c''b_I\lambda_c\boldsymbol{u_I}\right)\delta\boldsymbol{u}\\
+\xi^4&\left(\frac{1}{2}\cancelto{0}{\ddot{\phi}_c''}a_I^2\lambda_c^2\boldsymbol{u}_{II}+\cancelto{0}{\ddot{\phi}_c''}a_Ib_I\lambda_c^2\boldsymbol{u}_I+\cancelto{0}{\dot{\phi}_c'''}a_I\lambda_c\boldsymbol{u}_I\boldsymbol{u}_{II}+\frac{1}{2}\cancelto{0}{\dot{\phi}_c'''}b_I\lambda_c\boldsymbol{u}_I^2+\dot{\phi}_c''b_I\lambda_c\boldsymbol{u}_{II}+\frac{1}{2}\phi_c'''\boldsymbol{u}_{II}^2\right.\\
&\left.+\frac{1}{2}\phi_c^{iv}\boldsymbol{u}_I^2\boldsymbol{u}_{II}\right)\delta\boldsymbol{u}+\\
+\xi^5&\left(\cancelto{0}{\ddot{\phi}_c''}a_Ib_I\lambda_c^2\boldsymbol{u}_{II}+\frac{1}{2}\cancelto{0}{\ddot{\phi}_c''}b_I^2\lambda_c^2\boldsymbol{u}_I+\frac{1}{2}\cancelto{0}{\dot{\phi}_c'''}a_I\lambda_c\boldsymbol{u}_{II}^2+\cancelto{0}{\dot{\phi}_c'''}b_I\lambda_c\boldsymbol{u}_I\boldsymbol{u}_{II}+\frac{1}{2}\phi_c^{iv}\boldsymbol{u}_I\boldsymbol{u}_{II}^2\right)\delta\boldsymbol{u}\\
+\xi^6&\left(\frac{1}{2}\cancelto{0}{\ddot{\phi}_c''}b_I^2\lambda_c^2\boldsymbol{u}_{II}+\frac{1}{2}\cancelto{0}{\dot{\phi}_c'''}b_I\lambda_c\boldsymbol{u}_{II}^2+\frac{1}{6}\phi_c^{iv}\boldsymbol{u}_{II}^3\right)\delta\boldsymbol{u}+\xi\phi_c''\boldsymbol{u}_I\delta\boldsymbol{u}=
\end{aligned}
\tag{B.2}
$$

$$
\begin{aligned}
&\xi^2(\frac{1}{2}\phi_c'''\boldsymbol{u_I^2}+\phi_c''\boldsymbol{u_{II}}+\dot{\phi}_c''a_I\lambda_c\boldsymbol{u_I}\Big)\,\delta\boldsymbol{u}\\
+\xi^3&\left(\frac{1}{6}\phi_c^{iv}\boldsymbol{u_I^3}+\dot{\phi}_c''a_I\lambda_c\boldsymbol{u_{II}}+\phi_c'''\boldsymbol{u_I u_{II}}+\dot{\phi}_c''b_I\lambda_c\boldsymbol{u_I}\right)\delta\boldsymbol{u}\\
+\xi^4&\left(\dot{\phi}_c''b_I\lambda_c\boldsymbol{u}_{II}+\frac{1}{2}\phi_c'''\boldsymbol{u}_{II}^2+\frac{1}{2}\phi_c^{iv}\boldsymbol{u}_I^2\boldsymbol{u}_{II}\right)\delta\boldsymbol{u}+\\
&+\frac{1}{2}\xi^5\phi_c^{iv}\boldsymbol{u_I u}_{II}^2\delta\boldsymbol{u}+\frac{1}{6}\xi^6\phi_c^{iv}\boldsymbol{u}_{II}^3\delta\boldsymbol{u}+\xi\phi_c''\boldsymbol{u}_I\delta\boldsymbol{u}=0
\end{aligned}
\tag{C.2}
$$

C

Non-Linear Asymptotic Analysis

C.1. Initial Imperfect Post-buckling coefficients

C.1.1. Option 3: PN

Equation C.1 emerges after the substitution of the asymptotic expansions into the full potential energy following the work of Pignataro. The imperfect terms are underlined to emphasize the difference between the perfect and imperfect derivatives.

$$
\begin{aligned}
&\underline{\bar{\xi}\hat{\boldsymbol{u}}\tilde{\psi}_c'\delta\boldsymbol{u}} + \xi\left(\underline{\bar{\xi}\hat{\boldsymbol{u}}\dot{\tilde{\psi}}_c' a_I\lambda_c + \bar{\xi}\hat{\boldsymbol{u}}\tilde{\psi}_c''\boldsymbol{u}_I} + \phi_c''\boldsymbol{u}_I\right)\delta\boldsymbol{u} \\
&+\xi^2\left(\underline{\frac{1}{2}\bar{\xi}\hat{\boldsymbol{u}}\ddot{\tilde{\psi}}_c' a_I^2\lambda_c^2 + \bar{\xi}\hat{\boldsymbol{u}}\dot{\tilde{\psi}}_c'' a_I\lambda_c\boldsymbol{u}_I + \bar{\xi}\hat{\boldsymbol{u}}\dot{\tilde{\psi}}_c' b_I\lambda_c + \frac{1}{2}\bar{\xi}\hat{\boldsymbol{u}}\tilde{\psi}_c'''\boldsymbol{u}_I^2 + \bar{\xi}\hat{\boldsymbol{u}}\tilde{\psi}_c''\boldsymbol{u}_{II}} + \dot{\phi}_c'' a_I\lambda_c\boldsymbol{u}_I + \frac{1}{2}\phi_c'''\boldsymbol{u}_I^2\right. \\
&\qquad\left.+\phi_c''\boldsymbol{u}_{II}\right)\delta\boldsymbol{u} \\
&+\xi^3\left(\underline{\bar{\xi}\hat{\boldsymbol{u}}\ddot{\tilde{\psi}}_c' a_I b_I\lambda_c^2 + \bar{\xi}\hat{\boldsymbol{u}}\dot{\tilde{\psi}}_c'' a_I\lambda_c\boldsymbol{u}_{II} + \bar{\xi}\hat{\boldsymbol{u}}\dot{\tilde{\psi}}_c'' b_I\lambda_c\boldsymbol{u}_I + \bar{\xi}\hat{\boldsymbol{u}}\tilde{\psi}_c'''\boldsymbol{u}_I\boldsymbol{u}_{II}} + \frac{1}{2}\ddot{\phi}_c'' a_I^2 a_I^2\lambda_c^2\boldsymbol{u}_I + \frac{1}{2}\dot{\phi}_c''' a_I\lambda_c\boldsymbol{u}_I^2\right. \\
&\qquad\left.+\dot{\phi}_c'' a_I\lambda_c\boldsymbol{u}_{II} + \dot{\phi}_c'' b_I\lambda_c\boldsymbol{u}_I + \phi_c'''\boldsymbol{u}_I\boldsymbol{u}_{II} + \frac{1}{6}\phi_c^{iv}\boldsymbol{u}_I^3\right)\delta\boldsymbol{u} \\
&+\xi^4\left(\underline{\frac{1}{2}\bar{\xi}\hat{\boldsymbol{u}}\ddot{\tilde{\psi}}_c' b_I^2\lambda_c^2 + \frac{1}{2}\bar{\xi}\tilde{\psi}'''\boldsymbol{u}_{II}^2 + \bar{\xi}\hat{\boldsymbol{u}}\dot{\tilde{\psi}}_c'' b_I\lambda_c\boldsymbol{u}_{II}} + \frac{1}{2}\ddot{\phi}_c'' a_I^2\lambda_c^2\boldsymbol{u}_{II} + \ddot{\phi}_c'' a_I b_I\lambda_c^2\boldsymbol{u}_I + \dot{\phi}_c''' a_I\lambda_c\boldsymbol{u}_I\boldsymbol{u}_{II}\right. \\
&\qquad\left.+\frac{1}{2}\dot{\phi}_c''' b_I\lambda_c\boldsymbol{u}_I^2 + \dot{\phi}_c'' b_I\lambda_c\boldsymbol{u}_{II} + \frac{1}{2}\phi_c'''\boldsymbol{u}_{II}^2 + \frac{1}{2}\phi_c^{iv}\boldsymbol{u}_I^2\boldsymbol{u}_{II}\right)\delta\boldsymbol{u} \\
&+\xi^5\left(\ddot{\phi}_c'' a_I b_I\lambda_c^2\boldsymbol{u}_{II} + \frac{1}{2}\ddot{\phi}_c'' b_I^2\lambda_c^2\boldsymbol{u}_I + \frac{1}{2}\dot{\phi}_c''' a_I\lambda_c\boldsymbol{u}_{II}^2 + \dot{\phi}_c''' b_I\lambda_c\boldsymbol{u}_I\boldsymbol{u}_{II} + \frac{1}{2}\phi_c^{iv}\boldsymbol{u}_I\boldsymbol{u}_{II}^2\right)\delta\boldsymbol{u} \\
&+\xi^6\left(\frac{1}{2}\ddot{\phi}_c'' b_I^2\lambda_c^2\boldsymbol{u}_{II} + \frac{1}{2}\dot{\phi}_c''' b_I\lambda_c\boldsymbol{u}_{II}^2 + \frac{1}{6}\phi_c^{iv}\boldsymbol{u}_{II}^3\right)\delta\boldsymbol{u} = 0
\end{aligned}
\tag{C.1}
$$

C.1.2. Option 4: BN

The final and further longest expression for the fourth solution approach is presented in Equation C.2 after the asymptotic expansions are substituted into the full potential energy of Budiansky. The imperfect terms are underlined to highlight the difference between the perfect and imperfect terms.

$$
\begin{aligned}
&\underline{\bar{\xi}\hat{\boldsymbol{u}}\tilde{\psi}_c'\delta\boldsymbol{u} + \frac{1}{2}\bar{\xi}^2\hat{\boldsymbol{u}}^2\tilde{\psi}_c'\delta\boldsymbol{u}} + \xi\left(\underline{\frac{1}{2}\bar{\xi}^2\hat{\boldsymbol{u}}^2\dot{\tilde{\psi}}_c' a_I\lambda_c + \frac{1}{2}\bar{\xi}^2\hat{\boldsymbol{u}}^2\tilde{\psi}_c''\boldsymbol{u}_I + \bar{\xi}\hat{\boldsymbol{u}}\dot{\tilde{\psi}}_c' a_I\lambda_c + \bar{\xi}\hat{\boldsymbol{u}}\tilde{\psi}_c''\boldsymbol{u}_I} + \phi_c''\boldsymbol{u}_I\right)\delta\boldsymbol{u}\\
&+\xi^2\left(\underline{\frac{1}{2}\bar{\xi}^2\hat{\boldsymbol{u}}^2\ddot{\tilde{\psi}}_c' b_I\lambda_c + \frac{1}{2}\bar{\xi}^2\hat{\boldsymbol{u}}^2\dot{\tilde{\psi}}_c''\boldsymbol{u}_{II} + \frac{1}{2}\bar{\xi}\hat{\boldsymbol{u}}\ddot{\tilde{\psi}}_c' a_I^2\lambda_c^2 + \bar{\xi}\hat{\boldsymbol{u}}\dot{\tilde{\psi}}_c'' a_I\lambda_c\boldsymbol{u}_I + \bar{\xi}\hat{\boldsymbol{u}}\dot{\tilde{\psi}}_c' b_I\lambda_c + \frac{1}{2}\bar{\xi}\hat{\boldsymbol{u}}\tilde{\psi}_c'''\boldsymbol{u}_I^2}\right.\\
&\qquad\left.\underline{+\bar{\xi}\hat{\boldsymbol{u}}\tilde{\psi}_c''\boldsymbol{u}_{II}} + \dot{\phi}_c'' a_I\lambda_c\boldsymbol{u}_I + \frac{1}{2}\phi_c'''\boldsymbol{u}_I^2 + \phi_c''\boldsymbol{u}_{II}\right)\delta\boldsymbol{u}\\
&+\xi^3\left(\underline{\bar{\xi}\hat{\boldsymbol{u}}\ddot{\tilde{\psi}}_c' a_I b_I\lambda_c^2 + \bar{\xi}\hat{\boldsymbol{u}}\dot{\tilde{\psi}}_c'' a_I\lambda_c\boldsymbol{u}_{II} + \bar{\xi}\hat{\boldsymbol{u}}\dot{\tilde{\psi}}_c'' b_I\lambda_c\boldsymbol{u}_I + \bar{\xi}\hat{\boldsymbol{u}}\tilde{\psi}_c'''\boldsymbol{u}_I\boldsymbol{u}_{II}} + \frac{1}{2}\ddot{\phi}_c'' a_I^2 a_I^2\lambda_c^2\boldsymbol{u}_I + \frac{1}{2}\dot{\phi}_c''' a_I\lambda_c\boldsymbol{u}_I^2\right.\\
&\qquad\left.+\dot{\phi}_c'' a_I\lambda_c\boldsymbol{u}_{II} + \dot{\phi}_c'' b_I\lambda_c\boldsymbol{u}_I + \phi_c'''\boldsymbol{u}_I\boldsymbol{u}_{II} + \frac{1}{6}\phi_c^{iv}\boldsymbol{u}_I^3\right)\delta\boldsymbol{u}\\
&+\xi^4\left(\underline{\frac{1}{2}\bar{\xi}\hat{\boldsymbol{u}}\ddot{\tilde{\psi}}_c' b_I^2\lambda_c^2 + \frac{1}{2}\bar{\xi}\tilde{\psi}'''\boldsymbol{u}_{II}^2 + \bar{\xi}\hat{\boldsymbol{u}}\dot{\tilde{\psi}}_c'' b_I\lambda_c\boldsymbol{u}_{II}} + \frac{1}{2}\ddot{\phi}_c'' a_I^2\lambda_c^2\boldsymbol{u}_{II} + \ddot{\phi}_c'' a_I b_I\lambda_c^2\boldsymbol{u}_I + \dot{\phi}_c''' a_I\lambda_c\boldsymbol{u}_I\boldsymbol{u}_{II}\right.\\
&\qquad\left.+\frac{1}{2}\dot{\phi}_c''' b_I\lambda_c\boldsymbol{u}_I^2 + \dot{\phi}_c'' b_I\lambda_c\boldsymbol{u}_{II} + \frac{1}{2}\phi_c'''\boldsymbol{u}_{II}^2 + \frac{1}{2}\phi_c^{iv}\boldsymbol{u}_I^2\boldsymbol{u}_{II}\right)\delta\boldsymbol{u}\\
&+\xi^5\left(\ddot{\phi}_c'' a_I b_I\lambda_c^2\boldsymbol{u}_{II} + \frac{1}{2}\ddot{\phi}_c''' b_I^2\lambda_c^2\boldsymbol{u}_I + \frac{1}{2}\dot{\phi}_c''' a_I\lambda_c\boldsymbol{u}_{II}^2 + \dot{\phi}_c''' b_I\lambda_c\boldsymbol{u}_I\boldsymbol{u}_{II} + \frac{1}{2}\phi_c^{iv}\boldsymbol{u}_I\boldsymbol{u}_{II}^2\right)\delta\boldsymbol{u}\\
&+\xi^6\left(\frac{1}{2}\ddot{\phi}_c''' b_I^2\lambda_c^2\boldsymbol{u}_{II} + \frac{1}{2}\dot{\phi}_c''' b_I\lambda_c\boldsymbol{u}_{II}^2 + \frac{1}{6}\phi_c^{iv}\boldsymbol{u}_{II}^3\right)\delta\boldsymbol{u} = 0
\end{aligned}
\tag{C.2}
$$

C.2. Imperfection Form Factors

C.2.1. Option 3: PN

The displacement expansion is replaced into the full total potential energy expansion. Subsequently, the imperfect expansion for the load, provided in Equation 7.16, is substituted to replace $\xi\left(\lambda-\lambda_c\right)$. The emerging equation is rewritten to find Equation C.3. If the imperfection amplitude is set to zero, thus the underlining terms vanish, it equals the perfect equilibrium presented in Equation B.1.

$$
\begin{aligned}
&\xi\phi_c''\boldsymbol{u}_I\delta\boldsymbol{u}+\bar{\xi}\Big(-\frac{1}{2}\left(\lambda-\lambda_c\right)\ddot{\phi}_c''\alpha\lambda_c\boldsymbol{u_I}-\dot{\phi}_c''\alpha\lambda_c\boldsymbol{u_I}-\frac{1}{2}\left(\lambda-\lambda_c\right)^2\ddot{\phi}_c''\beta\boldsymbol{u_I}-\left(\lambda-\lambda_c\right)\dot{\phi}_c''\beta\boldsymbol{u_I}\\
&\qquad+\frac{1}{2}\left(\lambda-\lambda_c\right)^2\hat{\boldsymbol{u}}\ddot{\tilde{\psi}}_c'+\left(\lambda-\lambda_c\right)\hat{\boldsymbol{u}}\dot{\tilde{\psi}}_c'+\hat{\boldsymbol{u}}\tilde{\psi}_c'\Big)\delta\boldsymbol{u}\\
&+\xi\bar{\xi}\Big(\hat{\boldsymbol{u}}\tilde{\psi}_c''\boldsymbol{u}_I-\left(\lambda-\lambda_c\right)\dot{\phi}_c''\beta\boldsymbol{u_{II}}-\frac{1}{2}\left(\lambda-\lambda_c\right)\dot{\phi}_c'''\beta\boldsymbol{u_I}^2-\frac{1}{2}\left(\lambda-\lambda_c\right)^2\ddot{\phi}_c''\beta\boldsymbol{u_{II}}-\dot{\phi}_c''\alpha\lambda_c\boldsymbol{u_{II}}\\
&\qquad-\frac{1}{2}\dot{\phi}_c'''\alpha\lambda_c\boldsymbol{u_I}^2-\frac{1}{2}\left(\lambda-\lambda_c\right)\ddot{\phi}_c''\alpha\lambda_c\boldsymbol{u_{II}}\Big)\delta\boldsymbol{u}\\
&\qquad+\xi^2\Big(\phi_c''\boldsymbol{u_{II}}+\frac{1}{2}\phi_c'''\boldsymbol{u_I}^2+\dot{\phi}_c''a_I\lambda_c\boldsymbol{u_I}+\frac{1}{2}\left(\lambda-\lambda_c\right)\ddot{\phi}_c''a_I\lambda_c\boldsymbol{u_I}\Big)\delta\boldsymbol{u}\\
&+\xi^2\bar{\xi}\Big(\hat{\boldsymbol{u}}\tilde{\psi}_c''\boldsymbol{u}_{II}+\frac{1}{2}\hat{\boldsymbol{u}}\tilde{\psi}_c'''\boldsymbol{u}_I^2+\hat{\boldsymbol{u}}\dot{\tilde{\psi}}_c''a_I\lambda_c\boldsymbol{u_I}-\left(\lambda-\lambda_c\right)\dot{\phi}_c'''\beta\boldsymbol{u_I}\boldsymbol{u_{II}}-\dot{\phi}_c'''\alpha\lambda_c\boldsymbol{u_I}\boldsymbol{u_{II}}\Big)\delta\boldsymbol{u}\\
&+\bar{\xi}^2\Big(-\left(\lambda-\lambda_c\right)\hat{\boldsymbol{u}}\dot{\tilde{\psi}}_c''\beta\boldsymbol{u_I}-\hat{\boldsymbol{u}}\dot{\tilde{\psi}}_c''\alpha\lambda_c\boldsymbol{u_I}\Big)\delta\boldsymbol{u}+\xi\bar{\xi}^2\Big(-\left(\lambda-\lambda_c\right)\hat{\boldsymbol{u}}\dot{\tilde{\psi}}_c''\beta\boldsymbol{u_{II}}-\hat{\boldsymbol{u}}\dot{\tilde{\psi}}_c''\alpha\lambda_c\boldsymbol{u_{II}}\Big)\delta\boldsymbol{u}\\
&+\xi^3\Big(\frac{1}{2}\left(\lambda-\lambda_c\right)\ddot{\phi}_c''a_I\lambda_c\boldsymbol{u}_{II}+\frac{1}{2}\left(\lambda-\lambda_c\right)\ddot{\phi}_c''b_I\lambda_c\boldsymbol{u}_I+\frac{1}{2}\dot{\phi}_c'''a_I\lambda_c\boldsymbol{u}_I^2+\dot{\phi}_c''a_I\lambda_c\boldsymbol{u}_{II}+\dot{\phi}_c''b_I\lambda_c\boldsymbol{u}_I\\
&\qquad+\phi_c'''\boldsymbol{u}_I\boldsymbol{u}_{II}+\frac{1}{6}\phi_c^{iv}\boldsymbol{u}_I^3\Big)\delta\boldsymbol{u}\\
&+\xi^3\bar{\xi}\Big(-\frac{1}{2}\dot{\phi}_c'''\alpha\lambda_c\boldsymbol{u_{II}}^2-\frac{1}{2}\left(\lambda-\lambda_c\right)\beta\boldsymbol{u_{II}}^2+\hat{\boldsymbol{u}}\dot{\tilde{\psi}}_c''a_I\lambda_c\boldsymbol{u_{II}}+\hat{\boldsymbol{u}}\dot{\tilde{\psi}}_c''b_I\lambda_c\boldsymbol{u_I}+\hat{\boldsymbol{u}}\tilde{\psi}_c'''\boldsymbol{u_I}\boldsymbol{u_{II}}\Big)\delta\boldsymbol{u}\\
&\qquad+\xi^4\Big(\frac{1}{2}\left(\lambda-\lambda_c\right)\ddot{\phi}_c''b_I\lambda_c\boldsymbol{u_{II}}+\dot{\phi}_c'''a_I\lambda_c\boldsymbol{u_I}\boldsymbol{u_{II}}+\frac{1}{2}\dot{\phi}_c'''b_I\lambda_c\boldsymbol{u_I}^2+\dot{\phi}_c''b_I\lambda_c\boldsymbol{u}_{II}+\frac{1}{2}\phi_c^{iv}\boldsymbol{u}_I^2\boldsymbol{u}_{II}\\
&\qquad+\frac{1}{2}\phi_c'''\boldsymbol{u}_{II}^2\Big)\delta\boldsymbol{u}\\
&+\xi^4\bar{\xi}\Big(\hat{\boldsymbol{u}}\dot{\tilde{\psi}}_c''b_I\lambda_c\boldsymbol{u_{II}}+\frac{1}{2}\hat{\boldsymbol{u}}\tilde{\psi}_c'''\boldsymbol{u_{II}}^2\Big)\delta\boldsymbol{u}+\xi^5\Big(\frac{1}{2}\dot{\phi}_c'''a_I\lambda_c\boldsymbol{u}_{II}^2+\dot{\phi}_c'''b_I\lambda_c\boldsymbol{u}_I\boldsymbol{u}_{II}+\frac{1}{2}\phi_c^{iv}\boldsymbol{u}_I\boldsymbol{u}_{II}^2\Big)\delta\boldsymbol{u}\\
&\qquad+\xi^6\Big(\frac{1}{2}\dot{\phi}_c''''b_I\lambda_c\boldsymbol{u}_{II}^2+\frac{1}{6}\phi_c^{iv}\boldsymbol{u}_{II}^3\Big)\delta\boldsymbol{u}=0
\end{aligned}
\tag{C.3}
$$

C.2.2. Option 4: BN

The last possibility for deriving the imperfection form factors is obtained by substituting the expansion for the displacement into the full expansion of Budiansky. Consequently, the imperfect load expansion including both form factors is replaced for $\xi(\lambda - \lambda_c)$, resulting in the following equation after the terms are regrouped. If the imperfection amplitude is set to zero, thus the underlining terms vanish, it equals the perfect equilibrium presented in Equation B.1.

$$
\begin{aligned}
&\xi\phi_c''\boldsymbol{u}_I\delta\boldsymbol{u} + \underline{\bar{\xi}\left(-\frac{1}{2}(\lambda-\lambda_c)\ddot{\phi}_c''\alpha\lambda_c\boldsymbol{u_I} - \dot{\phi}_c''\alpha\lambda_c\boldsymbol{u_I} - \frac{1}{2}(\lambda-\lambda_c)^2\ddot{\phi}_c''\beta\boldsymbol{u_I} - (\lambda-\lambda_c)\dot{\phi}_c''\beta\boldsymbol{u_I}\right.}\\
&\qquad\underline{\left.+\frac{1}{2}(\lambda-\lambda_c)^2\hat{\boldsymbol{u}}\ddot{\tilde{\psi}}_c' + (\lambda-\lambda_c)\hat{\boldsymbol{u}}\dot{\tilde{\psi}}_c' + \hat{\boldsymbol{u}}\tilde{\psi}_c'\right)\delta\boldsymbol{u}}\\
&+\underline{\xi\bar{\xi}\left(\hat{\boldsymbol{u}}\tilde{\psi}_c''\boldsymbol{u}_I - (\lambda-\lambda_c)\dot{\phi}_c''\beta\boldsymbol{u_{II}} - \frac{1}{2}(\lambda-\lambda_c)\dot{\phi}_c'''\beta\boldsymbol{u_I}^2 - \frac{1}{2}(\lambda-\lambda_c)^2\ddot{\phi}_c''\beta\boldsymbol{u_{II}} - \dot{\phi}_c''\alpha\lambda_c\boldsymbol{u_{II}}\right.}\\
&\qquad\underline{\left.-\frac{1}{2}\dot{\phi}_c'''\alpha\lambda_c\boldsymbol{u_I}^2 - \frac{1}{2}(\lambda-\lambda_c)\ddot{\phi}_c''\alpha\lambda_c\boldsymbol{u_{II}}\right)\delta\boldsymbol{u}}\\
&\qquad+\xi^2\left(\phi_c''\boldsymbol{u_{II}} + \frac{1}{2}\phi_c'''\boldsymbol{u_I}^2 + \dot{\phi}_c''a_I\lambda_c\boldsymbol{u_I} + \frac{1}{2}(\lambda-\lambda_c)\ddot{\phi}_c''a_I\lambda_c\boldsymbol{u_I}\right)\delta\boldsymbol{u}\\
&+\underline{\xi^2\bar{\xi}\left(\hat{\boldsymbol{u}}\tilde{\psi}_c''\boldsymbol{u}_{II} + \frac{1}{2}\hat{\boldsymbol{u}}\tilde{\psi}_c'''\boldsymbol{u}_I^2 + \hat{\boldsymbol{u}}\dot{\tilde{\psi}}_c''a_I\lambda_c\boldsymbol{u_I} - (\lambda-\lambda_c)\dot{\phi}_c'''\beta\boldsymbol{u_I}\boldsymbol{u_{II}} - \dot{\phi}_c'''\alpha\lambda_c\boldsymbol{u_I}\boldsymbol{u_{II}}\right)\delta\boldsymbol{u}}\\
&\qquad\underline{+\bar{\xi}^2\left(-(\lambda-\lambda_c)\hat{\boldsymbol{u}}\dot{\tilde{\psi}}_c''\beta\boldsymbol{u_I} - \hat{\boldsymbol{u}}\dot{\tilde{\psi}}_c''\alpha\lambda_c\boldsymbol{u_I} + \frac{1}{2}\hat{\boldsymbol{u}}^2\tilde{\psi}_c' + \frac{1}{2}(\lambda-\lambda_c)\hat{\boldsymbol{u}}^2\dot{\tilde{\psi}}_c'\right)\delta\boldsymbol{u}}\\
&+\underline{\xi\bar{\xi}^2\left(-(\lambda-\lambda_c)\hat{\boldsymbol{u}}\dot{\tilde{\psi}}_c''\beta\boldsymbol{u_{II}} - \hat{\boldsymbol{u}}\dot{\tilde{\psi}}_c''\alpha\lambda_c\boldsymbol{u_{II}} + \frac{1}{2}(\lambda-\lambda_c)\hat{\boldsymbol{u}}^2\dot{\tilde{\psi}}_c'\right)\delta\boldsymbol{u} + \frac{1}{2}\xi^2\bar{\xi}^2\hat{\boldsymbol{u}}^2\tilde{\psi}_c''\boldsymbol{u_{II}}}\\
&+\xi^3\left(\frac{1}{2}(\lambda-\lambda_c)\ddot{\phi}_c''a_I\lambda_c\boldsymbol{u}_{II} + \frac{1}{2}(\lambda-\lambda_c)\ddot{\phi}_c''b_I\lambda_c\boldsymbol{u}_I + \frac{1}{2}\dot{\phi}_c'''a_I\lambda_c\boldsymbol{u}_I^2 + \dot{\phi}_c''a_I\lambda_c\boldsymbol{u}_{II} + \dot{\phi}_c''b_I\lambda_c\boldsymbol{u}_I\right.\\
&\qquad\left.+\phi_c'''\boldsymbol{u}_I\boldsymbol{u}_{II} + \frac{1}{6}\phi_c^{iv}\boldsymbol{u}_I^3\right)\delta\boldsymbol{u}\\
&+\underline{\xi^3\bar{\xi}\left(-\frac{1}{2}\dot{\phi}_c'''\alpha\lambda_c\boldsymbol{u_{II}}^2 - \frac{1}{2}(\lambda-\lambda_c)\beta\boldsymbol{u_{II}}^2 + \hat{\boldsymbol{u}}\dot{\tilde{\psi}}_c''a_I\lambda_c\boldsymbol{u_{II}} + \hat{\boldsymbol{u}}\dot{\tilde{\psi}}_c''b_I\lambda_c\boldsymbol{u_I} + \hat{\boldsymbol{u}}\tilde{\psi}_c'''\boldsymbol{u_I}\boldsymbol{u_{II}}\right)\delta\boldsymbol{u}}\\
&+\xi^4\left(\frac{1}{2}(\lambda-\lambda_c)\ddot{\phi}_c''b_I\lambda_c\boldsymbol{u_{II}} + \dot{\phi}_c'''a_I\lambda_c\boldsymbol{u_I}\boldsymbol{u_{II}} + \frac{1}{2}\dot{\phi}_c'''b_I\lambda_c\boldsymbol{u_I}^2 + \dot{\phi}_c''b_I\lambda_c\boldsymbol{u}_{II} + \frac{1}{2}\phi_c^{iv}\boldsymbol{u}_I^2\boldsymbol{u}_{II}\right.\\
&\qquad\left.+\frac{1}{2}\phi_c'''\boldsymbol{u}_{II}^2\right)\delta\boldsymbol{u}\\
&+\underline{\xi^4\bar{\xi}\left(\hat{\boldsymbol{u}}\dot{\tilde{\psi}}_c''b_I\lambda_c\boldsymbol{u_{II}} + \frac{1}{2}\hat{\boldsymbol{u}}\tilde{\psi}_c'''\boldsymbol{u_{II}}^2\right)\delta\boldsymbol{u}} + \xi^5\left(\frac{1}{2}\dot{\phi}_c'''a_I\lambda_c\boldsymbol{u}_{II}^2 + \dot{\phi}_c'''b_I\lambda_c\boldsymbol{u}_I\boldsymbol{u}_{II} + \frac{1}{2}\phi_c^{iv}\boldsymbol{u}_I\boldsymbol{u}_{II}^2\right)\delta\boldsymbol{u}\\
&\qquad+\xi^6\left(\frac{1}{2}\dot{\phi}_c'''b_I\lambda_c\boldsymbol{u}_{II}^2 + \frac{1}{6}\phi_c^{iv}\boldsymbol{u}_{II}^3\right)\delta\boldsymbol{u} = 0
\end{aligned}
\tag{C.4}
$$